6G Integrated Sensing and Communication System for the Factory of the Future

Departamento de Comunicaciones
Universitat Politècnica de València

A thesis submitted for the degree of
Doctor por la Universitat Politècnica de València
Valencia, December 2024

Author:
Andrea F. Ramos Pillasagua

Supervisor:
Prof. Jose F. Monserrat del Río

In memory of my magical
and endless love,
my grandma
Betita.

Abstract

Leveraging Fifth Generation (5G) technology to advance Industry 4.0 has marked a significant milestone in the historical evolution of cellular networks. This development aims to support smart factories with stringent communication requirements, as their operation is focused on meeting Quality of Service (QoS) standards, making the Industrial Internet of Things (IIoT) applications susceptible to unstable network performance.

Moreover, these applications frequently occur indoors, where high-density clutter poses additional challenges. Large metal structures, robots, and moving vehicles obstruct signal propagation and can significantly degrade communication performance. The first standardized channel model for Indoor Factory (InF) was introduced by the Third Generation Partnership Project (3GPP) in Release 16 to study and address these environmental particularities. This Thesis builds on this foundation and examines the modeling procedure, identifying limitations such as imprecise parameter characterization and a limited ability to capture the full geometric complexity of such environments.

Concerned about these limitations, this work takes a significant step forward by proposing a new technology to address challenges in industrial modeling. This approach opens the door to exploring one of the key emerging trends in Sixth Generation (6G) for IIoT applications: Integrated Sensing and Communications (ISAC) systems. ISAC systems hold the promising potential to overcome not only existing challenges but also introduce additional, valuable enhancements. As ISAC is a novel technology, no channel model has been specifically designed for it so far. To fill this need, this Thesis presents the development of an ISAC channel model as a foundational step in advancing this technology.

During this progress, fundamental features for building an ISAC channel model have been identified, which are often overlooked in the literature. In response, this work motivates the development of technical guidelines for ISAC modeling, forming an evaluation methodology.

An evaluation methodology is important for ISAC or any system, as it is essential for assessing performance and guiding future upgrades. Such a methodology does not exist for ISAC. This Thesis tackles these challenges by emphasizing the importance of considering the main features to construct an ISAC channel: Correlation between the sensing and communication channel and spatial consistency.

Building on the initial development of the ISAC framework, the next step involves testing ISAC in quasi-realistic environments. This Thesis presents an industrial use case that applies sensing-assisted beam training, demonstrating how ISAC can deal with the issue of multiple obstructions in such environments. Specifically, it explores the background subtraction technique in a predictive beamforming algorithm, which leverages target-related information obtained through sensing. Under these considerations, the findings indicate a substantial improvement in communication performance, particularly regarding signal-to-noise ratio (SNR) and effective data rate.

In other words, the results highlight ISAC's potential to tackle the geometrical complexities of the environment of interest effectively. This Thesis not only pioneers the background subtraction technique but also showcases its impact, paving the way for future applications to other sensing algorithms within the framework of ISAC and the factory of the future.

Resumen

El aprovechamiento de la tecnología de Quinta Generación (5G) para impulsar a la Industria 4.0 ha marcado un hito significativo en la evolución histórica de las redes celulares. Este desarrollo tiene como objetivo respaldar a las fábricas inteligentes con estrictos requisitos de comunicación, ya que su operatividad se centra en cumplir con los estándares de Calidad de Servicio (QoS), lo que hace que las aplicaciones del Industrial Internet de las cosas (IIoT) sean susceptibles a un rendimiento de red inestable.

Además, estas aplicaciones suelen ocurrir en interiores, donde la alta densidad de obstáculos presenta desafíos adicionales. Estructuras metálicas grandes, robots y vehículos en movimiento obstruyen la propagación de la señal y pueden degradar significativamente el rendimiento de las comunicaciones. El primer modelo de canal estandarizado para fábricas interiores (InF) fue introducido por el Third Generation Partnership Project (3GPP) en la Release 16 para estudiar y abordar estas particularidades ambientales.

Esta tesis se centra en esta base y examina el procedimiento de modelado, identificando limitaciones como la caracterización imprecisa de parámetros y la capacidad limitada para capturar toda la complejidad geométrica de tales entornos.

Preocupado por estas limitaciones, este trabajo da un paso significativo hacia adelante al proponer una nueva tecnología para abordar los desafíos en el modelado industrial. Este enfoque abre la puerta a explorar una de las tendencias emergentes clave en la Sexta Generación (6G) para aplicaciones IIoT: los sistemas de Integrated Sensing and Communications (ISAC). Los sistemas ISAC tienen un gran potencial para superar no solo los desafíos existentes, sino también para introducir mejoras adicionales y valiosas. Dado que ISAC es una tecnología novedosa, aún no se ha diseñado un modelo de canal específico para ella. Para cubrir esta necesidad, esta tesis presenta el desarrollo de un modelo de canal ISAC como un paso fundamental para avanzar en esta tecnología.

Durante dicho avance, se han identificado características fundamentales para construir un modelo de canal ISAC, las cuales suelen ser pasadas por alto en la literatura. En respuesta a esto, este trabajo motiva el desarrollo de directrices técnicas para el modelado ISAC, formando una metodología de evaluación.

Una metodología de evaluación es importante para ISAC o cualquier sistema, ya que es esencial para evaluar el rendimiento y orientar futuras mejoras. Actualmente, no existe una metodología de este tipo para ISAC. Esta

tesis aborda estos desafíos al enfatizar la importancia de considerar las características principales para construir un canal ISAC: correlación entre el canal de sensado y el de comunicación y consistencia espacial.

Basándose en el desarrollo inicial del marco ISAC, el siguiente paso consiste en probar ISAC en entornos cuasi-realistas. Esta tesis presenta un caso de uso industrial que aplica entrenamiento de haz asistido por sensado, demostrando cómo ISAC puede abordar el problema de las múltiples obstrucciones en tales entornos. Específicamente, explora la técnica de sustracción de fondo en un algoritmo de formación de haces predictiva, que aprovecha la información relacionada con el usuario obtenida a través del sensado. Bajo estas consideraciones, los hallazgos indican una mejora sustancial en el rendimiento de la comunicación, particularmente en lo que respecta a la relación señal a ruido (SNR) y la tasa de datos efectiva.

En otras palabras, los resultados destacan el potencial de ISAC para abordar eficazmente las complejidades geométricas del entorno de interés. Esta tesis no solo es pionera en la técnica de sustracción de fondo, sino que también muestra su impacto, allanando el camino para futuras aplicaciones a otros algoritmos de sensado dentro del marco ISAC y la fábrica del futuro.

Resum

L'aprofitament de la tecnologia de Cinquena Generació (5G) per a impulsar la Indústria 4.0 ha marcat un fita significativa en l'evolució històrica de les xarxes cel·lulars. Aquest desenvolupament té com a objectiu donar suport a les fàbriques intel·ligents amb estrictes requisits de comunicació, ja que el seu funcionament depén de complir amb els estàndards de Qualitat de Servei (QoS), cosa que fa que les aplicacions de l'Internet Industrial de les Coses (IIoT) siguen susceptibles a un rendiment de xarxa inestable.

A més, aquestes aplicacions solen produir-se en interiors, on la gran densitat d'obstacles presenta desafiaments addicionals. Grans estructures metàl·liques, robots i vehicles en moviment obstrueixen la propagació del senyal i poden degradar significativament el rendiment de les comunicacions. El primer model de canal estandarditzat per a fàbriques interiors (InF) va ser introduït pel Third Generation Partnership Project (3GPP) en la Release 16 per a estudiar i abordar aquestes particularitats ambientals.

Aquesta tesi es centra en aquesta base i examina el procediment de modelatge, identificant limitacions com ara la caracterització imprecisa dels paràmetres i la capacitat limitada per a captar tota la complexitat geomètrica d'aquests entorns.

Preocupat per aquestes limitacions, aquest treball fa un pas significatiu cap endavant en proposar una nova tecnologia per a abordar els desafiaments en el modelatge industrial. Aquest enfocament obri la porta a explorar una de les tendències emergents clau en la Sisena Generació (6G) per a aplicacions IIoT: els sistemes d'Integrated Sensing and Communications (ISAC). Els sistemes ISAC tenen un gran potencial per a superar no sols els desafiaments existents, sinó també per a introduir millores addicionals i valuoses. Com que ISAC és una tecnologia innovadora, encara no s'ha dissenyat un model de canal específic per a ella. Per a cobrir aquesta necessitat, aquesta tesi presenta el desenvolupament d'un model de canal ISAC com un pas fonamental per a avançar en aquesta tecnologia.

En el marc d'aquest avanç, s'han identificat característiques fonamentals per a construir un model de canal ISAC, les quals solen ser passades per alt en la literatura. En resposta a això, aquest treball motiva el desenvolupament de directrius tècniques per al modelatge ISAC, formant una metodologia d'avaluació.

Una metodologia d'avaluació és important per a ISAC o per a qualsevol sistema, ja que és essencial per avaluar el rendiment i orientar futures millores.

Actualment, no existeix una metodologia d'aquest tipus per a ISAC. Aquesta tesi aborda aquests desafiaments en destacar la importància de considerar les característiques principals per a construir un canal ISAC: correlació entre el canal de sensat i el de comunicació i consistència espacial.

Basant-se en el desenvolupament inicial del marc ISAC, el pas següent consisteix a provar ISAC en entorns quasi-realistes. Aquesta tesi presenta un cas d'ús industrial que aplica un entrenament de feix assistit per sensat, demostrant com ISAC pot abordar el problema de les múltiples obstruccions en aquests entorns. Específicament, explora la tècnica de sostracció de fons en un algoritme de formació de feixos predictiva, que aprofita la informació relacionada amb l'usuari obtinguda a través del sensat. Dins d'aquestes consideracions, les troballes indiquen una millora substancial en el rendiment de la comunicació, particularment pel que fa a la relació senyal-soroll (SNR) i la taxa de dades efectiva.

En altres paraules, els resultats destaquen el potencial d'ISAC per a abordar eficaçment les complexitats geomètriques de l'entorn d'interés. Aquesta tesi no sols és pionera en la tècnica de sostracció de fons, sinó que també mostra el seu impacte, obrint el camí a futures aplicacions en altres algoritmes de sensat dins del marc ISAC i la fàbrica del futur.

Acknowledgements

First of all, my sincerest thanks to the Spanish Ministry of Science, Innovation, and University, which funded this Thesis under Project Grant No. RTI2018-099880-B-C31. Receiving this opportunity in the middle of the pandemic crisis was a light at the end of the tunnel. It was a hard start. However, I am so grateful that I am leveraging this experience as much as I can.

I thank my supervisor, Prof. Jose F. Monserrat, for all his support. I am deeply grateful to the professor for his generous and insightful guidance. His teachings have sown the seeds that inspire me to become the researcher I aspire to be.

An enormous thanks to Prof. Henk Wymeersch for the sharing and technical experience at Chalmers University of Technology. He and his research group made my stay in Gothenburg feel like home. A special thanks to Musa Furkan Keskin for guiding me so well and being patient during my research stay.

Finally, I would like to thank every person I met during this long journey, whether a colleague or not. Thanks to the friends who are still with me and those who are no longer with me. This research work would not be possible without the emotional cushion provided by vitamin people, friends, and, of course, my family.

Andrea Ramos Pillasagua

Table of contents

List of Figures

List of Tables

Acronyms

2D Two Dimensions
1G First Generation
2G Second Generation
3D Three Dimensions
3G Third Generation
3GPP Third Generation Partnership Project
4G Fourth Generation
5G Fifth Generation
6G Sixth Generation
5G-ACIA 5G Alliance for Connected Industries and Automation
AI Artificial Intelligence
AoA Azimuth angle of Arrival
AoD Azimuth angle of Departure
AGV Automatic Guided Vehicle
AWGN additive white Gaussian noise
ASA Angular Spread Azimuth
ASD Angular Spread Departure
ABG alpha-beta-gamma
BS base station
CDF Cumulative Distribution Function
CIR Channel Impulse Response
CSI channel state information
CFAR constant false alarm rate
CRB Cramér–Rao bound
DS delay spread
DFRC Dual-Functional Radar-Communication
eMBB Enhanced Mobile Broadband
FCC Federal Communications Commission
GI Global Illumination
GBSM geometry-based stochastic model

Gbps gigabit-per-second
InH Indoor Hotspot
IMT International Mobile Telecommunications
ISAC Integrated Sensing and Communications
ITU International Telecommunications Union
InF Indoor Factory
InF-SL InF-Sparse Low
InF-DL InF-Dense Low
InF-SH InF-Sparse High
InF-DH InF-Dense High
InF-HH InF-High High
ISD inter-Site Distance
IIoT Industrial Internet of Things
iTEAM Institute of Telecommunications and Multimedia Applications
JCS Joint Communication and Sensing
KPI key performance indicator
KF Kalman Filter
LoS Line of Sight
LSP large-scale parameter
MIMO multiple-input multiple-output
mMIMO massive MIMO
mMTC massive Machine Type Communications
mmW millimeter wave
MPC Multipath Component
MSE Mean Square Error
MISO multiple input single output
MI Mutual Information
NLoS Non Line of Sight
NR New Radio
NGCS Next Generation Communication Systems
OFDM Orthogonal Frequency Division Multiplexing
PAP Power Angular Profile
QoS Quality of Service
RMa Rural Macro-cell
RT ray-tracing
Rx receiver
RCS Radar Cross Section
RSU Road Side Unit
RAN Radio Access Network
RAN1 RAN working group 1
RadCom radar-communication

RMS root mean square
RSRP Reference Signal Received Power
SF shadow fading
SNR signal-to-noise ratio
SHF super high frequency
SC Spatial Consistency
SAC sensing-assisted communications
SMS short messaging system
SSP small-scale parameter
SLAM simultaneous localization and mapping
SUT System Under Test
SINR signal-to-interference plus noise ratio
SIR signal-to-interference ratio
Tx transmitter
TRxP Transmission and reception point
TR Technical Report
Tbps terabit-per-second
TSG Technical Specification Group
UE User Equipment
UL Uplink
UMa Urban Macro-cell
UMi Urban Micro-cell
URLLC Ultra-Reliable and Low Latency Communications
UT User Terminal
UPA Uniform Planar Array
ULA uniform linear array
UPV Universitat Politècnica de València
V2X vehicle-to-anything
V2I vehicle-to-infrastructure
ZoA Zenith angle Of Arrival
ZoD Zenith angle Of Departure
ZSA Zenith spread Arrival
ZSD Zenith spread Departure

Notation

This section describes the notation used in this Thesis.

$\mathbf{A}$ (boldface capital letter) and $\mathbf{A}_k$ represent matrices.
$[\mathbf{A}]_{ij}$ is the element of matrix $\mathbf{A}$ in row i and column j.
$[\mathbf{A}]_{i:}$ represents the i-th row of matrix $\mathbf{A}$.
$[\mathbf{A}]_{:j}$ represents the j-th column of matrix $\mathbf{A}$.
$\mathbf{A}^\top$ denotes the transpose of $\mathbf{A}$.
$\mathbf{A}^*$ denotes the conjugate transpose or Hermitian transpose of $\mathbf{A}$.
$\mathbf{a}$ (boldface lower-case letter) and $\mathbf{a}_k$ represent vectors.
$[\mathbf{a}]_i$ represents the i-th element of vector $\mathbf{a}$.
a and A (not boldface italic letters) represent scalars.

Chapter 1

Introduction

1.1 Background

From a historical perspective, wireless communications first took shape with the advent of the radiotelegraphy system in the late 1890s. This pioneering technology eventually succeeded by what we now recognize as the telegraph and played a pivotal role in shaping the evolution of communication systems. The telegraph was a revolutionary invention worldwide since it brought a new paradigm of operating a system through the propagation of electromagnetic waves. From this invention, several technologies emerged that, many years later, served as a solid foundation for mobile communications. In 1973, the first cellular phone was created, marking an important milestone in the development of mobile communication. Since then, mobile communication has been a driving force in advancing society, satisfying users' needs and Quality of Service (QoS) requirements. With this motivation in mind, several generations of mobile communication have passed through the years.

The progression of mobile communications was initiated with the advent of the First Generation (1G), which relied primarily on analog technology for voice calls. The Second Generation (2G) transitioned to digital transmission technologies, enhancing the QoS for voice calls, which remained the primary service despite the short messaging system (SMS) introduction. Introduced at the turn of the 21st century, the Third Generation (3G) revolutionized the mobile horizon by enabling devices to access the Internet and share multimedia content through a mobile broadband network. Given the rapid evolution of smartphones and the high demand for multimedia services in the 2010s, the Fourth Generation (4G) emerged to overcome the limitation of 3G regarding data rate. This unprecedented service ushered in a new era of connectivity [1].

While the previous generations of mobile communications were historically focused on meeting the needs of individuals, the Fifth Generation (5G) breaks new ground by meeting the needs of interconnected machines and devices [2]. This feature refers to expanding capabilities to Industrial Internet of Things (IIoT) applications within the world of the fourth industrial revolution (Industry 4.0) [3].

The industry has been evolving and growing in parallel with the wireless communications world. Industry encompasses a systematic process in which raw materials are transformed into finished products facilitated by a specific energy source. These products may be destined for a final consumer or as raw materials for another industry. The industry has already gone through three revolutions. The first revolution introduced mechanization, the steam engine, and water power as an energy source, starting with the invention of the power loom in 1784. In 1870, given mass production and depending on electric power, the second revolution emerged with the deployment of the assembly line. The third, the programmable logic controller, revolutionized the industry in 1969, achieving the automation of machines [4].

With the advent of the Internet and the era of digitalization, a paradigm transformed the industrial world. This monumental shift, often termed "Industry 4.0" [5], signifies the integration of advanced technologies to revolutionize and enhance industrial processes for widespread benefits [6]. Within this integration of technologies, the convergence of 5G with Industry 4.0 marks a starting point toward achieving smart factories. This argument is strongly related to the IIoT applications, which enable a more agile and intelligent production environment through the interconnection of devices. In other words, it reflects the goal of seamlessly connecting machines, humans, and data.

To meet the mentioned goal, 5G can provide ultra-low latency and high-reliability communications, which are the main requirements of IIoT applications [7]. 5G enables industrial communication by efficiently allocating resources to meet the specific needs of different applications. This capability makes the network more scalable and can address many use cases.

The International Telecommunications Union (ITU), in the standardization process of International Mobile Telecommunications (IMT)-2020 [8], 5G services have been classified into three main categories, also called usage scenarios: Enhanced Mobile Broadband (eMBB), Ultra-Reliable and Low Latency Communications (URLLC), and massive Machine Type Communications (mMTC). The latter two usage scenarios are tailored for IIoT applications, supporting smart automation in production processes through real-time communication or enabling periodic machine monitoring for efficient smart manufacturing. To provide a visual example, Figure 1.1 illustrates an envisioned industrial scenario operated by 5G networks.

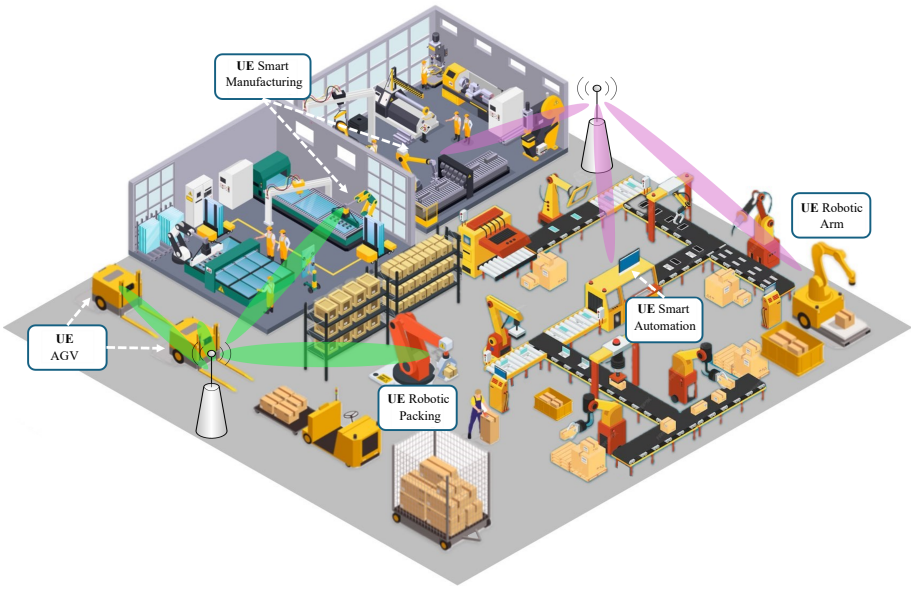

Figure 1.1: Beamforming communication in an industrial environment demonstrates the convergence of 5G technology and Industry 4.0 to create a smart factory

All these advantages and services of the 5G are mainly due to its spectrum, which operates in the mid-band (below 6 GHz) and millimeter wave (mmW) band. The latter band ranges frequencies between 30 - 100 GHz, corresponding with a wavelength range between 10 and 1 mm [9]. Given this range of wavelengths, the high propagation losses at mmW band exhibit increased sensitivity to the absence of Line of Sight (LoS), which can be influenced by obstacles or even fading produced by human presence. On a positive note, this characteristic serves as a subsidiary benefit, allowing communication signals to interact with the surroundings and effectively estimate the localization of objects, users, or machines within the given scenario [10].

In the context of indoor localization, the 5G network (or 5G-positioning) gained special attention since the Federal Communications Commission (FCC) established the location accuracy requirement for emergency calls. Since most wireless calls to 911 originate from indoor environments [11]. Effortlessly ensuring the security of individuals within buildings by locating and tracking them has become a valuable service facilitated by 5G. From the commercial use case

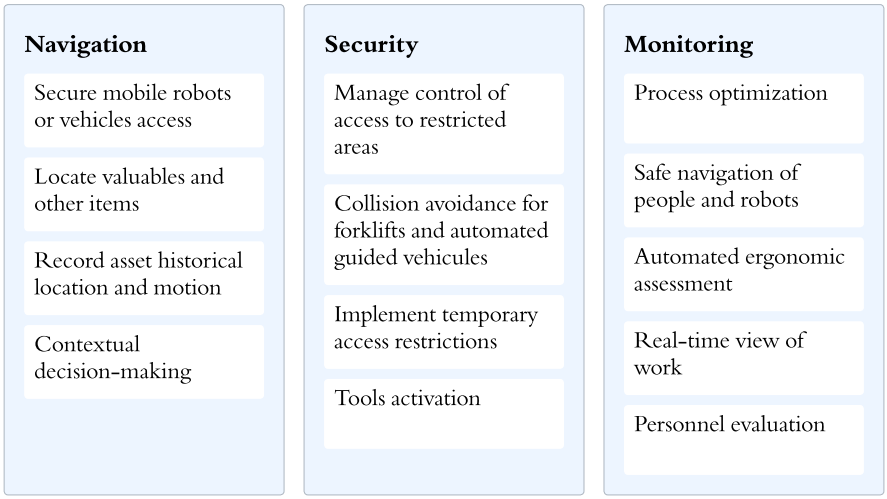

Figure 1.2: Key benefits of industrial localization

standpoint, 5G-positioning has also introduced navigation solutions specifically tailored to locate and track objects within industrial environments.

For instance, Figure 1.2 illustrates the main benefits of positioning in such environments. The first block is related to ensuring accurate navigation of automated robots and tracking of people in large factory warehouses. It can be a valuable resource to aid logistics and thus improve factory efficiency. The second block is the security perspective. The movements of devices or Automatic Guided Vehicle (AGV) in such environments may be dangerous. Without localization, collision accidents inside the factory can occur and endanger employees. The third block is monitoring, where localization can benefit the factory's production evaluation. Hence, localization has become a fundamental aspect of Industry 4.0 [12].

Given this growing interest, New Radio (NR) positioning was introduced in Release 16, where "Release" refers to a specific version of the 3GPP standards. Several mechanisms were presented in Technical Report (TR) 38.855 [13], particularly for industrial use cases promising sub-meter accuracy [14]. Then, in recent years, another advantage of localization has emerged. By knowing a user's or object's precise position, the base station (BS) can better orient the communication link, downlink, or uplink. Positioning could benefit communication techniques such as beamforming [15, 16]. The angle obtained from the

user's position allows for a high degree of direction beamforming, which might optimize the data transmission and improve the signal quality [17].

Despite the technical advancements that have emerged alongside 5G standardization, 5G may still fall short of meeting the demands of 2030 and beyond. Undoubtedly, in the Next Generation Communication Systems (NGCS), detection and localization would be an essential milestone to be included. This context helps readers understand one of the directions of emerging Sixth Generation (6G) trends.

1.2 Literature review

Given the above background, wireless technology analysis is essential for evaluating the performance of different solutions in various use cases, including positioning. Ideally, this analysis could use a pilot 5G network in relevant environments. However, this approach comes with significant costs and disrupts industrial production activities. Since real deployments for these scenarios are not feasible for testing the network [18], network simulations emerge as indispensable tools for evaluating industrial or any scenario. They eliminate the necessity for actual deployments and the consequential expenses, saving time and resources. For this reason, the ITU recommends theoretical channel modeling as an essential milestone for analyzing the behavior of wireless technology in a given scenario [19].

The channel model aims to replicate the electromagnetic propagation from a transmitter (Tx) to a receiver (Rx), where the scenario condition, such as obstacles or free space, can influence the behavior of radio propagation. The channel can provide the physical radio effect that should be considered to establish a communication system. There are two main types of channel modeling: analytical and physical models. The analytical channel model develops a mathematical description based on statistical distributions. In contrast, the physical channel model description is based on electromagnetic propagation properties that consider the environment's geometry. Here, there are three categories of physical models: stochastic models, deterministic models, and geometry-based stochastic models (GBSMs).

Initially, physical models may offer a more precise channel representation for evaluating any given use case. However, in complex environments like industrial scenarios, careful consideration is essential to identify the most suitable channel model for accurate analysis. Therefore, this section provides a comprehensive literature review to orient readers regarding channel models pertinent to such environments, elucidating how novel 6G paradigms contribute to these contexts.

1.2.1 3GPP industrial channel model

The IMT-2020 [8] encourages the radio channels to use a deterministic ray-tracing (RT) generation. Figure 1.3 [8] details this channel model procedure as a Map-based hybrid channel model. This extension allows for accurately studying the propagation condition in a given scenario described entirely by the environment's geometry. This model can include the reflection coefficients of wall and floor materials contributing to channel construction. Even though deterministic modeling provides more realistic results than any propagation channel, using RT algorithms may involve a high computational cost due to the high number of rays and operations needed to simulate a specific scenario or use case. Therefore, flexible channel models are expected to be considered to achieve an evaluation that tests all types of scenarios without computational effort.

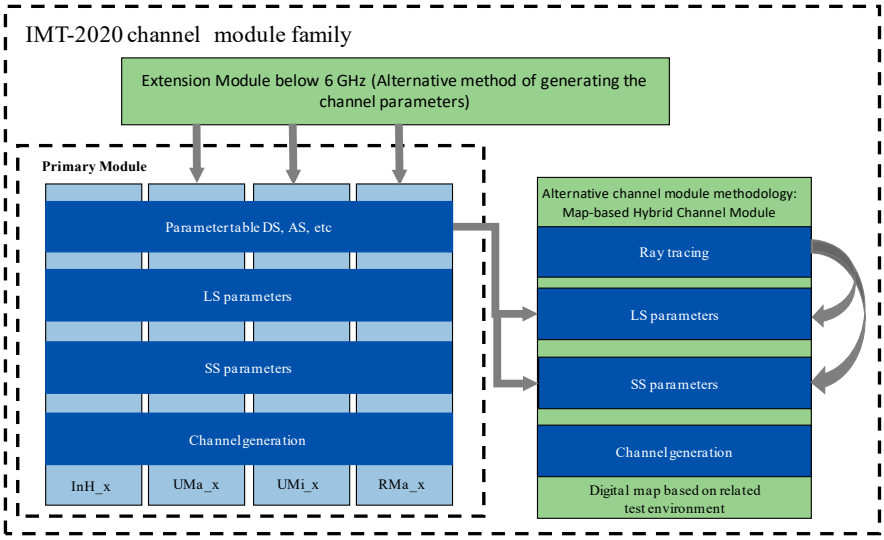

Figure 1.3: IMT-2020 recommended channel models

For instance, the GBSM, the Primary Module of Figure 1.3, might be ideal for geometrically complex scenarios. The characterization of the channel is based on real scenarios by previously performed measurement campaigns. The statistical distributions extracted from these realistic measurements determine every step of this procedure. Probability density functions define the type of communication for each scenario. The large-scale parameters (LSPs) for the

different scenarios are obtained from the antenna's separation and heights. The small-scale parameters (SSPs) refer to generating the output of delay, power, Azimuth angle of Arrival (AoA), Azimuth angle of Departure (AoD), Zenith angle Of Arrival (ZoA), Zenith angle Of Departure (ZoD), and among others information of the Multipath Components (MPCs). Eventually, these previous steps are used to parameterize and construct the channel.

If a brief literature review is performed, many channel models within the GBSM family are currently available, such as the QuaDRiGa channel model defined in [20]. Additionally, those described in European projects such as METIS [21], mmMAGIC [22], or WINNER [23]. Even though these channel models support a wide range of scenarios, i.e., Urban Macro-cell (UMa), Urban Micro-cell (UMi), Rural Macro-cell (RMa), and Indoor Hotspot (InH), only the Third Generation Partnership Project (3GPP) has introduced the study of Indoor Factory (InF) in the TR 38.901 from Release 16 [24] by request from the industry forum 5G Alliance for Connected Industries and Automation (5G-ACIA). The 3GPP channel model is the most widely used for evaluating mobile communication systems from 0.5 to 100 GHz, and NR Positioning (Release 16) recommends it as the basis for evaluation.

To provide a literature review on using the 3GPP channel model in the environment of interest, Table 1.1 describes the few contributions found in these aspects. Some research works, such as [25–31], use this channel model to evaluate and propose new localization methods. Others focus on improving performance for use cases like InF automation or collaborative robots. Finally, a large part is devoted to contributing realistic measurements to tune the parameterization of the current 3GPP-InF channel model.

Use case	**Contribution**	**Existing works**
Localization	Theoretical methods	[25–30]
	Carrier-phase measurements	[31]
Automation	Theoretical methods	[32, 33]
	Network deployment	[34]
Cooperative Robots	Theoretical methods	[35]
Any	Measurement comparison with 3GPP-InF channel model	[36–41]

Table 1.1: Research works that consider the 3GPP channel model for Indoor Factory

This literature review suggests that this channel model is not yet fully exploited. Factory environments are often particularly challenging for capturing

radio propagation properties. They can contain large, tall metal structures, robots, and moving vehicles. Typically, in mmW bands, a large amount of the transmitted signal is through the LoS link. The probability of LoS would be very low in InF. Mechanisms must be provided so that the whole area or all terminal users benefit from communication, even if it is not through direct links. Another noteworthy aspect is that this channel model was published in the last quarter of 2019, just a few months before the global deployment of 5G. Presumably, upcoming native 6G technologies will be able to tackle and delve deeper into this issue.

1.2.2 Integrated Sensing and Communication (ISAC)

In parallel to the previous study, the interest in 6G has gained significant attention since the frame of the 6G research began in 2019. Therefore, since then, numerous proposals for paradigms and enabling technologies have emerged for all areas of mobile communications. The vision and perspective of the 6G was mainly based on enhancing the radio interface.

Recently, the Report M.2516 [42] announced the 6G as the network that encompasses ultra-high data rates with a speed of terabit-per-second (Tbps) since the spectrum resource will operate in sub-THz and THz frequency bands, mainly ranging from around 100 GHz to 3 THz with the approval of FCC.

With the transition to super high frequency (SHF) bands, the advent of 6G opens up opportunities, paving the way for a seamlessly interconnected society (by humans and machines) driven by intelligence.

6G is expected to usher in a new era of connectivity and introduce improvement based on Artificial Intelligence (AI) and sensing technologies, representing the other key trend in this transformation.

In particular, sensing capabilities were initially introduced as a separate technology in the 5G vehicular network, primarily focusing on localization and tracking as in [43]. Over time, this notion evolved and gained strength, leading to a 6G-native technology known as Integrated Sensing and Communications (ISAC). Indeed, in terms of standardization, the ITU has already published novel usage scenarios for 6G in the Recommendation M.2160-0 [44], where ISAC, Ubiquitous Connectivity, and Artificial Intelligence and Communication have been announced as unprecedented usage scenarios. Figure 1.4 [44] illustrates these usage scenarios in blue. The rest are extensions of the previous ones from IMT-2020, of course, in a broader use that requires expanded and new capabilities. These are: eMBB, URLLC, and mMTC, which have become Immersive Communication, Hyper Reliable and Low-Latency Communication, and Massive Communication, respectively.

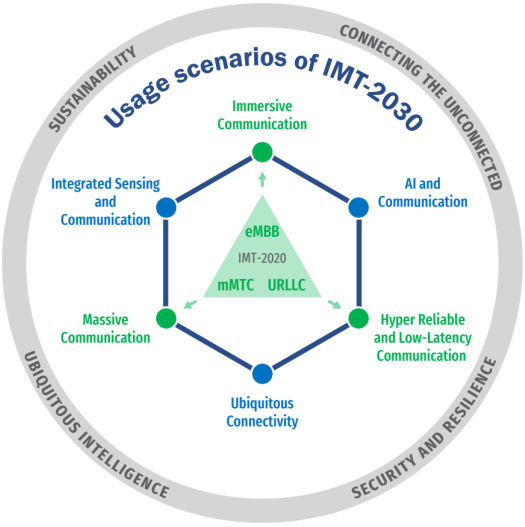

Figure 1.4: Overview of the 6G usage scenarios according to IMT-2030

Delving further into ISAC, it primarily involves the coexistence of sensing and communication capabilities in a single system. This technology will enable the sharing of hardware and spectrum resources of both systems to leverage each other. Since sensing capabilities can provide geometric and spatial information about the scenario, i.e., obstacles and movements of the environment, this novelty has emerged for both sensing-assisted communication and communication-assisted sensing cases. The communication system as a sensor will employ radio waves' transmission, reflection, and scattering to obtain helpful information from the environment, introducing new services such as high-accuracy localization, detection, imaging, and tracking. Using sensing information to improve communication will bring appealing benefits, such as reducing channel estimation resources or optimizing beam management [45].

In the literature, the ISAC framework was officially conceptualized in [46] since, over the years, there have been numerous research papers on the coexistence of radar and communications but never as both integrated into a single hardware architecture. Therefore, the authors emphasized the role of ISAC and defined this single terminology to refer to all systems that in the past were referred to as Dual-Functional Radar-Communication (DFRC), Joint Communication and Sensing (JCS), or radar-communication (RadCom) systems. In [47], the authors provide an extensive technical overview of ISAC, offering its

involvement in some use cases, especially smart factory scenarios. This contribution mentions how ISAC is a leading-edge solution for the smart factory, that in addition to achieving ultra-latency communications, the integration of sensing functionality enables factory users and robots to improve localization and tracking, considering those as indispensable services for efficient production.

Despite these benefits, the most technical ISAC contributions have been tested in vehicular and outdoor scenarios, as exemplified in [48–51]. While the vehicular scenarios are categorized as a "cleaner" environment with fewer obstructions, the industrial scenarios are more complex regarding cluttered environments. There seems to be a need for more attention paid to ISAC in industrial scenarios, which can also benefit from the integration of sensing. For instance, sensing capabilities can be used to obtain previous knowledge of the scenario, including the localization of users and robots. This information might allow an accurate communication beam to be constructed and pointed to the desired target. Given this negligibility, this Thesis offers a first step in evaluating ISAC systems in industrial scenarios.

1.2.3 ISAC channel model

As mentioned in Section 1.2.1, the 3GPP channel model has represented a fundamental tool for evaluating 5G networks. The same notion could be applied to the envisioned 6G networks. Since 6G encompasses emerging technologies, novel techniques must be employed for channel modeling, especially for a prevalent technology such as ISAC, which occurs in IMT-2030 standardization. Developing an ISAC channel model poses challenges, as it entails more than just replicating the propagation radio channel of the sensing and communication system. It also involves incorporating realistic assumptions to simulate the convergence between the two.

While the channel model provided by 3GPP offers propagation characteristics closely aligned with the reality of communication channels, it was not explicitly designed for sensing channel modeling. Nonetheless, it might likely provide valuable insights into generic radio propagation channels. Therefore, it can serve as a solid foundation for modeling sensing channels, ensuring the inclusion of their geometric attributes. The approach will definitely depend on the configuration of the sensing system, whether mono-static or bi-static. The Tx and Rx antennas are collocated in mono-static sensing. In contrast, like the communication system, bi-static sensing involves separating the Tx and Rx antennas.

In the literature, the first steps of evaluating ISAC were focused on signal processing methods, where analytical or discrete channel models have been used [52–54]. Parameters such as AoDs, AoAs, pathloss, or delays have been

generated without considering the geometrical characteristics of the scenario. Given the complexity of sensing functionalities due to the required geometrical accuracy, these channel models do not seem to fit these requirements.

Other studies [55–57] employ RT algorithms to accurately simulate environments for evaluating sensing functionalities, thereby positioning deterministic models as a convenient option for assessing ISAC. However, Section 1.2.1 already discussed the drawbacks of these models. Therefore, there is a clear need to generate affordable and synthetic channel models for consideration in the IMT-2030 standardization, which included the 3GPP channel model in its recommendations.

In [58], the authors introduce an adaptation of the 3GPP channel model to simulate the sensing channel and conduct compressive sensing analysis. However, their focus solely on the sensing channel neglects the correlated communication channel generation and lacks a method for generating both channels simultaneously.

Similarly, in [59], the authors modify the 3GPP channel model, but this time to encompass sensing and communication channel generation. They mention the assumption of channel correlation (between sensing and communication) due to shared scatterers in the scenario but do not comprehensively study why this is a fundamental behavior in ISAC. In addition, they overlook a crucial aspect of the 3GPP model and most GBSMs, namely spatial consistency.

The GBSMs channels have generally been drop-based. A drop still represents the channel impulse response between the Tx and the Rx at a given time. When the network layout has more Rx or the Rx are moving, the physical channel model is generated independently for each moment of motion and each Rx. Moreover, the environment's geometry is not considered, and drop-based models cause a lack of channel consistency among different channel realizations, even for close locations in space with similar Tx-Rx distances.

Spatial consistency or correlation is mandatory to overcome this constraint and obtain matching channels for closely located Rxs or a continuous channel evolution for an Rx moving around a nearby area. Whereas spatial consistency is inherent to deterministic models, since the physical environment is known and this information is used in simulations, drop-based stochastic models must be adjusted.

1.3 Problem and thesis scope

Having reviewed the literature, some problems were identified. First, the industrial scenarios where 5G was introduced were not mature enough regarding channel modeling. Notably, it was not until 2019 that the 3GPP introduced the

channel model for industrial applications in Release 16. This occurred a year ahead of worldwide 5G deployments. In parallel, there was a pressing need to advance toward the 6G framework, directing research efforts towards emerging trends and enabling technologies essential for developing 6G.

Within 6G, ISAC appears promising, where literature suggests its potential to address the limitations of factory environments. Despite its advantages, the ISAC framework has not yet focused on such scenarios and requires further experimentation before standardization. One crucial aspect awaiting completion is establishing a channel model and a methodology for evaluating ISAC. Finally, the sensing capabilities of ISAC might solve the central issue in the factory environment: the cluttered density.

This line of reasoning has given rise to the following hypotheses:

- Hypothesis 1: The emergence of 6G technologies may have caused the 3GPP-InF channel model to not be fully exploited.
- Hypothesis 2: ISAC systems open new paradigms for industrial environments. It is important to develop an ISAC channel model to evaluate it.
- Hypothesis 3: Developing an evaluation methodology gives criteria to assess an ISAC system in any scenario.
- Hypothesis 4: ISAC may potentially meet the industry's needs by leveraging sensing to enhance communication systems.

1.4 Thesis objectives

This Thesis addresses the inherent challenges prevalent in industrial environments, renowned for their complexity within cluttered scenarios. The primary aim is to discern the appropriate system and channel model conducive to evaluating industrial use cases effectively.

The road to achieve this goal may be lengthy. Therefore, initial progress can be achieved by the following partial objectives:

- To comprehensively study the legacy 3GPP channel model in industry scenarios.
- To identify the key factors that the ISAC systems must capture to be suitable for industrial or any scenario.
- To implement a standardizable ISAC channel model.

- To develop an evaluation methodology for the ISAC systems in an industrial environment or any scenario.
- To perform an initial evaluation of an IIoT use case using the ISAC systems.

1.5 Thesis outline

The Thesis is divided into five chapters. The first chapter is related to the introduction, and the last chapter concludes and offers the future lines of the developed work. A brief description of the rest of the chapters is provided below:

Chapter 2 comprehensively studies the 3GPP channel model for indoor factory. The initial motivations that led to the standardization of this model in Release 16 are presented. Furthermore, the channel parameterization is examined in detail, focusing on the specific adjustments made to the 3GPP base model. This study also inspired implementing a calibration process and an in-depth analysis of its limitations.

Chapter 3 introduces a novel ISAC channel model, as ISAC has been identified as the key 6G technology to address the limitations outlined in the previous chapter. This chapter highlights the opportunity to explore this emerging technology from the ground up. The proposed ISAC channel model is evaluated through a comparison with deterministic simulations conducted using the RT tool. Finally, the angular correlation analysis results between communication and detection channels highlight one of the crucial features to be considered in the ISAC channel modeling framework.

Chapter 4 presents an evaluation methodology for the ISAC system. It details the key features that ISAC channel modeling should address, as does the ITU in previous standardizations. A use case is provided as an example to demonstrate the practicality of the proposed methodology. The results from this use case underscore the critical technical criteria that should be considered for ISAC system evaluation.

Chapter 5 introduces an industrial use case centered on sensing-assisted beam training. It addresses the challenge of managing high clutter density in industrial environments by employing background subtraction within a predictive beamforming algorithm. This approach leverages mono-static sensing to enhance communication performance, ensuring a robust communication link for an AGV.

1.6 Thesis publications

The work developed during this Thesis has materialized in the following publications.

Journals

[J1] **A. Ramos** et al., "Evaluation Methodology for 6G Sensing-Assisted Communication System Performance," in IEEE Access, vol. 12, pp. 7841-7852, 2024.

[J2] M. Cantero, S. Inca, **A. Ramos**, M. Fuentes, D. Martín-Sacristán and J. F. Monserrat, "System-Level Performance Evaluation of 5G Use Cases for Industrial Scenarios," in *IEEE Access*, vol. 11, pp. 37778-37789, 2023.

Conferences

[C1] **Ramos, A.**, Keskin, M. F., Wymeersch, H., Inca, S., & Monserrat, J. F. (2024)."Enhancing Sensing-Assisted Communications in Cluttered Indoor Environments Through Background Subtraction," 2024 IEEE Wireless Communications and Networking Conference (WCNC), Dubai, United Arab Emirates, 2024, pp. 1-6

[C2] López-Reche, A., Prado-Alvarez, D., **Ramos, A.**, Inca, S., Monserrat, J. F., Zhang, Y., ... & Chen, Y. (2022, December). "Considering correlation between sensed and communication channels in GBSM for 6G ISAC applications". In *2022 IEEE Globecom Workshops (GC Wkshps)* (pp. 1317-1322). IEEE.

[C3] **Ramos, Andrea**, et al."Implementation and Calibration of the 3GPP Industrial Channel Model for ns-3." Proceedings of the 2022 Workshop on ns-3. 2022.

Chapter 2

Legacy Channel Modeling for Industrial Scenarios

According to the International Telecommunications Union (ITU), link-level simulations can provide a criterion for evaluating and optimizing wireless communication network resources within a given scenario [8]. The ITU defines it as a method to study the performance between the base station (BS) and the User Equipment (UE) under specific channel conditions. The channel is the medium through which the transmitted signal propagates between these two network elements, accounting for all the obstacles and environmental factors affecting the signal propagation.

In the case of industrial environments, modeling the channel can be challenging due to the multiple propagation components resulting from high reflection, diffraction, or absorption caused by the presence of metallic structures, walls, and machinery. The effects above vary significantly between Indoor Factory (InF) and other scenarios. As an initial approach, the Third Generation Partnership Project (3GPP) introduced a channel model for InF scenarios in Release 16, marking one of the first channel models designed exclusively for such environments.

Despite the considerable standardization efforts that have been undertaken, further exploration of these scenarios is necessary, primarily since the related Release 16 for Fifth Generation (5G) in factories was published in 2019, coinciding with the start of studies for Sixth Generation (6G). This trend suggests that the new 6G is gaining prominence even as the potential of an existing one, i.e., 5G remains under-exploited. Given this context, it is essential to begin this Thesis by examining how 3GPP approaches channel modeling in industrial

scenarios. This study is due to the necessity of thorough exploration to ensure effective implementation in factory use cases.

This chapter comprehensively examines the InF channel model from the 3GPP, covering the initial administrative steps for inclusion in standardization to the modeling process and calibration results. Furthermore, the model's limitations are discussed, drawing on insights from this Thesis and existing literature.

2.1 Toward Release 16

The 3GPP included the Indoor Hotspot (InH) channel model under the Technical Report (TR) 38.901 in Release 14 [60]. This environment was then the only representation for indoor scenarios. The InH channel model represents an office environment classified into Mixed Office and Open Office. The Mixed Office is related to cubicle areas, walled offices, and corridors, while the Open Office mainly comprises more open spaces.

Even though the Mixed Office environment has more obstructions, it lacks the complex features of industrial environments. Unlike offices, industrial scenarios have unique obstacles, such as many machines and metal structures directly affecting the propagation. Therefore, a channel model designed explicitly for factories is needed to accurately emulate these complexities to meet the Industrial Internet of Things (IIoT) application requirements outlined in the previous chapter. The 3GPP has been one of the first to publish an industrial channel model in Release 15 of TR 38.901 [61].

The logistics process for the standardization of the industrial channel model started with a new study item requested by the industry forum 5G Alliance for Connected Industries and Automation (5G-ACIA). The 5G-ACIA is an organization dedicated to ensuring that the specific interests of the industrial sector are appropriately considered in the 5G standardization. This request occurred at the 3GPP-Technical Specification Group (TSG) of Radio Access Network (RAN) #81 meeting [62]. Then, the standardization process was carried out by 3GPP RAN working group 1 (RAN1) [63], which is the technical body in charge of the physical layer specification.

RAN1 began the discussion in November 2018 at the RAN1 #95 meeting to model the features needing modification. During 2019, at the RAN #96, #96b, and #97 meetings, the electromagnetic interference and network layout, frequency bands, and reclassification for each sub-scenario of the measurement results were established, respectively. Finally, the channel model of the InF scenarios was fully established at the RAN #98 meetings and delivered in Release-16 of the TR 38.901 [24].

All changes in the version above are mainly oriented to the InF channel model. These modifications included new features regarding the scenario description and channel parametrization. This will be further detailed in the following sections.

2.2 3GPP channel generation procedure

This section overviews the modifications performed in TR 38.901 to include InF scenarios. Figure 2.1 illustrates the conventional channel generation procedure, comprising three key segments: general parameters, large-scale parameters (LSPs), small-scale parameters (SSPs), and coefficient generation.

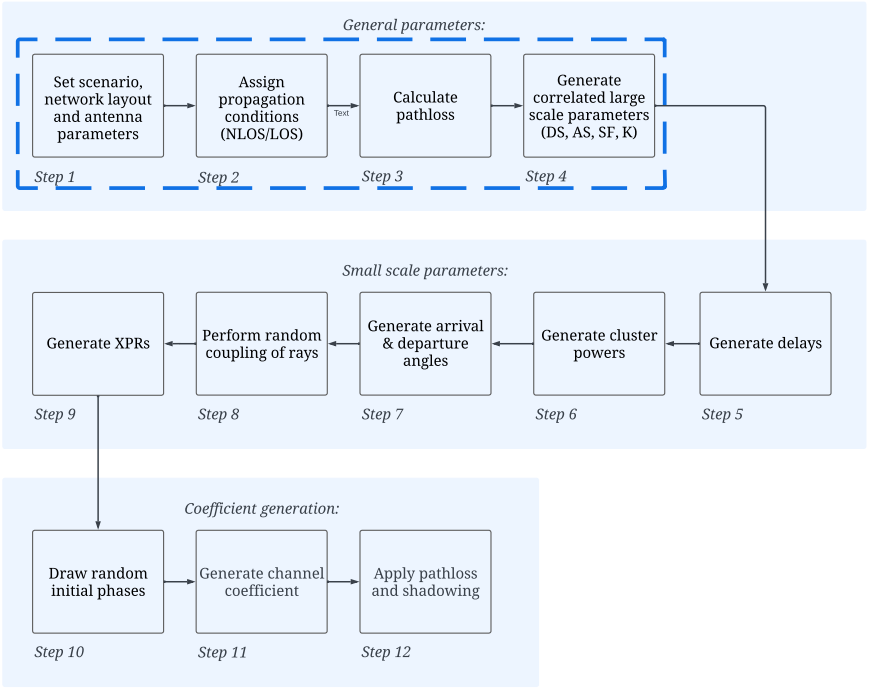

Figure 2.1: 3GPP conventional channel generation procedure of the TR 38.901

The initial segment is intricately linked to the overall parametrization of the channel within the designated scenario. In addition to InF, 3GPP also

encompasses the following scenarios: Urban Macro-cell (UMa), Urban Micro-cell (UMi), Rural Macro-cell (RMa), and InH.

Subsequent segments remain the same for all scenarios. Hence, the changes pertinent to the InF scenario primarily manifest in the initial steps, marked by blue dashed lines in Figure 2.1. The clarity of the scenario description (Step 1) holds paramount importance as it profoundly influences the interpretation of the subsequent steps.

2.2.1 Environment description

At the beginning of this chapter, it was mentioned that the industrial scenario encompasses a variety of environments, such as warehouses, manufacturing plants, assembly halls, and production areas. In these scenarios, the propagation of wireless communication signals is subject to frequency fading, induced by specular reflections from metallic structures and obstruction by machinery and personnel. Numerous obstructions render this scenario particularly intricate and complex to model accurately. Consequently, 3GPP has established a sub-classification to address the complexity inherent in such environments. This results in four Non Line of Sight (NLoS) sub-scenarios and a Line of Sight (LoS) sub-scenario. NLoS sub-scenarios refer to environments that have low LoS probability; these are InF-Sparse Low (InF-SL), InF-Dense Low (InF-DL), InF-Sparse High (InF-SH), and InF-Dense High (InF-DH), which are illustrated in Figure 2.2.

Clutter density and antenna height are the main criteria for classifying the four NLoS sub-scenarios. The terms “Sparse” and “Dense” determined the clutter density, referring to the quantity of machinery and other objects in the room. For instance, InF-SL and InF-SH (Figures 2.2a and 2.2c [64]) have sparse clutter, i.e., less obstruction in the scenario. In contrast, the InF-DL and InF-DH (Figures 2.2b and 2.2d [64]) have high clutter density. The clutter density parameter can vary according to the values in Table 2.1. This depends on the desired percentage of clutter that can be added to the scenario.

On the other hand, the terms “High” and “Low” define the height of the antennas of the BS. For instance, InF-SH and InF-DH should have the antennas BS above the height of obstacles or clutter. Unlike the InF-SL and InF-DL, the antennas are below the clutter. In addition, the height of the BS antennas can also vary as long as they achieve the condition of being below or above the clutter, as described in Table 2.1. Meanwhile, in all four NLoS sub-scenarios, the UE antennas are below the clutter.

Other parameters, such as ceiling height, room size, and effective clutter height, are shown in Table 2.1 for setting up the network layout. The latter is the average height of objects placed in the environment. Moreover, the distance

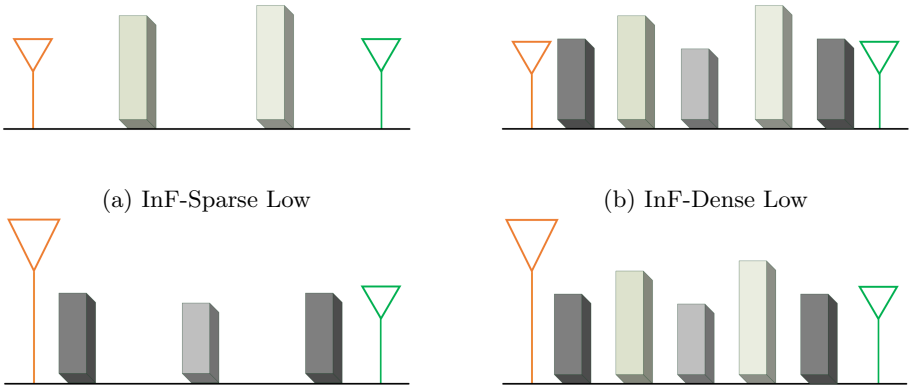

(a) InF-Sparse Low

(b) InF-Dense Low

(c) InF-Sparse High

(d) InF-Dense High

Figure 2.2: NLoS sub-scenarios definition. The orange antennas represent the BSs and the green one the UEs

typical clutter size is average and varies with the clutter density. Naturally, the mentioned geometric description significantly influences the channel condition, determining whether the UE is in LoS or not in each time instant.

Finally, the InF-High High (InF-HH) scenario represents a sub-scenario characterized by favorable geometric conditions. Here, the BS maintains 100% LoS probability because its antennas and those of the UE are located above the clutter. This configuration establishes an unobstructed communication link.

	Parameters	**Indoor factory sub-scenarios**				
		InF-SL	**InF-DL**	**InF-SH**	**InF-DH**	**InF-HH**
Layout	Room size	Rectangular: 20-160000 m^2				
	Ceiling height	5-25 m	5-15 m	5-25 m	5-15 m	5-25 m
	Effective clutter height	Ceiling height, 0-10 m				
Test environment	Distance typical clutter size	10 m	2 m	10 m	2 m	Any
	Clutter density	$\leq$ 40 %	$\geq$ 40%	$\leq$ 40%	$\geq$ 40%	Any
	BS	Below clutter		Above clutter		Above clutter
	UE condition	LoS and NLoS				100% LoS
	UE height	Below clutter				Above clutter

Table 2.1: Geometric description for Indoor Factory according to TR 38.901

2.2.2 Propagation condition

As mentioned in the previous section, the clutter density directly affects the channel condition. Therefore, new probability models must be designed within the channel modeling procedure. The 3GPP LoS probability determines whether receiver (Rx) nodes' positions are in LoS or NLoS conditions at a given distance. Consequently, either of these selected propagation conditions will define the channel state that will later be an important input for generating the large-scale parameters, small-scale parameters, and channel coefficients (Figure 2.1). Hence, the 3GPP recommends the probability function adapted for each NLoS sub-scenario, which is defined as

$$\mathrm{Pr}_{\mathrm{LOS,subsce}}(d_{\mathrm{2D}}) = e^{-\left(\frac{d_{\mathrm{2D}}}{k_{\mathrm{subsce}}}\right)}, \tag{2.1}$$

where d_{2D} is the 2D-distance between UE and BS, and k_{subsce} is a constant determined for each NLoS sub-scenario, This is expressed as

$$k_{\mathrm{subsce}} = \begin{cases} -\dfrac{d_{\mathrm{clutter}}}{\ln(1-r)} & \text{for InF-SL, InF-DL} \\ -\dfrac{d_{\mathrm{clutter}}}{\ln(1-r)}\dfrac{h_{\mathrm{BS}}-h_{\mathrm{UE}}}{h_{\mathrm{c}}-h_{\mathrm{UE}}} & \text{for InF-SH, InF-DH,} \end{cases} \tag{2.2}$$

where d_{clutter} is clutter distance, r is clutter density, h_{c} is effective clutter height, h_{BS} is BS height, and h_{UE} is UE height. Note that Table 2.1 details the value of mentioned notations.

To provide a better understanding, Figure 2.3 [64] illustrates the LoS probability function in (2.1) according to the clutter density and the 3D-distance. Considering both heights, the latter is the distance between the BS and UE. The LoS probability is represented by the range 0 to 1, where yellow is the lowest probability and blue is the highest. According to 3GPP specifications in Table 2.1, the part above the 0.4 clutter density in Figure 2.3 corresponds to Dense sub-scenarios. In contrast, the part below 0.4 corresponds to Sparse sub-scenarios.

In addition, it can be seen how the LoS probability decreases if the 3D-distance or the clutter density increases, as in (2.1) describes. The sub-scenarios with higher antennas (i.e., InF-SH and InF-DH) have higher LoS probability than those with lower antennas (i.e., InF-SL and InF-DL).

This reasoning solidifies the theory that the 3GPP LoS probability model is custom-designed to suit the geometrical conditions of each NLoS sub-scenario. Meanwhile, the probability model for InF-HH has been omitted, given the 100% LoS probability in this sub-scenario.

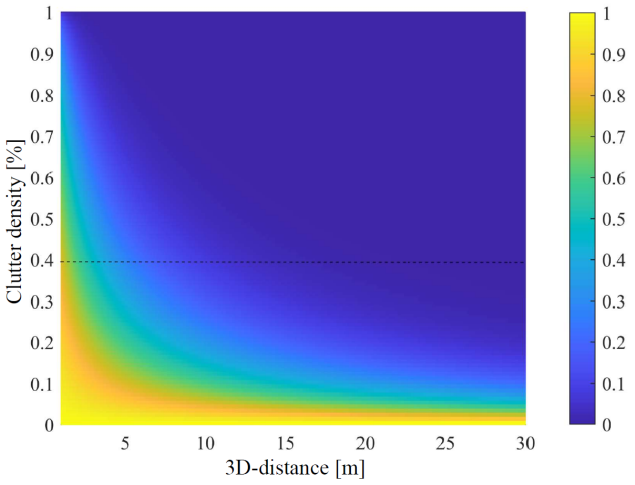

(a) InF-SH and InF-DH

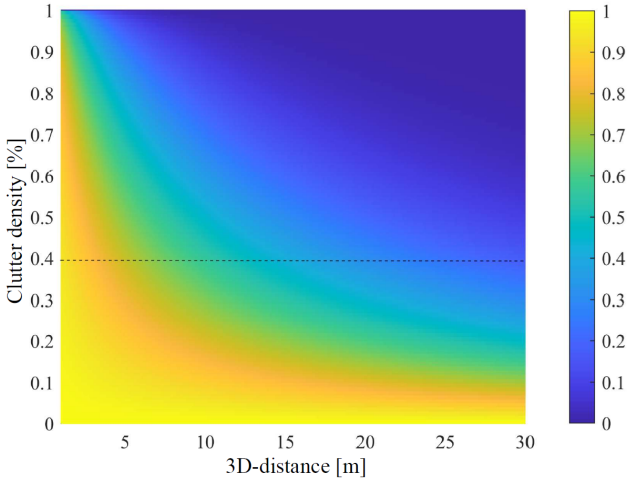

(b) InF-SL and InF-DL

Figure 2.3: LoS Probability by varying the k_{subsce} according to (2.2)

2.2.3 Pathloss generation

According to the 3GPP channel modeling procedure (Figure 2.1), the next step is the pathloss calculation. The 3GPP TR 38.901 uses alpha-beta-gamma (ABG) model

$$PL^{\mathrm{ABG}}(f_c, d_{3D}) = 10 \cdot \alpha \cdot \log_{10}(d_{3D}) + \beta + 10 \cdot \gamma \cdot \log_{10}(f_c) + X_\sigma, \quad (2.3)$$

where α is the pathloss exponent representing the degradation of the signal with the distance, β is an intercept parameter, and the exponent frequency-dependent is γ, reflecting how the frequencies affect pathloss. The symbol X_σ represents the shadow fading (SF), constructed by a normal distribution with zero mean, given by a standard deviation of σ. The symbol $d_{3\mathrm{D}}$ is the 3D-distance in meters, and fc denotes the center frequency in GHz.

The ABG model emulates the attenuation of electromagnetic waves propagating through space, especially for millimeter wave (mmW) and sub-6 GHz frequencies. The 3GPP considers this model valuable to represent the signal degradation caused by metallic structures, walls, or machinery in industrial environments. Therefore, the following are modeled particularly for each sub-scenario of InF. First, it is necessary to previously know the channel condition since the 3GPP has proposed different pathloss models for LoS and NLoS conditions.

When a high percentage of LoS probability is obtained, the pathloss model for all sub-scenarios is given by:

$$PL_{\mathrm{LOS}}(f_c, d_{3D}) = 31.84 + 21.50 \log_{10}(d_{3D}) + 19 \log_{10}(f_c), \;\; \sigma_{\mathrm{LOS}} = 4.3. \quad (2.4)$$

Otherwise, when LoS probability is affected by the clutter density and antenna height, the following pathloss models are given for the NLoS condition as a function of each sub-scenario.

- NLoS condition for InF-SL:

$$PL_{\mathrm{SL}}(f_c, d_{3D}) = 33.00 + 25.50 \log_{10}(d_{3D}) + 20 \log_{10}(f_c), \;\; \sigma_{\mathrm{SL}} = 5.7 \quad (2.5)$$

$$PL_{\mathrm{NLOS}} = \max(PL_{\mathrm{SL}}, PL_{\mathrm{LOS}}) \quad (2.6)$$

- NLoS condition for InF-DL:

$$PL_{\mathrm{DL}}(f_c, d_{3D}) = 18.6 + 35.70 \log_{10}(d_{3D}) + 20 \log_{10}(f_c), \;\; \sigma_{\mathrm{DL}} = 7.2 \quad (2.7)$$

$$PL_{\mathrm{NLOS}} = \max(PL_{\mathrm{DL}}, PL_{\mathrm{LOS}}, PL_{\mathrm{SL}}) \tag{2.8}$$

- NLoS condition for InF-SH:

$$PL_{\mathrm{SH}}(f_c, d_{3D}) = 32.40 + 23.00\log_{10}(d_{3D}) + 20\log_{10}(f_c), \quad \sigma_{\mathrm{SH}} = 5.9 \tag{2.9}$$

$$PL_{\mathrm{NLOS}} = \max(PL_{\mathrm{SH}}, PL_{\mathrm{LOS}}) \tag{2.10}$$

- NLoS condition for InF-DH:

$$PL_{\mathrm{DH}}(f_c, d_{3D}) = 33.63 + 21.9\log_{10}(d_{3D}) + 20\log_{10}(f_c), \quad \sigma_{\mathrm{DH}} = 4.0 \tag{2.11}$$

$$PL_{\mathrm{NLOS}} = \max(PL_{\mathrm{DH}}, PL_{\mathrm{LOS}}) \tag{2.12}$$

The above pathloss models are tested by considering several simulation seeds for each sub-scenario to offer readers a more comprehensive understanding. The UE is placed at a 3D-distance ranging from 0 to 60 meters in the high band frequency (30 GHz), where mobility has not been considered.

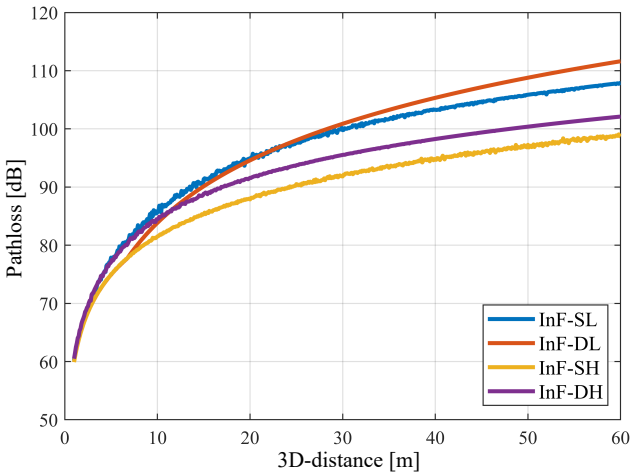

Figure 2.4: Pathloss models performance for each NLoS sub-scenario

Figure 2.4 [64] shows the average pathloss, where it can be noted that as the 3D-distance increases, the pathloss levels worsen significantly for all sub-scenarios. The impact of LoS probability on the pathloss behavior at some 3D distance can be reflected, with InF-DL being the worst case and InF-SH being the best case. In addition to the clutter density percentage, antenna height plays an essential role in the channel conditions through the pathloss.

2.2.4 Large-scale parameters

The LSPs involve statistical properties to emulate realistic propagation conditions. The 3GPP has published these parameters obtained by physical measurements. The LSPs depend on the scenario of interest. Therefore, Table 7.5-6 Part-3 of the TR 38.901 [65] incorporates new values of Ricean K-factor, root mean square (RMS) delay spread (DS), Angular Spread Azimuth (ASA), Angular Spread Departure (ASD), Zenith spread Arrival (ZSA) and Zenith spread Departure (ZSD) for the new InF scenario.

The DS measures a mobile communications channel's Multipath Component (MPC) profile. It is generally defined as the difference between the time of arrival of the earliest component, e.g., the LoS component if there exists, and the time of arrival of the latest MPC. During the DS modeling, the 3GPP had four candidate models: Distance-dependent model, antenna-dependent model, frequency-dependent model, and volume-dependent model. The distance-dependent model using the 2D-distance might not fit because the DS can change with antenna height [66, 67]. The antenna-dependent model was discarded due to insufficient research support [3]. Finally, the frequency-dependent model is used for conventional indoor scenarios (like InH). Still, InF cannot be comparable with this latter since in [68], the authors realized the DS does not change with the frequency.

Given the complexity of the channel and many reflective elements, they decided on the volume-dependent model and the total surface area. The expression of DS is detailed in Table 2.2, which follows a normal distribution, and the mean depends on both LoS and NLoS conditions. The symbol V is the volume in m^3, and S is the total surface area of each sub-scenario in m^2. As the room size of each sub-scenario is different, the floor, walls, and ceiling are the primary inputs to obtain V/S. In this way, V/S changes according to the parameters of scenarios defined in Table 2.1.

On the other hand, the angular spread encompasses ASD, ASA, ZSD, and ZSA, representing the propagation channel's spatial features in a multiple-input multiple-output (MIMO) system. The hall's volume affects the angular spread, mainly for ASA, which increases based on the distance. Table 2.2 summarizes the models for obtaining the mentioned LSPs. It is important to emphasize

Scenarios		Indoor Factory	
		LoS	NLoS
Delay spread (DS) lgDS = $\log_{10}$(DS/1s)	μ_{lgDS}	$\log_{10}(26(\frac{V}{S})+14)-9.35$	$\log_{10}(30(\frac{V}{S})+32)-9.44$
	σ_{lgDS}	0.15	0.19
AOD spread (ASD) lgASD = $\log_{10}$(ASD/1°)	μ_{lgASD}	1.56	1,57
	σ_{lgASD}	0.25	0.2
AOA spread (ASA) lgASA = $\log_{10}$(ASA/1°)	μ_{lgASA}	$-0.18\log_{10}(1+fc)+1.78$	1.72
	σ_{lgASA}	$0.12\log_{10}(1+fc)+0.2$	0.3
ZOA spread (ZSA) lgZSA = $\log_{10}$(ZSA/1°)	μ_{lgZSA}	$-0.2\log_{10}(1+fc)+1.5$	$-0.13\log_{10}(1+fc)+1.45$
	σ_{lgZSA}	0.35	0.45
ZOD spread (ZSD) lgZSD = $\log_{10}$(ZSD/1°)	μ_{lgZSD}	1.35	1.2
	σ_{lgZSD}	0.35	0.55
K-factor (K) [dB]	μ_{K}	7	N/A
	σ_{K}	8	N/A

Table 2.2: Large-scale parameters of Indoor Factory under the LoS and NLoS channel condition

that these parameters do not depend on the type of sub-scenario explained in the previous section.

2.2.5 Small-scale parameters

The LSPs explained in the previous section are used as input to determine the SSPs. The small-scale fading model characterizes the MPCs (also called rays by the 3GPP) that the UE or Rx experiences at a given spatial position by generating clusters. Each cluster contains a specific number of paths or rays. Thus, SSPs define the delay, power, and cluster angles in both azimuth and elevation. A simplified representation of these parameters is shown in Figure 2.5, illustrating a cluster as an example. The number of clusters (N) and rays (M) depend on the type of scenario. In the case of InF, 25 and 20 are the values of N and M, respectively.

Following Figure 2.1, the SSPs are entirely generated from Step 5 to Step 9. Nevertheless, this Section pretends to highlight the changes inherited from the LSPs affect each SSP step, which are summarized in Table 2.3 and further explained below:

- **Cluster delays (Step 5):** The DS value is the input to generate the cluster delays. First, the exponential distribution of τ_n' is determined, where r_τ is the proportionality factor of the delay distribution, $X_n \sim$ uniform (0,1) for each cluster index $n = 1, ..., N$. An additional process is introduced in the case of the LoS condition. Scaling of delays is required to compensate for the effect of LoS peak besides the delay spread. The

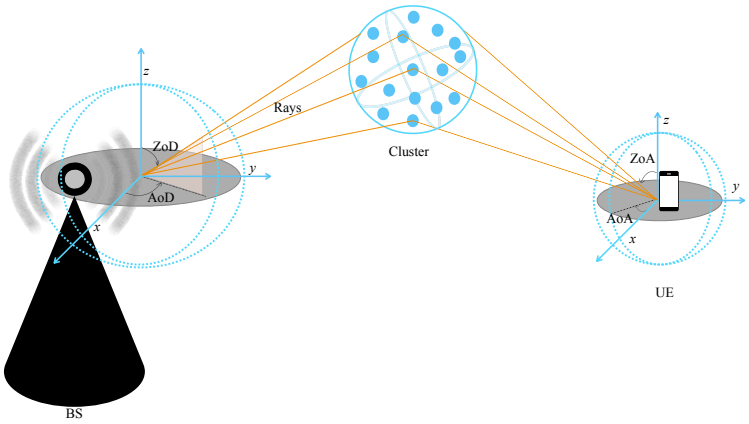

Figure 2.5: Geometric definition of small-scale parameters in the 3GPP TR-38.901

heuristically determined Ricean K-factor (K) dependent scaling constant is C_τ. The K[dB] is generated in step 4. Finally, the delays are generated by the expression of item 3 and for NLoS by item 2 in Table 2.3.

- **Cluster powers (Step 6):** They also change their distributions since their primary input is the previously generated cluster delays (τ_n). Here, the exponential delay distribution (P'_n) for cluster powers can be obtained based on a single-slope exponential power delay profile. In Table 2.3, The $Z_n \sim N(0, \zeta^2)$ is the shadowing term per cluster in [dB]. Using the scaled delays is unnecessary in the case of the LoS condition. Therefore, only for this process $C_\tau = 1$ from τ_n. Finally, item 2 defines the cluster powers by P_n for the conditions of both LoS and NLoS.

  Item 3 generates cluster powers that will only be used to create cluster angles (Step 7). These special cluster powers are denoted as $\bar{P}_n$. In the case of the LoS condition, an additional component is considered only for the first cluster ($P_{1,\mathrm{LoS}}$), where the K_R is the Ricean K-factor generated on a linear scale. In the NLoS conditions, the $\bar{P}_n$ procedure is the same as for cluster powers generation.

  From this point, all generations of cluster delay, cluster powers, and cluster angles powers are removed with the condition of -25 dB power compared to the maximum cluster power from P_n. Only the most potent clusters are retained.

- **Cluster AoDs and AoAs (Step 7):** The generation of Azimuth angle of Arrival (AoA) and Azimuth angle of Departure (AoD) follow the same procedure detailed below:

  1. The input to obtain the inverse Gaussian function (ϕ'_n) is RMS angle spread detonated as AS in Table 2.3. The AS represents the values of ASA for AoA or ASD for AoD obtained from LSPs. The C'_ϕ is the scaling factor for the azimuth angle generation, and its constant values depend on the number of clusters. These are detailed in Table 7.5-2 of TR 38.901.
  2. The generation of AoD or AoA (ϕ_n) is given by item 2 in Table 2.3. X_n is a random variable with uniform distribution to the discrete set of $\{1, -1\}$, and the component of $Y_n \sim N(0, (\text{AS}/7)^2)$ that introduces random variation. Here, the AS value could be ASA or ASD. In the LoS case, the first cluster of each element (X_1, Y_1, ϕ'_1) is enforced to the LoS direction. Finally, the ϕ_{LoS} is defined as the LoS direction, in other words, the true AoD or AoA obtained by geometry calculation.
  3. Item 3 in Table 2.3 provides the azimuth angles for each ray m within the cluster n. For this, the input parameters are the cluster azimuth angles ϕ_n and the c_{AS}, which is the cluster-wise RMS azimuth spread (ASA or ASD). Then, the α_m is the ray offset angles within a cluster, where Table 7.5-3 of the TR 38.901 provides the values.

- **Cluster ZoAs (Step 7):** The generation of Zenith angle Of Departure (ZoD) or Zenith angle Of Arrival (ZoA) assumes the composite PAS in the zenith dimension of all clusters is Laplacian. Hence, first, the ZoA generation follows the next procedure:

  1. Expression of item 1 in Table 2.3 represents the inverse Laplacian function, where ZS represents the RMS angle spread ZSA or ZSD, depending on the zenith angle to be calculated. The C'_θ is the scaling factor for zenith angle generation, depending on the number of clusters considered. Table 7.5-2 of the TR 38.901 details these constants' values.
  2. Only cluster ZoA generation follows a similar procedure to AoD or AoA, except the component $Y_n \sim N(0, (\text{ZSA}/7)^2)$. The θ_{LoS} is defined as the ZoA LoS direction
  3. Finally, the rays of ZoA within the clusters are obtained from the input parameters of c_{ZSA} and the α_m, where the offset angle values are provided by Table 7.5-3 of the TR 38.901.

SSPs	LoS	NLoS
Delays	1) $\tau_n' = r_\tau \mathrm{DS} \ln(X_n)$ 2) $C_\tau = 0.7705 - 0.0433K$ $+0.0002K^2 + 0.000017K^3$ 3) $\tau_n = \frac{\mathrm{sort}(\tau_n' - \min(\tau_n'))}{C_\tau}$	1) $\tau_n' = r_\tau \mathrm{DS} \ln(X_n)$ 2) $\tau_n = \mathrm{sort}(\tau_n' - \min(\tau_n'))$
Powers	1) $P_n' = \exp(-\tau_n \frac{r_\tau - 1}{r_\tau \mathrm{DS}}) \cdot 10^{\frac{-\mathrm{Z}_n}{10}}$ 2) $P_n = \frac{P_n'}{\sum_{n=1}^{N} P_n'}$	
	3) $\bar{P}_n = \frac{1}{K_R+1} P_n + \delta(n-1) P_{1,\mathrm{LoS}}$, where $P_{1,\mathrm{LoS}} = \frac{K_R}{(K_R+1)}$	3) $\bar{P}_n = P_n$
AoDs/ AoAs	1) $\phi_n' = \frac{2(\mathrm{AS}/1.4\sqrt{-\ln(\bar{P}_n / \max(\bar{P}_n))})}{C_\phi}$	
	where $C_\phi = C_\phi' \cdot (1.1035 - 0.028K$ $-0.002K^2 + 0.0001K^3)$ 2) $\phi_n = (X_n \phi_n' + Y_n) - (X_1 \phi_1'$ $+Y_1 - \phi_{\mathrm{LoS}})$	where $C_\phi = C_\phi'$ 2) $\phi_n = X_n \phi_n' + Y_n + \phi_{\mathrm{LoS}}$
	3) $\phi_{n,m} = \phi_n + C_{\mathrm{AS}} \alpha_m$	
ZoAs	1) $\theta_n' = \frac{\mathrm{ZS} \ln(\bar{P}_n / \max(\bar{P}_n))}{C_\theta}$	
	where $C_\theta = C_\theta' \cdot (1.3086 + 0.0339K$ $-0.0077K^2 + 0.0002K^3)$ 2) $\theta_n = (X_n \theta_n' + Y_n) + (X_1 \theta_1'$ $+Y_n - \theta_{\mathrm{LoS}})$	where $C_\theta = C_\theta'$ 2) $\theta_n = X_n \theta_n' + Y_n + \theta_{\mathrm{LoS}}$
	3) $\theta_{n,m} = \theta_n + C_{\mathrm{ZS}} \alpha_m$	
ZoDs	2) $\theta_n = (X_n \theta_n' + Y_n) + (X_1 \theta_1'$ $+Y_n - \theta_{\mathrm{LoS}})$	2) $\theta_{n,ZoD} = X_n \theta_n' + Y_n$ $+\theta_{\mathrm{LoS}} + \mu_{\mathrm{offset,ZoD}}$
	3) $\theta_{n,m,ZoD} = \theta_{n,ZoA} + (3/8)(10^{\mu_{\mathrm{lgZSD}}} \alpha_m)$	

Table 2.3: Small-scale parameters affected by the changes of Indoor Factory channel modeling

- **Cluster ZoDs (Step 7):** The expression of item 1 in Table 2.3 of the generation of ZoA is the same as generating ZoD. Then, an additional offset is added to create the n cluster ZoD generation. The $\mu_{\text{offset,ZoD}}$ is given by the Table 7.5-6,7,8 of the 38.901. The component $Y_n \sim N(0, (\text{ZSD}/7)^2)$, and θ_{LoS} is defined as the ZoD LoS direction.

  Finally, the rays of ZoD within the clusters follow the expression of item 3 in Table 2.3, where μ_{lgZSD} is the mean of the ZSD log-normal distribution, and Table 7.5-3 of the TR 38.901 provides the α_m values.

The ray angles from Step 7 are randomly coupled between AoDs-AoAs and ZoDs-ZoAs in Step 8. In Step 9, the cross-polarization power ratios are generated, which, according to 3GPP Table 7.5-6, is a log-normal distribution with a standard deviation of 12 for LoS and 11 for NLoS, with a mean value of 6 for both conditions. These steps have been significant for generating the following channel coefficients procedure, which remains unchanged to obtain the InF channel matrix (see Figure 2.1).

2.3 Calibration procedure

The 3GPP recommends that channel models undergo a calibration process during implementation. This Thesis adheres to this guideline, and this section details the process to provide a complete understanding of the model. Firstly, the simulation scenarios should follow the 3GPP specifications, including the scenario layout, antenna configuration, and communication parameters for any propagation sub-scenarios, i.e., InF-SL, InF-DL, InF-SH, or InF-DH.

A total of 180 User Terminals (UTs) uniformly distributed and 18 BSs based on inter-Site Distance (ISD) of the respective sub-scenarios have been deployed. All users in the mapped area are attached to the BS server based on the best pathloss. All these configurations are detailed in Table 2.4 and have been implemented in the ns-3 simulator [69]. The InF channel model has been developed as a new module in the mentioned simulator and published in [70].

Several key performance indicators (KPIs) have been covered for link-level simulations: Coupling loss, Geometry with noise, Geometry without noise, and Delay spread. These KPIs are compared with results from the simulation campaigns of companies like Ericsson, ZTE, Huawei, and Nokia. The 3GPP has made these benchmark results publicly available in the document R1-1909704 [71]. The performance metrics should align closely with the benchmarks to validate the calibration, demonstrating similar trends.

Even though both 3.5 and 28 GHz frequency bands have been simulated, as established in Table 2.4, this section shows only those results obtained at

Parameters	Value
BS Deployment	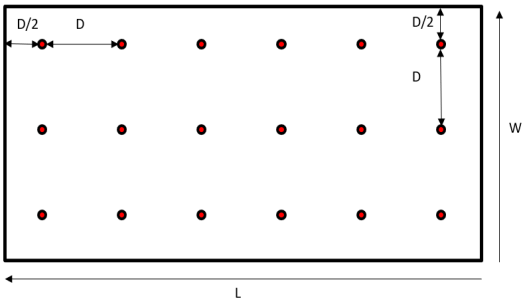
Room size	Small-hall → L = 120 m, W = 60 m, D = 20 m Big-hall → L = 300 m, W = 150 m, D = 50 m
Ceiling height	10 m
UE height	1.5 m
gNB height	Low sub-scenarios: 1.5 m High sub-scenarios: 8 m
UE attachment	Based on pathloss
Carrier frequency	3.5 GHz and 28 GHz
Bandwidth	100 MHz and 400 MHz
Numerology	1 and 3
Clutter density	Low clutter density: 20% High clutter density 60%
Clutter height	Low clutter density: 2 m High clutter density: 6 m
Clutter size	Low clutter density: 10 m High clutter density: 2 m

Table 2.4: Calibration simulation assumptions according to 3GPP specifications

28 GHz, which are displayed as "ns-3" results (blue lines) in the subsequent Figures (from 2.6 to 2.9 [70]).

2.3.1 Coupling loss

The Coupling loss represents the difference between the received and transmitted signal power. It captures all attenuation between the UE and the serving BS. Here, both antenna gains at the Rx and transmitter (Tx) are 0 dB for the

Reference Signal Received Power (RSRP) computation. Moreover, the total transmit power per Transmission and reception point (TRxP) is 30 dBm. This parameter has been freely assigned due to the lack of information in the 3GPP specifications.

Therefore, Figure 2.6 shows the Coupling loss for each InF sub-scenario. The performances show that the range of values is slightly different. The high scenarios (i.e., InF-SH and InF-DH) have narrower ranges, and the low ones (i.e., InF-SL and InF-DL) have higher top values. Overall, the trend is very similar to the results obtained in [71], which leads to the conclusion that the channel model is validated in this aspect.

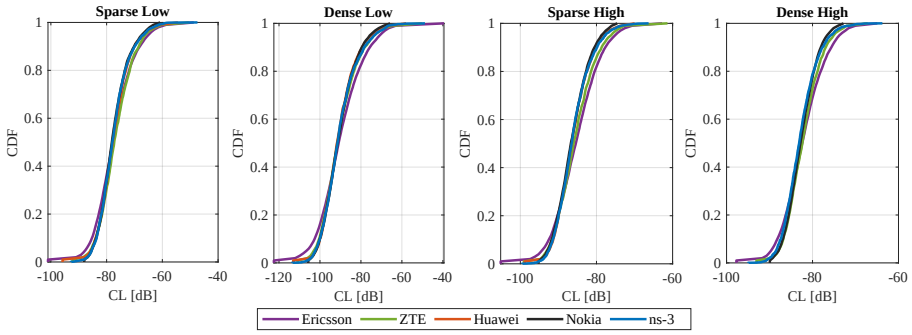

Figure 2.6: Coupling loss for four NLoS sub-scenarios at 28 GHz

2.3.2 Geometry with noise

This KPI is better known as signal-to-interference plus noise ratio (SINR), which captures and measures the received signal quality compared to the unwanted interference and noise. The results are shown in Figure 2.7, where low scenarios (InF-SL and InF-DL) have the highest levels of SINR. Nearly all sub-scenarios fit perfectly, except for InF-DH, where the curve shifts left at intermediate Cumulative Distribution Function (CDF) values. This indicates that while some users experience the worst SINR, most receive an improved SINR.

2.3.3 Geometry without noise

Unlike SINR, the Geometry without noise or signal-to-interference ratio (SIR) does not consider the noise. It only encloses the strength of the received signal and the interference from the serving BS.

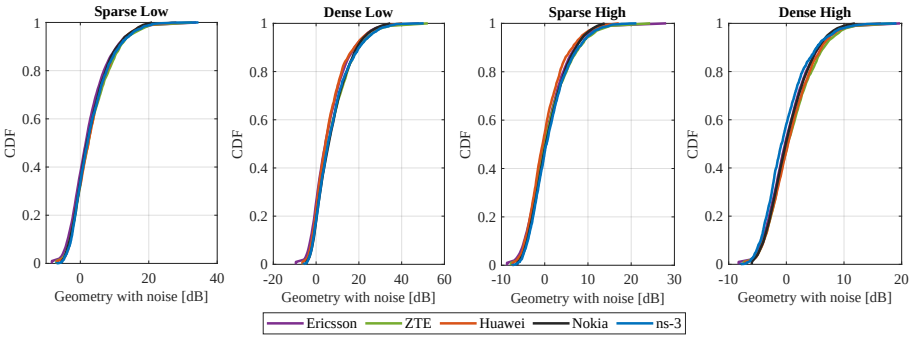

Figure 2.7: Geometry with noise for four NLoS sub-scenarios at 28 GHz

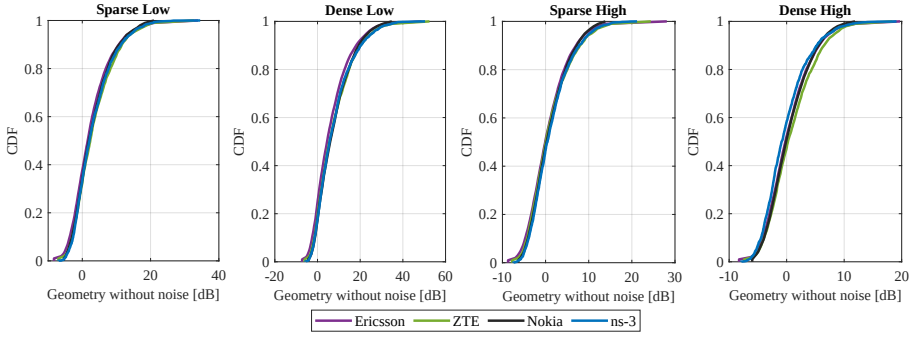

Figure 2.8: Geometry without noise for four NLoS sub-scenarios at 28 GHz

Figure 2.8 illustrates the SIR of ns-3 compared to the enterprises. The trends of InF-SL, InF-DL, and InF-SH closely follow the behavior of the other performance, indicating that most users experience improved geometry without noise. Then, the InF-DH curve is slightly positioned to the left. This is consequently about the lower geometry values without noise achieved, which suggests that more users receive worse signals in this sub-scenario.

Additionally, from an overall point of view, the ns-3 plots are almost aligned in the four sub-scenarios with the other companies' performances. This proves that this channel is validated with this KPI.

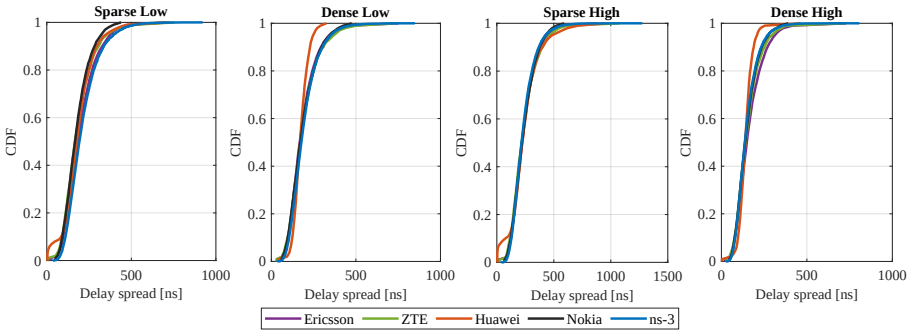

Figure 2.9: Delay spread for four NLoS sub-scenarios at 28 GHz

2.3.4 Delay spread

The DS performance is obtained following the description of Section 2.2.4. Thus, Figure 2.9 illustrates the DS, which shows highly accurate results compared to the other references. While Huawei's results (red line) differ from the rest of the references in some areas, this Thesis's results align with those obtained by other entities evaluating the same models. Even though the T-doc R1-1907968 [72] suggests modifying some parameters that may improve DS, this work shows results with the initial configuration proposed by 3GPP since the results fulfill the expectations.

2.4 Associated limitations

Over the last few years, the 3GPP model has evolved by incorporating various extensions to accommodate the latest generations of mobile communications and their technological advancements. Consequently, the 3GPP geometry-based stochastic model (GBSM) has become a valuable tool for assessing current 5G networks. However, the 3GPP model has been compared with other more realistic channel models, highlighting, for instance, the method to characterize the clusters for the channel.

The 3GPP model uses a joint delay-angle probability density function to emulate a group of traveling MPCs, each with unique departure and arrival angles centered around a mean propagation delay. Alternatively, *time clusters* and *spatial lobes* can be used to parameterize the channel, closely aligning with realistic measurement behavior [73, 74]. This indicates that while 3GPP provides geometric properties for channel modeling, it is relatively simple and less accurate, particularly in its parameter characterization.

Another noteworthy aspect is that the 3GPP model does not locate the scatterers (the spatial point of path reflection) and leaves free interpretation that the paths can have one or multiple hops. Including scatterer locations would help maintain spatial consistency since SSPs (Section 2.2.5), much of their process is randomly generated. In other words, if two users are nearby, the scatterers assigned to each can be completely different, leading to spatial incoherence [75]. Ideally, the same scattering environment should have other users.

Locating the scatterers could also help to achieve a more accurate understanding of the environment, as this process might allow for precise acquisition of the scattered power for each path [76]. The 3GPP randomly distributes power regardless of how many bounces a path has experienced. This Thesis emphasizes power terms because, in industrial scenarios, metallic surfaces will substantially impact propagation paths.

Despite the 3GPP channel model being a pioneering standard for the industrial scenario and offering insights into propagation characteristics, the characterization of industrial environments began relatively late, as highlighted in Section 2.1. Despite this, IIoT applications remain a primary focus in 5G usage scenarios. The environment's complexity and unexplored nature have probably been the main attributes of this slowness, emphasizing the crucial role of further investigation that needs to be carried out by the audience.

On the other hand, in [36], the authors found that the LSP of the 3GPP model did not align well with their measurement results, as well as those reported in [77]. Consequently, they concluded that industrial environments are unique and emphasized the need for further evaluation, particularly regarding dense or diffuse MPC. Observing this behavior suggests that 3GPP model for InF may not fully capture the complexity of industrial environments. In realistic scenarios, these environments often exhibit more significant variability due to the presence of machinery and dynamic changes within the factory. The static nature of 3GPP models might not effectively account for these variations.

2.5 Conclusion

This chapter has analyzed the 3GPP channel for industrial scenarios, detailing the particular environment features such as clutter density, distance, and antenna height. These features impact the channel modeling since new characterization has been necessary to introduce, such as the propagation condition and pathloss generation of new models. In addition, new LSPs have been introduced, consequently affecting the generation of SSPs. A calibration process has also been performed to study the model further, considering the specific

parameters proposed by 3GPP TR-38.901. The results have been compared against those in document R1-1907968. Said results show a similar trend for all the metrics considered, i.e., Coupling loss, Geometry with noise, Geometry without noise, and DS. These results indicate that the calibration procedure has been effectively carried out.

Although researchers have come a long way in this field, there are still limitations, especially with this model, which may struggle to meet the demands of IIoT applications. In addition, the standardization of the industrial channel model coincided with the start of 6G studies. This suggests that 6G may introduce new technologies capable of addressing these geometric constraints. This Thesis seeks to advance this exploration by investigating a new 6G trend designed to be compatible with and meet the unique demands of these environments: Integrated Sensing and Communications (ISAC) systems.

Chapter 3

ISAC Channel Modeling

As highlighted in Chapter 1, Integrated Sensing and Communications (ISAC) is a promising technology expected to address industrial scenarios' geometric complications. Even though ISAC has been mainly oriented to vehicular environments, this Thesis argues that sensing can be utilized to reduce channel estimation time, optimize beam management [47, 78], and identify the most effective paths to the user even under Non Line of Sight (NLoS) conditions. These applications are particularly advantageous in complex environments, such as factories. However, before exploring the advantages and applications that ISAC can offer, it is essential to focus on the crucial step in creating any wireless communication system: channel modeling.

The current channel models for ISAC in the literature are purely stochastic, offering only a general understanding of the performance of evaluated solutions. While sensing-only systems have been assessed realistically with consideration of the scenario's geometry, the coexistence of sensing and communication systems demands similarly comprehensive channel modeling. A suitable approach that balances stochastic and realistic modeling is the geometry-based stochastic model (GBSM). Similar to realistic or deterministic models, it accounts for the geometry of the scenario, making it a suitable choice. Indeed, one of the most well-recognized models in this category is the Third Generation Partnership Project (3GPP) model. Despite the limitations discussed in the previous chapter, the 3GPP channel model has been selected for the International Mobile Telecommunications (IMT)-2020 standardization [8]. This decision suggests that similar 3GPP-like channel models might be chosen for future standardization, such as IMT-2030.

According to these trends, the development of new channel models will be driven not only by introducing new frequency bands but also by integrating

emerging technologies. Therefore, this chapter proposes a new GBSM for ISAC systems, using the conventional 3GPP-GBSM [65] as a basis. This approach is validated by comparing it with realistic measurements obtained through a ray-tracing (RT) tool. It might be an initial step toward an ISAC deployment framework.

3.1 System model

The sensing mono-static channel must be incorporated to develop ISAC channel modeling so that the transmitter (Tx) and receiver (Rx) antenna positions are in the exact location. With this configuration, this proposal assumes the sensing transmitted signal undergoes a single bounce before returning to the base station (BS). In this manner, the sensing channel obtains information about the obstacles or scatterers in the scenario, including the User Equipment (UE).

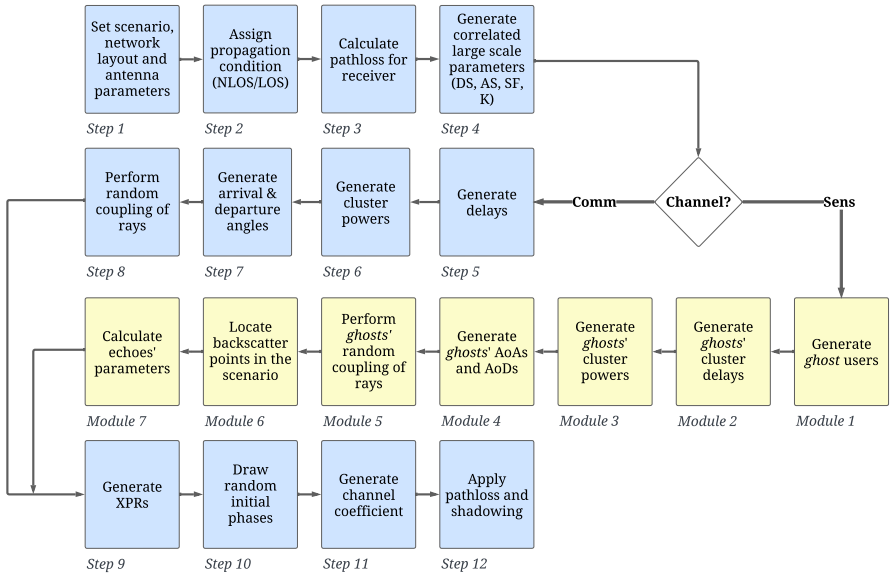

Figure 3.1: ISAC channel model block diagram based on the well-known 3GPP channel model

The sensing and communication channels operate as two systems in one hardware where a crucial correlation is assumed in this novel ISAC channel

modeling. Since both channels interact with the identical scatterers in the scenario, their multipath directions may resemble each other, leading to certain similarities in the channel realizations.

Considering this context, the well-known 3GPP channel model from the Technical Report (TR) 38.901 is used as a basis to design the ISAC channel model. Figure 3.1 shows the 3GPP conventional diagram procedure modified to add new modules (yellow blocks in the figure) to obtain the sensing mono-static channel. The conventional 3GPP steps related to scenario layout, antenna parameters, propagation condition, pathloss, and large-scale parameter (LSP) remain unchanged. The modifications begin from the decision block that generates either the sensing or communication channels. The procedure for obtaining the conventional communication channel remains the same. Finally, this processing provides both sensing and communication channels.

3.1.1 Generate ghost-users

The 3GPP channel model was designed to replicate the propagation behavior of Multipath Components (MPCs) or rays that reflect off the objects in the scenario (scatterer points) before arriving at the Rx or UE. As discussed in Chapter 2, the MPCs are characterized by small-scale parameters (SSPs), which are statistical functions based on measurements performed considering the link between Tx and Rx (physically separated). This implies that the 3GPP channel model requires this physical configuration to obtain the channel parameters.

However, some strategies must be employed to characterize the sensing paths or echoes due to the co-location of the Tx and Rx in a mono-static configuration. The primary effort identifies where echoes reflect and return to the BS, known as backscatter points. To address the limitation of mono-static configurations, this model introduces additional users or *ghost-users* only to generate the associated cluster SSPs for each *ghost-user* conventionally. This information encloses delays and angles that can obtain backscatter points by geometric calculation.

The backscatter points are illustrated in Figure 3.2 with blue dots. From this step, the information on the backscatter points can characterize the echoes (black dashed lines) that construct the sensing channel in the further modules.

The *ghost-users* method can ensure a correlation between the communication and sensing channels. For instance, at least one *ghost-user* shall be located at the exact location of the real Rx, i.e., the UE. This way ensures that some communication scatter points match the sensing backscatter points.

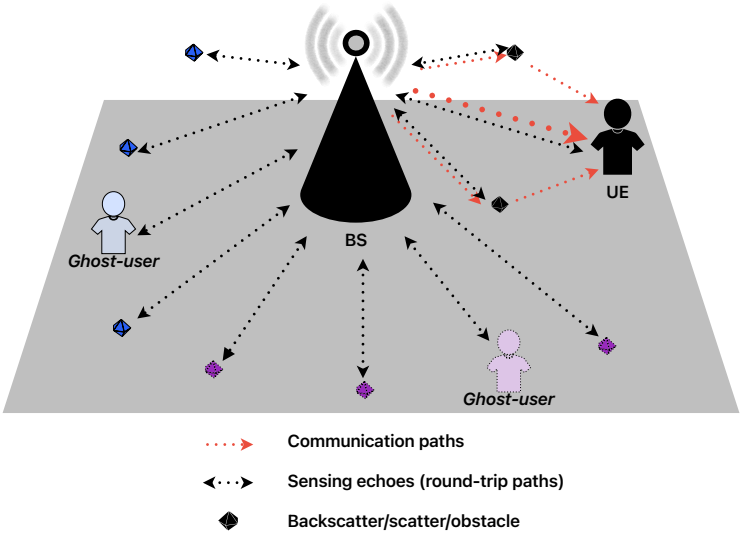

Figure 3.2: Clutter geometry for ISAC channel modeling

3.1.2 Locate sensing backscatter points

The 3GPP defines the clusters as a set of rays arranged randomly. Each cluster energy could radiate by multiple bounces before reaching any Rx. Therefore, this geometry might obtain plenty of degrees of freedom when generating the Azimuth angle of Arrival (AoA) to simulate the scenario. Hence, the specific location of the backscatter points cannot be determined, and the modeling of echoes would be complex. Thus, the treatment of AoAs is especially essential to this process. This subsection uses the term "AoAs" to refer to the trajectory of the directions that supposedly reach the *ghost-users*.

Module 5 in Figure 3.1 focuses on the intersection of direction pairs (AoD and AoA) using random coupling. When considering a single bounce, the intersection points can simply be geometrically calculated in the scenario. Thus, these intersected points can be regarded as the backscatter points. However, two possible cases may occur in the intersection process: (1) The intersected point can be inside the room (Figure 3.3a). Here, no modification is needed. (2) The intersected point can be outside the room or not intersected, like the gray dot in Figure 3.3b. In the latter case, an accepted range is considered and defined as the green area in Figure 3.3. Thus, the gray dot is reconstructed

by adjusting the AoA with the angle range formed from the *ghost-users* toward where the Azimuth angle of Departure (AoD) collides with the wall, as determined by the solid line arrow.

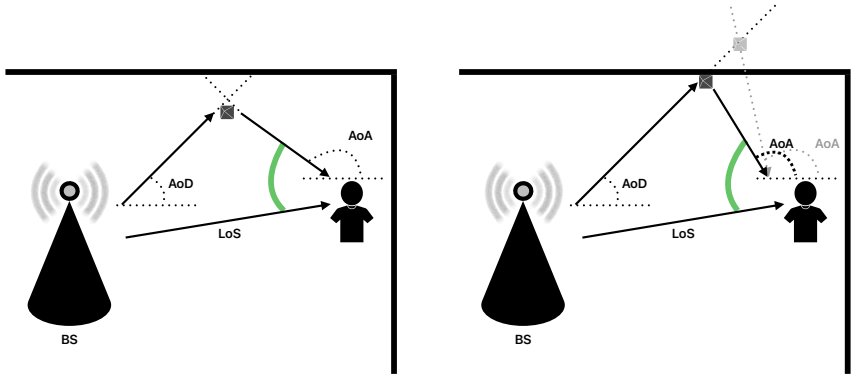

(a) Case 1: Inside the room (b) Case 2: Outside the room

Figure 3.3: Backscatter point calculation methods

3.1.3 Calculate echoes' parameters

So far, the SSPs have been generated for the clusters between the Tx and the *ghost-users* aiming to locate the backscatter points. However, these parameters, such as delays and powers, should not coincide with the characterization of echoes. Since the echoes should reflect in the backscatter point and return to the BS, the following details determine this particularity.

- **Sensing echo angles:** The AoAs shall be determined according to the mono-static configuration. This subsection uses the term "AoAs" to refer to the arrival angle at the BS when the echoes are finally returned. Since the Tx is also the Rx, the AoDs and AoAs are the same. In this procedure, the AoAs are overwritten by the AoDs previously generated. The AoAs of the *ghost-users* are not considered to create the sensing channel.
- **Sensing echoes pathloss:** This computation might be a new instance of a pathloss model using the distance from the Tx to each backscatter

point and back. The Radar Cross Section (RCS) is incorporated as the interaction with the backscatter point. Practically, this model shifts from the global pathloss experienced by the Rx (as the 3GPP) to a per echo pathloss calculation. Therefore, the new pathloss model per echo has been based on the radar equation [79], in which the radar channel gain (G_c) is defined as

$$G_c = \frac{c^2\sigma}{(4\pi)^3 f^2 R^4}, \tag{3.1}$$

where c is the speed of light, σ is the RCS area, f is the radar frequency, and R represents the distance to the backscatter point. In this sense, the pathloss model equation can be derived as,

$$PL(\text{dB}) = 2\alpha - G_\sigma(dB), \tag{3.2}$$

$$\begin{cases} \alpha = 20log_{10}f + 20log_{10}R + 20log_{10}4\pi - 20log_{10}c, \\ G_\sigma = 10log_{10}\sigma + 20log_{10}f + 10log_{10}4\pi - 20log_{10}c, \end{cases} \tag{3.3}$$

where α is the one-way free space loss, and G_σ is the backscatter point loss factor. Therefore, (3.2) can be rewritten in terms of the 3GPP pathloss model as

$$PL_2(\text{dB}) = 2PL_1 - G_\sigma(\text{dB}), \tag{3.4}$$

where PL_2 denotes the pathloss experienced in the path created from the Tx to a certain backscatter point in the scenario and back to the Tx (round-trip). Thereby, PL_1 refers to the conventional 3GPP multipath pathloss model used (one way).

- **Sensing echo delays:** Since the backscatter point locations are given in the previous process, the delay of each echo is calculated by obtaining the trajectory distance of the BS-k-th backscatter point. Considering that echoes are round trip, each l echo delay can be given by

$$\tau_l = 2d_{\text{BS}-k}. \tag{3.5}$$

  Note that L echo delays are calculated over the absolute delays specified in TR 38.901, Section 7.6.9 [65].

- **Sensing echo powers:** With the sensing echo delays, the 3GPP specification, Step 6 can compute sensing echo powers.

3.1.4 Generate the sensing channel coefficients

According to Figure 3.1, the generation of sensing channel coefficients follows the conventional procedure of the 3GPP specification. The sensing channel matrix is generated with a specific correlation level. This resemblance between the sensing and communication channels can be pre-established. The method above of the *ghost-user* (Section 3.1.1) might allow control over this correlation. For instance, a high correlation might be obtained if only one *ghost-user* is considered and placed in the exact location of the UE. On the other hand, a low correlation could result if several *ghost-users* can be placed in positions adjacent to the UE, and a minimum correlation could occur if *ghost-users* are in any direction of the scenario away from the UE.

3.2 Comparison with a deterministic model

This section compares realistic measurements to evaluate the designed ISAC channel model. The analysis presented here is based on findings from [80], where MPCs were obtained using RT tools. Examining realistic echoes with realistic measurements may give an intuition over the channel behavior and the considered features. The main feature to be analyzed is the correlation between communication and sensing channels, for which some key performance indicators (KPIs) have been selected under different simulation assumptions.

3.2.1 Simulation assumptions

Simulations under similar conditions have been performed for the presented approach and the deterministic model based on the RT tool. The tool for the deterministic channel is a proprietary simulator further described in [81].

As separate cases, the simulations have been performed for Line of Sight (LoS) and NLoS conditions following the geometry configuration detailed in Table 3.1. The BS is placed in the center of the scenario for both simulation cases. The UE is considered a target, which moves from the center to the upper right corner of the room. To guarantee LoS condition in the deterministic simulation, the scenario has no obstacles, as shown in Figure 3.4a [80]. In contrast, in Figure 3.4b [80] for NLoS, a large orange obstacle has been used to hide LoS.

The proposed ISAC channel model uses a *ghost-user* method to shape this correlation within a stochastic modeling framework. Since the main interest is to analyze the correlation between communication and sensing channels in stochastic modeling, two levels of correlation have been established: *Low* and *High* level. The *Low* level of correlation considers 2 *ghost-users*. For the *High*

Parameters	Value
Room size (WxL)	20 m x 20 m
Room height	8 m
BS antenna height	6 m
UE antenna height	1.5 m
Number of BS	1
Number of UE	1
BS antenna array	8 x 1
UE antenna array	1 x 1

Table 3.1: Geometry configuration applied for stochastic and deterministic simulations

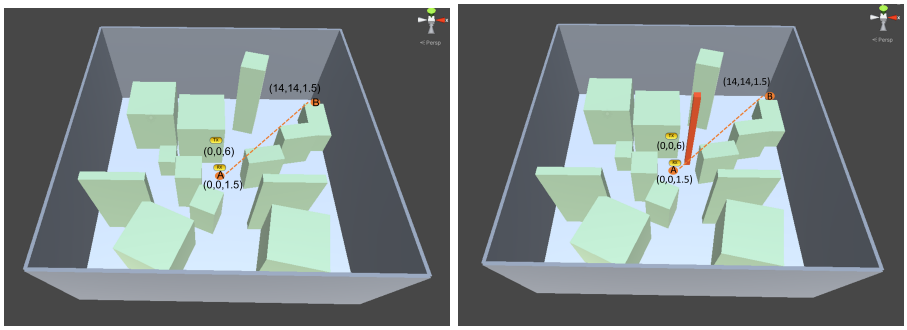

(a) LoS condition (b) NLoS condition

Figure 3.4: Visual description of the indoor scenario modeled for RT-based deterministic simulation

level of correlation, there is no *ghost-user*. Therefore, only the echoes from the UE that arrive at the BS are considered.

In realistic environments, such as deterministic channel models, the geometry of the scenario determines the number of echoes. Consequently, the assumptions defining the level of correlation will vary. At the *Low* level, thousands of echoes are considered to characterize the sensing channel. In contrast, only the most relevant echoes related to the UE are considered for the High level.

3.2.2 Angular correlation analysis

Analyzing the angular distribution of the MPCs might provide significant input to evaluate the correlation between the communication and sensing channels. The Power Angular Profiles (PAPs) might serve as a KPI, providing an angular view of the MPCs that characterize each channel. The simulation is divided into several snapshots of the UE time trajectory. To perform a fair comparison, the same snapshot of the communication and sensing channel is selected to compare the resulting AoDs. The PAPs present the normalized power in the given direction for each component angle.

The approach results in LoS and NLoS conditions are presented in Figure 3.5. Some MPCs of the communication channel (blue stemplot) are concentrated around 45°, which coincides with the direction of the orange dashed line in Figure 3.4. Meanwhile, the echoes of the sensing channel (red stemplot), the power is distributed in all sensing directions given by the omnidirectional configuration. The UE cannot be identified among all the echoes because the BS receives echoes from everywhere (ground, nearer backscatter point, etc.), so it is not easy to differentiate which echoes are related to the UE in this condition.

A similar performance is appreciated in Figure 3.6 from deterministic simulation, but here, the power of the echoes is more evenly distributed. This behavior is because the distance between the ground and the BS is shorter than between the BS and UE. Therefore, these echoes bounce back with almost the same power. On the other hand, the MPCs of the communication channel coincide with 45° directions. However, some MPCs are in the opposite direction, around 200°, corresponding to some obstacles placed on the left central side of the hall.

Comparing both models, an angular correlation between communication and sensing MPCs can be noticed since some sensing paths coincide with those of the communication. However, from the channel estimation perspective, the results suggest that MPCs unrelated to the user's direction are included in the sensing channel estimation. If this sensing estimation is employed to assist the communication channel estimation, it may lead to erroneous communication signals indicating directions unrelated to the UE.

Therefore, prior knowledge results are provided by assuming that the BS can filter out the most relevant echoes related to UE. This way, the sensing channel might enclose the power and angular information from the UE. Specifically, the angular range considered for this study comprises the area above the diagonal from the upper left to the lower right. This implies that the BS will filter out the most relevant 50% of echoes, being able to obtain a sensing channel matrix more correlated with the communication equivalent.

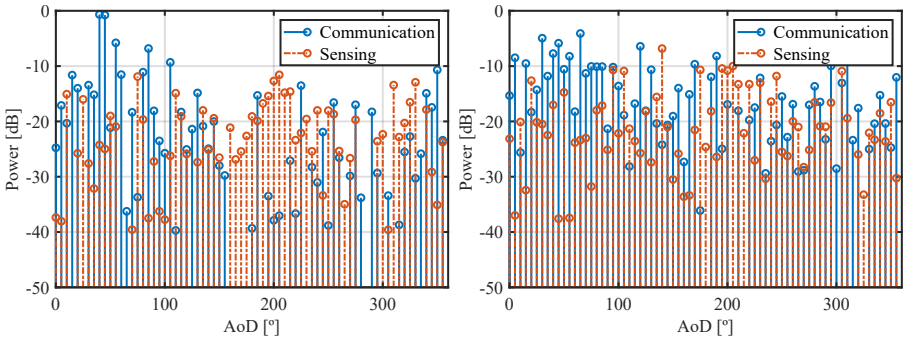

(a) LoS condition (b) NLoS condition

Figure 3.5: PAPs of proposed ISAC channel model

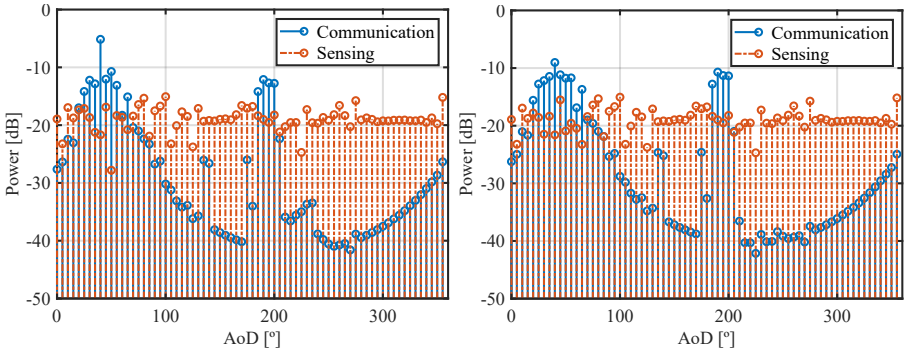

(a) LoS condition (b) NLoS condition

Figure 3.6: PAPs of deterministic channel model

Considering the previous assumption, Figure 3.7 and Figure 3.8 illustrate the PAPs from the proposed and deterministic channel model, respectively. In contrast to previous performances, the sensing MPCs concentrate the power in the relevant directions, i.e., toward the UE. This behavior is noticed for both statistic and deterministic simulations in LoS and NLoS conditions. In deter-

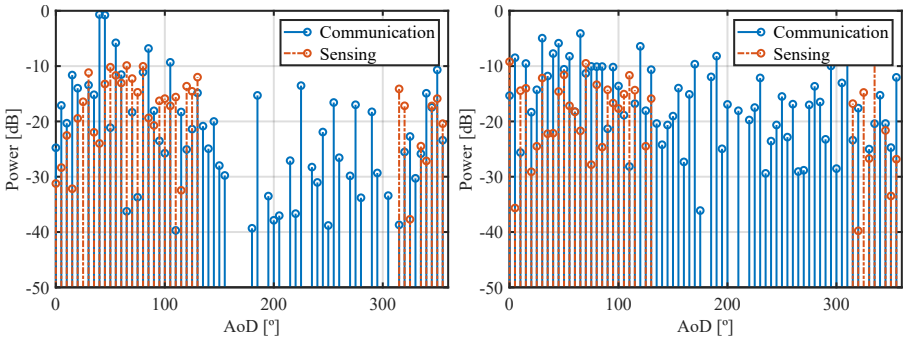

(a) LoS condition (b) NLoS condition

Figure 3.7: PAPs of proposed ISAC channel model with prior knowledge

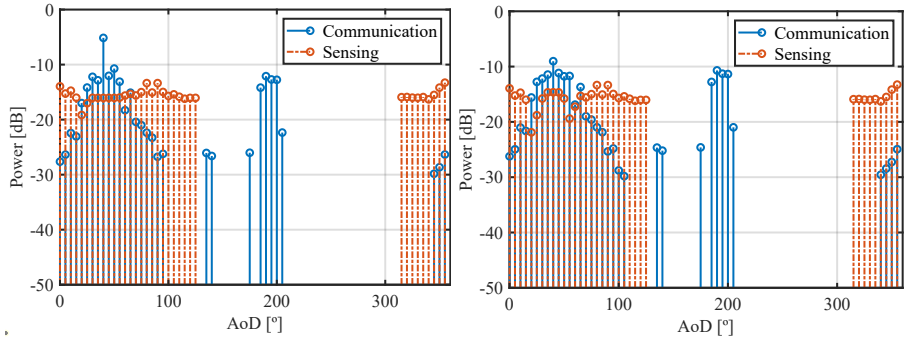

(a) LoS condition (b) NLoS condition

Figure 3.8: PAPs of deterministic channel model with prior knowledge

ministic simulation, some important transmission directions may be ignored since filtering is also applied to communication performance.

3.2.3 Quantitative correlation analysis

Since particular sensing MPCs overlap with communication MPCs, establishing a correlation between the two channels becomes feasible. While PAP offers

a broad understanding, a thorough investigation into the channel coefficients of each system is imperative. The channel matrix is the primary outcome for replicating any wireless system. Hence, this subsection examines the correlation coefficient between the sensing and communication channels. This statistical measure provides quantitative insight into their degree of linear correlation. Thus, the correlation coefficient can be given as

$$p(\mathbf{C}, \mathbf{S}) = \frac{cov(\mathbf{C}, \mathbf{S})}{\sigma_{\mathbf{C}} \sigma_{\mathbf{S}}}, \tag{3.6}$$

where $\mathbf{C}$ and $\mathbf{S}$ are the communication and sensing channels matrix of a single time slot, respectively. The expression $cov(\mathbf{C}, \mathbf{S})$ is the covariance between $\mathbf{C}$ and $\mathbf{S}$. The symbols $\sigma_{\mathbf{C}}$ and $\sigma_{\mathbf{S}}$ represent the standard deviation of $\mathbf{C}$ and $\mathbf{S}$, respectively.

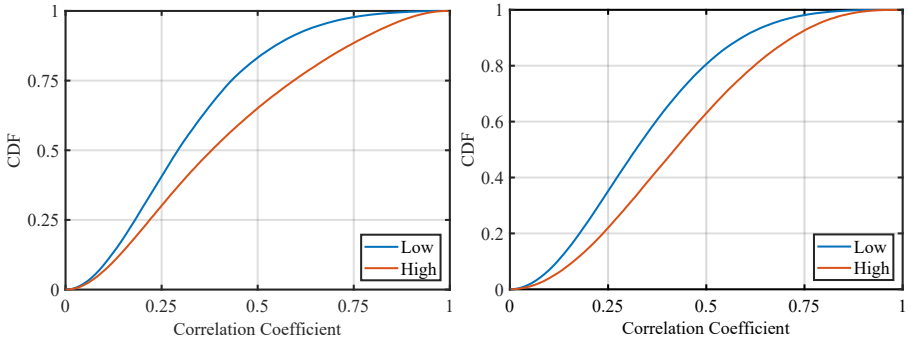

(a) LoS condition (b) NLoS condition

Figure 3.9: Correlation analysis of proposed ISAC channel model

The results are given by the Cumulative Distribution Function (CDF) of the correlation coefficient for the two levels of knowledge defined in Section 3.2.1. They use the filtering procedure explained in the previous subsection about the prior knowledge, where the sensing channel is constructed only according to the directions of the relevant MPCs. Figures 3.9 and 3.10 show the proposed and deterministic channel models, respectively. A notable contrast in correlation emerges between the low and high levels.

There is a marked increase in the average correlation between the two levels, with a 30.98% rise in LoS conditions and a 10.89% increase in NLoS conditions from the proposed channel model. Notably, the high level exhibits a more sig-

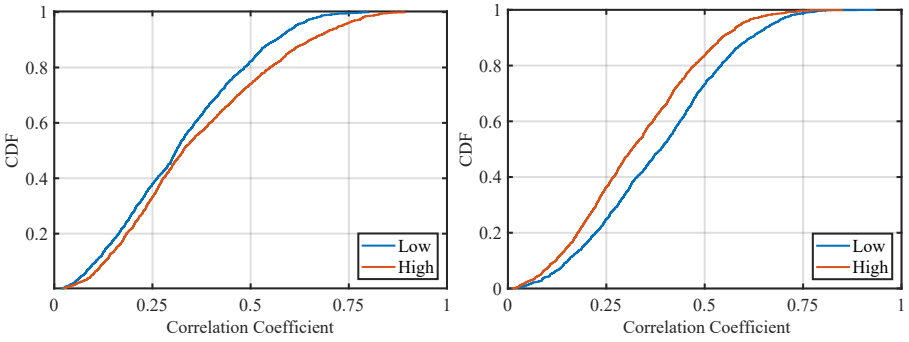

(a) LoS condition (b) NLoS condition

Figure 3.10: Correlation analysis of deterministic channel model

nificant number of correlated coefficients. Similar trends are observed in deterministic simulations. Consistently, the average correlation coefficient increases by 6.45% in LoS conditions. At the same time, NLoS condition decreases up to 17.95%. This latter behavior is given by the low level in deterministic, which considers all the echoes, while the high level only finds the relevant ones. Here, filtering is detrimental since the sensing channel loses half of the information, producing a non-similarity between channels.

Finally, comparing the proposed and deterministic models reveals a consistent parallel pattern in their behavior. Consequently, leveraging the proposed ISAC channel model proves valuable for evaluating future ISAC applications under the condition of prior knowledge.

3.3 Conclusion

Despite the limitations detailed in the previous chapter, the 3GPP model has been chosen as the foundation for constructing the new GBSM for ISAC systems. Its significance in the context of standardization is substantial, making it an ideal basis for this purpose.

The modeling has been compared with realistic measurements from the RT tool to verify the suitability of the modeling and understand the sensing channel's new features. During this development, the correlation between the communication and sensing channels has identified the main feature of constructing ISAC channels.

The results have shown that this correlation level depends on prior knowledge of the UE position. Assuming this knowledge, the sensing channel encloses only the echoes related to the UE. Under these considerations, this modeling provides initial insights of ISAC channel and how sensing might provide relevant information to improve channel estimation or beam alignment with the user. Although the results of the PAPs have provided an intuition of the ISAC channel model, further research is needed to evaluate ISAC systems and incorporate new inputs properly.

Even though the ISAC system is currently unexplored in industrial scenarios, this Thesis hypothesizes that it holds promising benefits for Industrial Internet of Things (IIoT) applications. The ISAC channel model presented here is a crucial first step in evaluating the feasibility of the ISAC system in these environments, as an appropriate channel model is essential for emulating any wireless communication system.

Chapter 4

Evaluation Methodology for ISAC Applications

Given that industrial scenarios require specialized treatment, particularly concerning channel modeling, as discussed in Chapters 1 and 2, Integrated Sensing and Communications (ISAC) system could significantly enhance communication reliability in these environments. Since channel modeling is crucial in developing any wireless system, establishing a methodology to evaluate this new system might be the next step toward standardization and construction of a comprehensive system.

A practical evaluation methodology is a vital compass to guide the improvement and growth of any system. Having a structured and reliable evaluation methodology is essential because it allows the research community to assess the current state to identify strengths and weaknesses, set clear objectives, and measure performance towards the desired achievement. The International Telecommunications Union (ITU) has identified ISAC as a key trend for Sixth Generation (6G) technology, highlighting the increasing importance of sensing in communication systems [42]. Consequently, like previous technologies, the ITU may develop guidelines for assessing this emerging technology.

The literature lacks contributions proposing a methodology for evaluating ISAC systems. Existing ISAC research [53, 78, 82, 83] primarily focuses on functionalities, advantages, and techniques that enhance communications through sensing. Given this interest, it is time to introduce evaluation criteria that consider aspects such as signal processing and channel modeling, particularly to explore how sensing can be leveraged to benefit communication.

Therefore, this chapter presents a methodology for evaluating the ISAC system, especially for sensing-assisted communication applications. The main

elements of this methodology involve characterizing the propagation conditions for sensing channel modeling, specifically by considering the correlation between the sensing and communication channels and ensuring their spatial correlation. This latter allows an accurate assessment of scenarios where users are expected to receive similar channel contributions, such as those involving user mobility or multiple users nearby.

Despite the limitations of the ISAC channel model presented in the previous chapters, it has been employed to develop the proposed evaluation methodology. Consequently, this Thesis does not suggest using any specific ISAC channel model but highlights the key characteristics that should be considered. Finally, a sensing-assisted communications (SAC) application is presented as an example to show the applicability of the proposed methodology. The content of this chapter is based on findings from [45].

4.1 Sensing-assisted channel estimation

Initially, sensing capabilities were introduced as a separate service, deriving valuable applications such as localization and mapping, imaging, or human activity recognition [78]. However, in recent years, it has become more evident that sensing can improve the performance of existing communication systems. One of the most attractive and promising applications is channel acquisition through sensing capabilities.

Acquiring a reliable channel estimate is a critical element in ensuring effective communication. Ideally, this procedure should involve frequent estimations, particularly in systems with many antenna ports or scenarios characterized by rapid channel fluctuations. Nonetheless, this estimation process often necessitates allocating pilot resources within a frame for channel estimation instead of data transmission, thereby introducing overhead in *Throughput*, as fewer bits are transmitted per frame. Efficient estimation is a prerequisite for facilitating swift user access to resources while minimizing overhead consumption. Within this context, the integration of sensing capabilities can confer distinct advantages by enhancing channel acquisition through leveraging prior knowledge of the environment.

This work presents fast channel acquisition as an applicable example of the evaluation methodology for ISAC system. This use case addresses the estimation of communication channels by leveraging the information available from sensing. The aim is to replace the pilot-based channel estimation procedure using the knowledge of the echoes from sensing. For this alternative method to successfully enable data transmission, the information provided by the communication pilots and the sensing echoes must be similar. Hence, both com-

munication and sensing channels must exhibit correlation because they share common Multipath Components (MPCs).

4.2 Evaluation methodology

The ITU defines an evaluation methodology as a set of the necessary tools, steps, parameters, and procedures designed to assess a communication system on a technical basis. Establishing unified guidelines in the form of a methodology allows for the consistent evaluation of systems, enabling performance results from one system to be reasonably compared with those of others. Regarding the elements that should be part of an evaluation methodology for wireless communication systems, at a minimum, it must include an appropriate selection of key performance indicators (KPIs) to quantify system performance, criteria on how these KPIs will be measured, and a channel model to have realistic modeling of the propagation condition [8]. The determination of the latter two allows the evaluation to be replicated.

Consequently, when considering new ISAC designs, it seems reasonable to follow the above guidelines, intended for communication-only systems, to design an evaluation methodology for sensing-assisted communication systems since one of their main goals is to boost communication performance by leveraging sensing capabilities. Therefore, similar considerations to those described above are followed in this work.

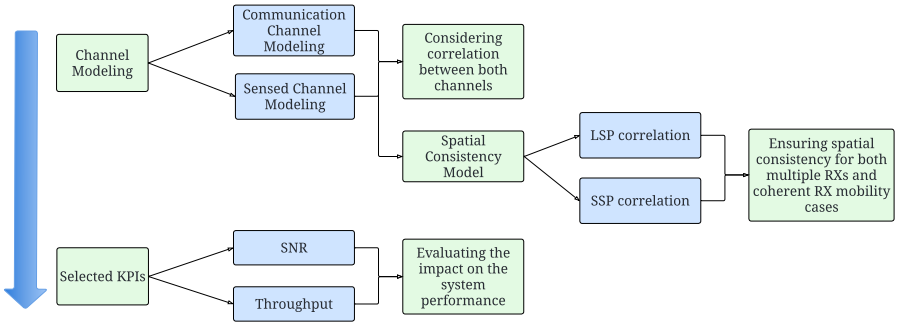

Figure 4.1: Summary of the main elements considered for evaluating sensing-assisted communication systems

Figure 4.1 summarizes the fundamental elements considered for this procedure. Firstly, the main features related to the characterization of the sensing channel in Section 4.2.1 are presented, i.e., considering the correlation between

sensing and communication channel and the spatial consistency. Then, in Section 4.2.2, some KPIs are introduced to illustrate the performance achieved by the system, together with the criteria for measuring them. Finally, the step-by-step procedure to evaluate a sensing-assisted communication system for a given use case is provided in Section 4.2.3.

4.2.1 Sensing channel modeling

When evaluating the performance of an ISAC system, both the communication channel and the sensing channel must be considered if accurate conclusions about system performance are to be drawn. In conventional communication systems, a radio channel model emulates electromagnetic wave propagation by accounting for the geometric characteristics of the scenario. This approach enables highly accurate predictions of channel behavior under real-world conditions [8]. Thus, a similar perspective to the sensing channel is conducted for ISAC. Several prominent features are presented for mono-static sensing configurations.

Correlation with the communication channel

Within an analysis of ISAC, the authors in [57] employed sensing devices integrated into the infrastructure of Road Side Unit (RSU). The sensing performance is highly correlated with the communications one, achieved by aligning angular information in the measurements. The azimuth power spectrum was used to assess the power originating from different angles, revealing substantial similarities between both systems.

The correlation between the sensing and the communication channel might also be evident in applications such as simultaneous localization and mapping (SLAM) integrated into Fifth Generation (5G) radio systems. For instance, the study conducted in [55] used such correlation to enhance environment reconstruction, providing an advanced mapping solution that enables more effective tracking against potential changes in the radio environment.

While the contributions mentioned above focused on different objectives, both concluded a realistic correlated behavior of communication and sensing channels and relied on it. This is a solid motivation to model ISAC systems using a geometry-based stochastic model (GBSM) model, given that if communication and sensing channels are modeled based on the geometry of the scenario, both would be characterized by the same scenario setup, meaning that an identical set of obstacles would influence signal propagation similarly in both cases. Furthermore, sensing and communication channels share the same fraction of the transmission path between the transmitter (Tx) and the

scatterers or backscatter points. This behavior was introduced in the previous chapter in Figure 3.2, showing the commonalities between communication paths and sensing paths. Given these inherent shared MPCs, a correlation between the two channels can be inferred. Some similar strategies are presented in the literature, such as the ones in [59, 80, 84, 85].

Modeling the sensing channel to ensure correlation with the communication channel can instigate new strategies, such as filtering the echo trajectories based on this correlation, as was explained in Chapter 3. This approach might guarantee that the sensing channel retains the most accurate contributions related to the environment. Consequently, more significant benefits can be derived from echoes without additional communication resources. In summary, not considering the existing correlation between the sensing and the communication channels may lead to wrong conclusions when assessing 6G candidate technologies.

Spatial consistency

As already pointed out, correlation is a crucial element in enabling the evaluation of ISAC systems. In addition to the correlation between the sensing and the communication channels, a proper assessment of the potential performance of a sensing-assisted communication system requires a spatially consistent channel. In this context, Spatial Consistency (SC) can be understood as a procedure to guarantee spatial correlation between channel realizations, i.e., to generate matching channels for receivers that are on a similar distance from the Tx, a smooth channel evolution for a receiver (Rx) moving around a nearby area, or even receivers close to each other can share identical scatterers. The receivers experiment with similar propagation conditions, so channel parameters such as delays and angles are consistent. Such situations must be considered when modeling the channel since scenarios with multiple receivers and mobility are expected to reflect the potential benefits of ISAC.

One of the significant drawbacks of GBSMs in dealing with mobility or multiple receivers is their drop-based nature. A drop can be defined as a still representation of the channel impulse response between the Tx and the Rx at a given time. Although SC is intrinsic to some parameters included in the GBSMs, e.g., distance-dependent path loss, the environment's geometry is not used to identify scatterers that give rise to the different propagation paths. Instead, the effective scatterers are distributed in a geometry determined by several random processes and probability functions derived from channel measurement campaigns and divided into two abstraction layers: the large-scale fading, which is characterized by large-scale parameters (LSPs), and the small-scale fading, described by small-scale parameters (SSPs). Therefore, whereas

SC is inherent to deterministic models since the physical environment is known and this information is used in simulations, drop-based GBSMs need to be adjusted. These models already include methods to ensure LSP correlation, but SSPs remain uncorrelated.

Regarding the large-scale fading model, LSPs refer to parameters whose variation is only significant over longer distances. In other words, these LSPs, e.g., delay and angular spreads and shadow fading, remain constant for several meters; therefore, there is a need to generate spatially correlated parameters. A common approach to model such correlation, and the one followed in the Third Generation Partnership Project (3GPP) GBSM, is a two-step procedure introduced in [86], in which the influence of exponential autocorrelation for each LSP and cross-correlation between all LSPs is generated separately.

As for the small-scale fading model, it characterizes the MPCs that the Rx experiences at a given spatial position by generating clusters defined by a set of SSPs. Some SSPs considered in the 3GPP GBSM are cluster delays, powers, Azimuth angle of Departures (AoDs), and Azimuth angle of Arrivals (AoAs) for both azimuth and elevation dimensions and polarization phases. These SSPs are calculated by combining one or more random variables drawn from a specific probability distribution defined through LSP (e.g., cluster delays are derived from a uniform random variable and the delay spread). For this reason, even if LSPs are correlated, the cluster generation procedure produces uncorrelated MPCs and, as a result, uncorrelated channel realizations.

The 3GPP Technical Report (TR) 38.901 [65], in which the GBSM is described, also features a collection of extensions that enable SC. This method combines a Two Dimensions (2D) filtered random process to generate correlated cluster and ray-specific random variables and two alternatives, Procedure A and Procedure B, to replace the stepwise generation of SSPs. In Procedure A, cluster delays and angles are geometrically updated at each location. In contrast, in Procedure B, the probability distributions of the random variables used to generate delays, angles, and cluster powers are modified. Hence, in one way or another, steps of the original channel model related to generating cluster delays, powers, and angles are replaced.

For the use case presented in this chapter, SC is implemented as indicated in Procedure A. Details on the implementation of this model are described in Appendix A. This procedure considers the velocity vector of the Rx and the time elapsed between channel realizations to update delays and angles from the previous ones. An update distance constraint is set to 1 m for these velocity and time parameters. Therefore, for the model to behave correctly, there should not be more than 1 m distance between receivers, or a Rx should not have moved more than 1 m between consecutive channel realizations. Additionally,

the implementation method presented in Appendix A assumes that the Tx has no mobility.

4.2.2 Key performance indicators

Usually, KPIs for ISAC evaluation are divided into two categories: information-theoretic and estimation-theoretic metrics [87]. On the one hand, information-theoretic focuses on channel capacity performance metrics, e.g., Mutual Information (MI) and KPIs derived by Shannon's theorem. Although the authors of [87] present MI as a promising candidate for evaluating ISAC, they also conclude that there are still some open problems. On the other hand, estimation-theoretic metrics include the Cramér–Rao bound (CRB), Mean Square Error (MSE), or detection probability.

For the present study, two metrics are chosen to evaluate the proposed use case as an example: the signal-to-noise ratio (SNR) and the *Throughput*. Firstly, the SNR is selected to assess the impact on the system performance by sensing-assisted communication. Secondly, the *Throughput* is used to quantify the improvement that can be achieved by the sensing-assisted solution due to the faster channel acquisition or the overall sensing gain.

The SNR at the Rx side and the *Throughput* experienced by the user have been calculated following the expressions (4.1) and (4.2), respectively.

$$\mathrm{SNR} = \frac{p|\mathbf{H}\mathbf{w}\mathbf{w}^{*}\mathbf{H}^{*}|}{N_0} \tag{4.1}$$

$$Throughput = \frac{\tau_c - \tau_p}{\tau_c} B \log\left(1 + \mathrm{SNR}\right) \tag{4.2}$$

In the above equations, $\mathbf{H}$ is the channel matrix, $\mathbf{w}$ can be any suitable precoder, p denotes the transmitted power, N_0 refers to the noise power, τ_c is the coherence interval length, τ_p is the training phase length, and B represents the system bandwidth.

4.2.3 System evaluation methodology

After reviewing the fundamental components to be considered in an evaluation methodology for sensing-assisted communication systems, it is essential to review the evaluation procedure. Figure 4.2 depicts the stages of this procedure. The step-by-step operation is as follows:

1. *Use case requirements.* A clear description of the use case, including its main requirements, should be a starting point for establishing an appropriate configuration or a precise implementation. This block addresses

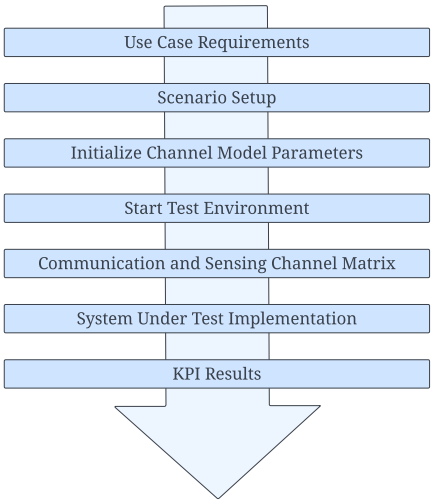

Figure 4.2: Outline of the stages that make up the evaluation methodology

the system implications derived from the use case and the necessary modifications to be made.

2. *Scenario setup.* The environment, network layout, and antenna array parameters are established. This step refers to the definition of the geometrical conditions of the scenario, together with the antenna configuration. The existence of the Line of Sight (LoS) propagation condition is also defined at this stage.

3. *Initialize channel model parameters.* In this step, it is decided whether to simulate the traditional communication channel or the sensing channel. Accordingly, the original 3GPP GBSM or the modified model for the sensing channel is used. Non-geometrical parameters such as frequency, number of clusters, or channel fading are also defined.

4. *Start test environment.* The system simulation starts after configuring all the parameters and setting the scenario.

5. *Communication and sensing channel matrix.* The communication and sensing channel coefficients are generated and structured as a Channel Impulse Response (CIR) matrix of size $N_t \times N_r$, where N_t is the number of transmitting antennas, and N_r is the number of receiving antennas.

6. *System Under Test (SUT) implementation.* Within this stage, the necessary modifications identified at the beginning of the procedure are implemented, e.g., beamformer designs, tracking or localization algorithms, or signal processing techniques, among others.

7. *KPI results.* SNR and *Throughput* results are obtained from the simulation. Other KPIs of interest to the use case can be added to provide additional information on system performance evaluation.

4.3 Example application of the evaluation methodology

To demonstrate the applicability of the evaluation procedures outlined in Section 4.2.3, this section presents the numerical results of the sensing-assisted channel estimation application described in Section 4.1. A comparative analysis of various benchmarks and the use case method are also discussed.

4.3.1 Simulation scenario

The evaluation scenario consists of a 20 m $\times$ 20 m indoor scenario shown in Figure 4.3. In this scenario, the Tx is in the center and equipped with 64 antenna elements distributed in an 8 $\times$ 8 Uniform Planar Array (UPA) at a height of 6 m. In contrast, the single-antenna of the Rx is 1.5 m high. Initially, the communication Rx is placed in the center of the stage and moves to the upper right corner with a constant speed of 3 km/h, with LoS propagation condition throughout the trajectory. The working frequency is 28 GHz, and the available bandwidth is 100 MHz. Table 4.1 summarizes the parameters used to carry out the simulations.

4.3.2 Use case assumption

Following the SUT implementation (step 6, Section III-D) of the proposed methodology, a beam training technique has been designed to select the transmitted codebook using sensing information. The sensing channel is used to estimate the geometry of the scenario and the user location [47, 53] represented by its angular information. This information is used to identify the most suitable beam in the codebook. Since the ISAC solution can retrieve the same information from data echoes as from pilot echoes, in later frames, the Tx does not require the transmission of sensing-specific pilots. Therefore, this approach can substitute conventional beam training techniques in a communication-only system.

Parameters	Value
Frequency	28 GHz
Bandwidth	100 MHz
Transmit power	21 dBm
Scenario dimensions	20 m × 20 m
Tx antenna height	6 m
Rx antenna height	1.5 m
Tx antenna configuration	UPA 8 × 8
Rx antenna elements	Single antenna
Rx noise figure	9 dB
Tx/Rx antenna pattern	Omnidirectional
Rx speed	3 km/h
Communication channel model	3GPP TR 38.901
Sensed channel model	Chapter 3
Spatial consistency model	3GPP - Procedure A
Frame duration	10 ms [88]
Number of simulations	100

Table 4.1: Simulation assumptions for the example use case

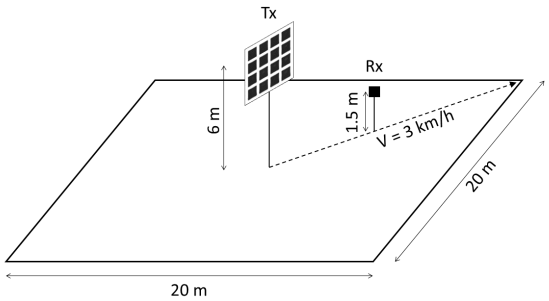

Figure 4.3: Scenario layout for simulations

It should be noted that both communication-only and sensing-assisted communication may require feedback signaling to share common ground and establish the communication link between Tx and Rx. Thus, the feedback stage is neglected in the performance study conducted in this use case.

The Tx must know the channel and available precoders to select the beam. On the one hand, for the latter, the Tx creates a set of precoding matrices as follows:

$$w_n = e^{-i2\pi \frac{d}{\lambda}(n_x cos(\phi) sin(\theta) + n_y sin(\phi) sin(\theta))}; \quad n_x \in 1, \ldots, N_x, n_y \in 1, \ldots, N_y \tag{4.3}$$

$$\mathbf{w} = \begin{bmatrix} w_1 \\ w_2 \\ \vdots \\ w_n \end{bmatrix}, \tag{4.4}$$

where d is the distance between antenna elements, λ is the wavelength of the carrier, and θ and ϕ are the elevation and azimuth LoS angles, respectively.

The symbols n_x and n_y denote the coordinate index pair of each antenna element in a UPA of N total antenna elements configured in a $N_x \times N_y$ distribution, where n_x and n_y correspond to the horizontal and vertical indexes of the array, respectively, and n is the precoder index which sweeps the vertical and horizontal array indexes of the UPA. For the numerical analysis, the azimuth and elevation are sampled from 0 to 180 degrees with a step of 5 degrees. The spatial power spectrum is given by

$$\hat{n} = \arg\max_n |\mathbf{w}^* \mathbf{H}_{\text{sen}}|^2, \tag{4.5}$$

$$w^{\text{sen}} = w_{\hat{n}}, \tag{4.6}$$

which determines the weight of every precoder created at every angle of the sweeping range. Thus, the ideal precoder is selected by the highest power in the scanning process, being $\mathbf{H}_{\text{sen}}$, the sensing CIR matrix. The latter is constructed assuming that the Tx has an approximate knowledge of the Rx position (as mentioned in [80]). This allows for the precise filtering of echo contributions. Consequently, in this case, the ideal precoder is selected based on the echoes associated with the user or those nearby.

Assuming that the channel state information (CSI)-based procedure performs beam selection every 10 ms of the frame duration (the duration of the frame), it can be naturally deduced that the performance may decrease compared to a system that constantly updates the beam selection and performs the data transmission simultaneously, as is the case with the sensing-assisted solution.

4.3.3 Benchmarks

Four solutions are compared to provide a comparative analysis of the proposed methodology. (1) *SAC* refers to *sensing-assisted communication* (beam selection) with the assumptions explained above. Moreover, the solution proposed in this chapter includes the correlation between sensing and communication channels and SC. (2) *CSI-based* beam selection refers to a conventional beam training solution as in [89]. It analyzes all available beams in the predefined codebook using communication system resources. This procedure is defined in Figure 4.4, in which a significant part of the resources are used to find the best beam.

After the beam selection, the Tx sends a downlink feedback signal informing the Rx of the chosen beam and the required parameters to establish the communication link. Communication can begin since the Tx and the Rx already have the information to transmit. SC has been considered for this benchmark. (3) *SAC without correlation* is a system like (1) in which correlation between the communication and the sensing channel is not included [90], i.e., two independent GBSM models are used for the communication and sensing channels. (4) *SAC without SC* refers to a model in which GBSM is used, including channel correlation, but without any guarantee of spatial consistency. As explained in Section 4.2.1, the absence of SC is a significant drawback in dealing with mobility or multiple receivers. Therefore, this benchmark considers the correlation between the channels without generating spatially consistent channel realizations, as done in [59, 84, 85].

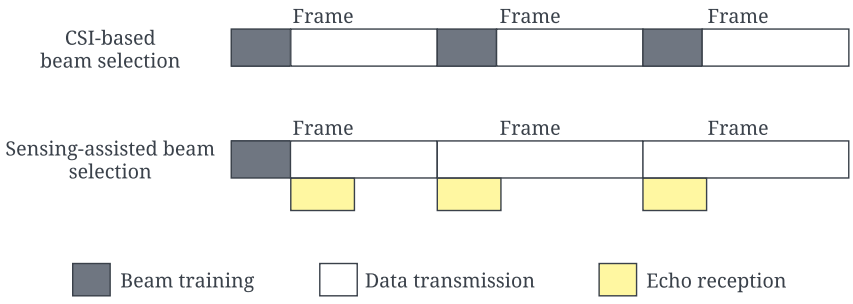

Figure 4.4: Frame structure in a DL transmission

4.3.4 Numerical results

After delving into the use case and mentioning the possible vulnerabilities in a sensing-assisted communication system without the crucial elements of the proposed methodology, this section provides a comparative analysis of the four solutions discussed before.

Figure 4.5 illustrates the Cumulative Distribution Functions (CDFs) of the SNR of the studied schemes. *SAC without correlation* and *SAC without SC* have obtained lower SNR levels than the other two schemes. *SAC without correlation* emulates a sensing channel that generates a different backscatter distribution from the communication channel. Consequently, the echo information to assist the communication system is inaccurately applied, which results in this degradation.

On the other hand, since there is no coherent mobility in the solution of *SAC without SC*, the channel realizations at each instant of the trajectory are generated differently, i.e., the SSPs are generated spatially uncorrelated in each time slot. This method introduces variations in the channel gain that negatively impact system performance. The smooth channel evolution is required to make the best of the sensing channel estimations.

Comparing the proposed *SAC* solution with the applied methodology and conventional *CSI-based* beam selection, it can be observed that *SAC* slightly outperforms the *CSI-based* scheme by 0.17 dB on the median. The *SAC* solution does not introduce a significant enhancement in terms of SNR. Still, it saves many resources dedicated to channel estimation, which will impact $Throughput$.

Figure 4.6 shows the $Throughput$ CDFs for the four solutions. The conventional communication system employs a *CSI-based* beam selection process, and resources within the transmitted frame are utilized. This process might introduce an overhead of 18%, as defined in [91] for CSI acquisition. In contrast, for any SAC solution, the beam selection process co-occurs with the data transmission process. This results in negligible overhead as the Tx leverages echo information for optimal precoder selection, as Figure 4.4 shows. Even without considering the overhead for *SAC without correlation* and *SAC without SC*, they failed to achieve satisfactory levels of $Throughput$ due to the mistaken channel estimation.

The comparison between *CSI-based* and proposed *SAC* reveals that even with the slight enhancement in terms of SNR level experienced when using the *SAC* solution, the reduced overhead allows the *SAC* approach to yield a 25.38% enhancement in terms of $Throughput$ over the *CSI-based* beam selection method. The *CSI-based* beam selection process inherently penalizes the experienced data rate as it uses many pilots before data transmission occurs.

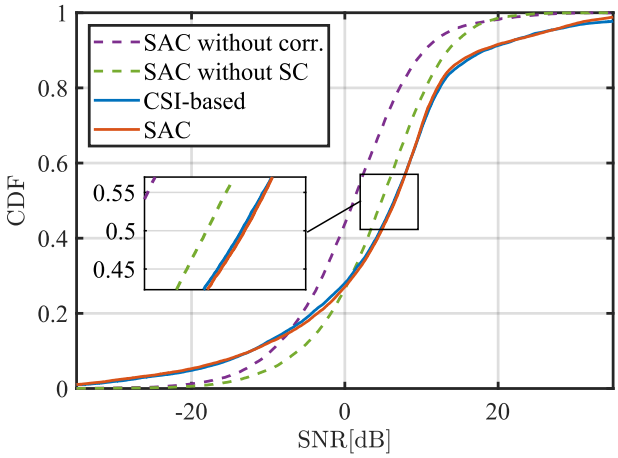

Figure 4.5: SNR performance of various benchmarks

The beam selection and link establishment procedure are simplified by taking advantage of the available sensing information, resulting in an almost overhead-free solution. In this case, communication would be more reliable and could be applied to more complex use cases and scenarios.

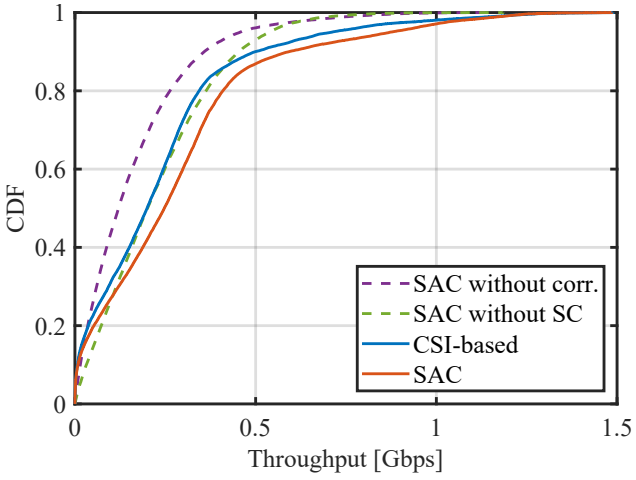

Figure 4.6: Throughput performance of various benchmarks

4.4 Conclusions

This chapter has proposed an ISAC system assessment methodology, describing two critical points identified. Firstly, it is essential to include channel modeling in a proposed methodology, where appropriate models must capture the particularities of both detection and communication channels. Features such as the correlation between channels and spatial consistency are necessary to reproduce a realistic behavior of the ISAC system. Secondly, appropriate KPIs must be selected to show the performance of the evaluated system. In this case, SNR and *Throughput* were chosen to quantify the robustness and efficiency of the sensing-assisted communication case.

In addition, a sensing-assisted application has been described and examined as an example of applying the proposed methodology for ISAC systems. The results underscore the importance of incorporating the suggested sensing channel modeling features.

Moreover, the convergence of both systems can be advantageous over established communication systems by harnessing the fast access and low overhead that ISAC envisions. It should be noted that the use case presented in this chapter refers to a simplified environment. However, the sensing-assisted communication system is likely better exploited in complex or further elaborated scenarios, e.g., industrial scenarios. Further research is required for these complex cases since more complex sensing algorithms are needed.

Chapter 5

Industrial Use Case: Sensing-assisted Beam Training

Throughout the last two chapters, Integrated Sensing and Communications (ISAC) systems have been introduced step by step, highlighting the fundamental elements that must be considered to build and simulate this system. A clear criteria for creating an ISAC system can be obtained following the proposed evaluation methodology.

To summarize, the inherent characteristics of this system include spatial consistency and correlation between sensing and communication channels. These features have been considered when using a geometry-based stochastic model (GBSM). However, deterministic models, such as those provided by ray-tracing (RT) tools, naturally incorporate these characteristics for a more realistic performance. Therefore, this Thesis proposes an alternative system modeling constructed using realistic channel parameters generated from RT tools, specifically tailored for a new industrial use case in realistic industrial environments.

Generally, a use case is known by the application or example of a particular technology to solve a relevant problem involving the user. In this case, the issue of the industrial use case is the presence of obstacles that result in multiple reflections, leading to many Multipath Components (MPCs). Consequently, establishing highly directional communication would be very difficult and would probably depend on the precise location of the user [92, 93]. With

this motivation in mind, sensing localization should serve as a security feature in smart factories and assist in establishing accurate communication links.

Therefore, this chapter introduces a new use case for the ISAC system in industrial scenarios. This approach offers a practical experiment to explore the performance of sensing-assisted communications (SAC) in such environments, providing valuable insights into the essential requirements for developing ISAC systems while highlighting essential interactions and potential future workflows.

The remainder of the chapter further describes the presented use case, a detailed description of the RT tool, and the development of the system model constructed by the RT dataset. Additionally, some beam training algorithms have been developed to leverage sensing information better, offering a novel solution for application in cluttered scenarios. Finally, the results are compared with several benchmarks, highlighting the impact of incorporating sensing localization to improve communication performance.

5.1 Sensing-assisted beam training

With the increasing number of antennas in massive MIMO (mMIMO) and the use of narrower beam patterns in higher frequencies to cope with higher losses, beam training techniques are becoming a trending topic. Beam training focuses on the procedures for selecting and maintaining the transmitting and receiving beams. To obtain a beam pair for the transmitter (Tx) and receiver (Rx) and be able to initialize the communication, some delay, pilot signaling, and signal processing are introduced, significantly impacting overall system performance. As the number of possible beams increases, the complexity of the problem grows exponentially, and the effective performance drops. Therefore, multiple solutions have been proposed in the literature to reduce the beam pair searching time, including algorithms that simplify the beam pair search, using prior information to aid the beam training, machine learning approaches [94], and beam tracking.

The introduction of sensing and location capabilities in the communication scheme has enabled the generation of novel technologies to boost legacy beam training. These novel approaches might reduce pilot signaling, suppress Uplink (UL) feedback, increase spectrum efficiency, and minimize signal processing costs. Some interesting works on this topic can be found in [49, 52, 95, 96]. Using the prior information and the sensing information, the set of possible beams is significantly reduced, the tracking of the optimal beams is eased, and the system can also benefit from the sensing signal to be aware of the context. Moreover, the authors in [53, 54, 97] consider employing beam prediction (beam tracking), which ensures integration and coordination gains in these procedures.

Given the above advantages, the localization of User Equipment (UE) may not only be a necessary factory service (as mentioned in Chapter 1) but also a sensing functionality that improves communications. However, the mentioned contributions related to sensing-assisted beam training have been performed on vehicle-to-anything (V2X) or vehicle-to-infrastructure (V2I) communication, where environments are "cleaner" with fewer obstructions. Most likely, in more clutter-dense scenarios, detecting the user among obstacles may be challenging, as in Indoor Factory (InF).

The cluttered scenario can directly impact the sensing capabilities in industrial environments; the received sensing signal includes all echoes unrelated to the target or UE. In such a case, it is essential to differentiate the part of the received sensing signal that encloses relevant sensing information about the target. However, this is not an easy task. One way to tackle this problem is to perform background subtraction.

Background subtraction techniques have been widely used in signal processing, especially video and imaging applications, to mitigate background noise and detect the target of interest [98]. On this basis, this Thesis argues that background subtraction might be employed as a specialized strategy to improve the performance of predictive beamforming algorithms.

5.2 Simulation tool overview

The channel modeling based on quasi-realistic measurements using RT has been utilized for years [99]. The Institute of Telecommunications and Multimedia Applications (iTEAM) group at Universitat Politècnica de València (UPV) has developed an RT tool using the Unity 3D platform. This tool leverages powerful graphic engines to achieve ultra-realistic scenes and accurately emulate real environments and conditions. Such capabilities enable more accurate and reliable calculations of propagation phenomena, allowing the emulation of any wireless system.

This simulation tool uniformly launches rays from the Tx to the scenario through a Raycast function. This function allows the rays to intersect all the obstacles. The trajectories of each ray are calculated based on the physical characteristics of the materials in the scenario, such as roughness, thickness, and physical dimensions. Each element in the scenario includes physical and electromagnetic information for materials like metal, wood, plasterboard, glass, and concrete. This characterization follows the recommendations of the International Telecommunications Union (ITU), specifically for the 18-40 GHz frequency bands.

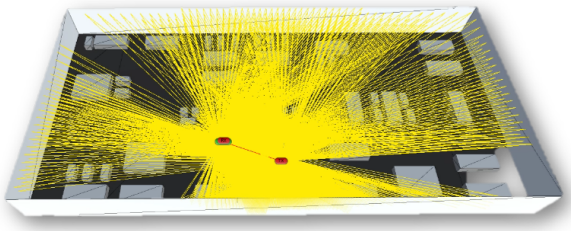

Figure 5.1: Simulations performed in the RT tool considering a single bounce

The RT tool provides various propagation mechanisms, including direct rays, specular reflections, diffuse scattering, and diffraction. Those properties are emulated by the Global Illumination (GI) model, a group of algorithms. Despite these advantages, this work restricts the rays to only one hop before reaching the respective Rx for sensing and communication simulations. This approach helps to avoid the cost and complexity of more comprehensive computations. Figure 5.1 shows a graphical example of the simulations and the distribution of the rays in the scenario. It can be seen how the rays are obstructed by the high density of clutter in the hall.

Finally, the parameters of communication and sensing rays, such as reflection coefficients (α_k^c, α_k^s), angles (θ_k^c, θ_k^s), and delays (τ_k^c, τ_k^s), are provided from the RT simulator. This data is processed using the following system model description.

5.3 System model

Considering a downlink communication scenario, the base station (BS) has multiple-antenna and a single-antenna in the UE. An ISAC BS transmits data symbols to the UE (i.e., the target) while collecting the mono-static sensing signal. This setup detects and tracks the UE, facilitating beam tracking by leveraging the principles of SAC.

5.3.1 Sensing signal model

Given a precoder $\mathbf{f}$, the mono-static sensing signal across N subcarriers can be given as

$$\mathbf{y}_n^{\text{sen}} = \mathbf{H}_n \mathbf{f} x_n + \mathbf{z}_n^s \in \mathbb{C}^{N_{\text{R}} \times 1} \ , \tag{5.1}$$

where x_n is the Orthogonal Frequency Division Multiplexing (OFDM) transmitted signal, $\mathbf{z}_n^s$ denotes the additive white Gaussian noise (AWGN) with zero mean with a variance σ_N^2. The sensing channel can be denoted as:

$$\mathbf{H}_n = \sum_{k=1}^{K} \alpha_k^s e^{-j2\pi n \Delta f \tau_k^s} \mathbf{a}_{\text{R}}(\theta_k^s) \mathbf{a}_{\text{T}}^{\top}(\theta_k^s) \in \mathbb{C}^{N_{\text{R}} \times N_{\text{T}}} \ , \tag{5.2}$$

where α_k^s is the complex channel gain, Δf denotes subcarrier spacing, and τ_k^s is the delay. The BS operates with uniform linear array (ULA), which has N_{T} transmit antennas and N_{R} receive antennas where θ_k^s is the Azimuth angle of Departure (AoD) and the Azimuth angle of Arrival (AoA). The transmit steering vector is the same as the receive steering vector given by the monostatic sensing configuration. Thus, both steering vectors, namely $\mathbf{a}_{\text{T}}(\theta_k^s)$ and $\mathbf{a}_{\text{R}}(\theta_k^s)$ can be denoted as:

$$\mathbf{a}(\theta_k^s) = [1, e^{-j\pi \sin(\theta_k^s)}, \ldots, e^{-j\pi(N_T - 1)\sin(\theta_k^s)}]^{\top}, \tag{5.3}$$

considering half-wavelength antenna spacing.

5.3.2 Communication signal model

In the case of the communication signal, a multiple input single output (MISO) downlink communication is assumed, and the received signal at the UE can be written as

$$y_n^{\text{com}} = (\mathbf{h}_n^{\text{com}})^{\top} \mathbf{f} x_n + z_n^c \in \mathbb{C} \ , \tag{5.4}$$

where

$$\mathbf{h}_n^{\text{com}} = \sum_{k=1}^{\widetilde{K}} \alpha_k^c e^{-j2\pi n \Delta f \tau_k^c} \mathbf{a}_{\text{T}}(\theta_k^c) \in \mathbb{C}^{N_{\text{T}} \times 1}. \tag{5.5}$$

The remaining notations have already been defined above. However, in this context, the notation "c" is introduced to distinguish communication-related parameters specifically.

5.4 Key performance indicators

The previous chapter highlighted that a crucial step in evaluating ISAC is determining the appropriate key performance indicator (KPI), which could vary depending on the use case. In the context of SAC, sensing information is utilized to design the communication precoder of the form

$$\mathbf{f} = \mathbf{a}_{\mathrm{T}}^{*}(\theta) \in \mathbb{C}^{N_{\mathrm{T}} \times 1}, \tag{5.6}$$

for a certain beamforming angle θ. The selection of the beamforming angle depends on the specific method. Discrete frames with duration T are considered, comprising beam training and data transmission. After beam training, a vector $\mathbf{f}$ is determined.

As in the previous chapter, the signal-to-noise ratio (SNR) is selected as the standard metric to compare conventional and new communication performance from this use case. By providing the quality of the received signal, the communication SNR at the UE is achieved after the beam training period and can, therefore, be denoted as

$$\mathrm{SNR}_{r,n} = \frac{P|(\mathbf{h}_n^{\mathrm{com}})^{\top}\mathbf{f}|^2}{\sigma_N^2} \ . \tag{5.7}$$

Since this use case aims to ensure high-quality communication, the effective data rate is a KPI for assessing the quality of service provided by the new ISAC performance. The effective data rate measures the amount of valuable data transmitted to the UE, crucial in Industrial Internet of Things (IIoT) applications. Therefore, given the SNR, the effective data rate can be formulated as follows:

$$R_{\mathrm{eff}} = \left(\frac{T-D}{T}\right) \sum_{n=1}^{N} \log_2(1 + \mathrm{SNR}_{r,n}), \tag{5.8}$$

where D is the time needed for beam training.

5.5 Beam training algorithms

To address the issue of how the number of passive scatterers influences beam misalignment in an InF environment, this section presents several beam training algorithms, including SAC approaches and the conventional communication-only methods. The effort focuses on designing a downlink precoder using sensing information. Since the UE moves over discrete time t, beam tracking or predictive beamforming might be implemented to enhance resource optimization.

5.5.1 Conventional beam training

Conventional beam training [89] has been selected as the baseline method (i.e., communication-only system) to compare proposal one. The algorithm aims to find the optimal receiving beamforming weight by looping the best SNR among all sampling angle directions. Consider a set of M beamforming directions $\mathbf{\Theta} = \{\theta_1, \ldots, \theta_M\}$ with corresponding precoders $\mathbf{f}_m = \mathbf{a}_{\mathrm{T}}^*(\theta_m)$.

Considering the channel is static during each time t, the corresponding received vector at the UE can be denoted as

$$y_{n,m}^{\mathrm{com}} = (\mathbf{h}_n^{\mathrm{com}})^\top \mathbf{f}_m x_{n,m} + z_{n,m}^{\mathrm{c}}. \tag{5.9}$$

The optimal precoder is selected by maximizing the received power

$$\hat{m} = \arg\max_m \sum_{n=1}^{N} |y_{n,m}^{\mathrm{com}}|^2, \tag{5.10}$$

$$\hat{\theta}^c = \theta_{\hat{m}}, \tag{5.11}$$

which is then used in (5.6) for beamforming for communication. This process occupies a certain amount of time $D = M/\Delta f$. Better estimation would be obtained as more time and resources are used to transmit the beams for scanning. However, this process could introduce a high overhead since, in each transmitted frame, the BS sends downlink pilots for beam training and then the data transmission.

5.5.2 Proposed method

According to the localization literature [100], obtaining a coarse estimate of the parameter and using it as a starting point for the process is essential. In this step, mono-static sensing can offer significant assistance without consuming communication resources. Nevertheless, estimating parameters can be complex for scenarios with many obstacles, such as InF, as the echoes from the user need to be more distinguishable from the rest of the echoes in the scenario. To this end, background subtraction is proposed as a subroutine in the proposed method.

Background subtraction

The estimation of the AoD or AoA based on background subtraction proceeds as follows:

1. *Learning stage:* The scenario is previously sensed *without the UE*. The received measurement echo signal at the BS can be expressed as

$$\mathbf{y}_{n,m}^{\text{ref}} = \tilde{\mathbf{H}}_n \mathbf{f}_m x_{n,m} + \mathbf{z}_{n,m}^{s} \in \mathbb{C}^{N_{\text{R}} \times 1} , \tag{5.12}$$

   where $\tilde{\mathbf{H}}_n$ is the sensed channel without considering the UE, i.e., considering echoes only from the rest of the scenario. The pairs $(\mathbf{f}_m, \mathbf{y}_{n,m}^{\text{ref}})$ are stored in a database. The selected beamforming directions cover a fine grid of angles.

2. *Inference stage:* Assuming that BS transmits with a precoder $\mathbf{f}$, the received signal can be formulated as in (5.1).

3. *Background subtraction:* Find the index m for which $\mathbf{f}_m$ is as close as possible to the current precoder $\mathbf{f}$, i.e.,

$$\hat{m} = \arg\min_{m} \|\mathbf{f} - \mathbf{f}_m\|. \tag{5.13}$$

   From the database, the corresponding $\mathbf{y}_{n,\hat{m}}^{\text{ref}}$ is selected to compute the subtracted signal:

$$\mathbf{y}_n^{\text{sub}} = \mathbf{y}_n^{\text{sen}} - \mathbf{y}_{n,\hat{m}}^{\text{ref}}. \tag{5.14}$$

4. *Selecting the best beam*: Finally, conventional beamforming is applied to estimate AoD/AoA at mono-static sensing. The best beam to transmit is selected in the angular range $\theta \in [-\pi/2, \pi/2]$. The best angle is obtained by maximizing the subtracted measurement signal $\mathbf{y}_n^{\text{sub}}$, as:

$$\hat{\theta}^{\text{sub}} = \arg\max_{\theta} \sum_{n=1}^{N} |\mathbf{a}_{\text{R}}^{*}(\theta) \mathbf{y}_n^{\text{sub}}|^2, \tag{5.15}$$

   where $\mathbf{a}_{\text{R}}(\theta)$ is the steering vector defined in (5.3).

To give a visual evaluation, Figure 5.2 [101] shows the background subtraction. The optimal angle is obtained as input for the following time step to construct the predictive beamforming.

Predictive beamforming

Since the UE is moving along a linear trajectory, the Kalman Filter (KF) algorithm can be applied to track the dynamic state information. This enables the precise prediction of the state of the UE, and this information might be utilized in constructing the predictive beamforming. To delve deeper into the

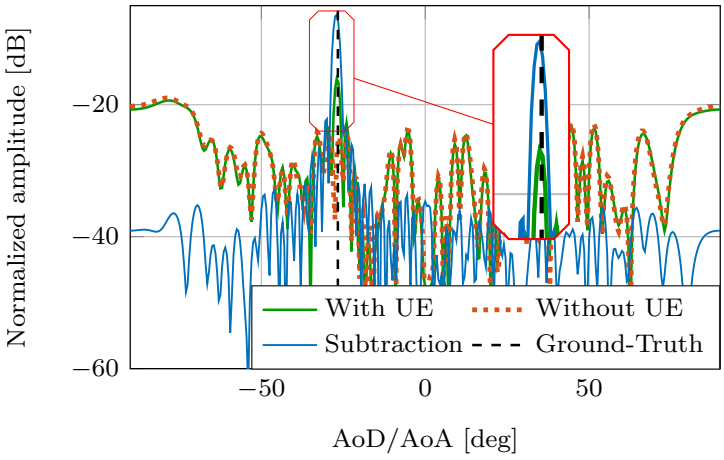

Figure 5.2: Beam selection estimation based on background subtraction

process, it is essential to establish an initial state. In this context, the estimated AoD obtained from conventional beam training at $t = 1$ (Section 5.5.1) is considered the initial state as $\hat{\mathbf{x}}_t = (\hat{\theta}^c, v)$, where $\mathbf{x}$ is the state vector filtered in every time step, and v is a preset constant velocity.

The state error covariance matrix should also be determined at the startup. Hence, it can be defined initially as $\mathbf{P} = \text{diag}(\bar{\sigma}_\theta^2, \bar{\sigma}_v^2)$, which would be naturally updated in every tth step. Then, the state vector is predicted using the state evolution model, which in this case is denoted as $\hat{\mathbf{x}}_{t|t-1} = \mathbf{F}\hat{\mathbf{x}}_{t-1}$, where $\mathbf{F}$ is the transition matrix defined by the system dynamics where acceleration has been ignored for simplicity. Next, the process noise covariance matrix is related to the uncertainty of the predictive results, which can be expressed as $\mathbf{Q} = \text{diag}(\sigma_\theta^2, \sigma_v^2)$.

Following Algorithm 1, another important aspect is the uncertainty information, also called measurement. This information obtains the desired state to update the following time steps. Since the uncertainty can be obtained through an independent system [102], this is where the background subtraction can be used. In this explanation, the estimated AoD from the background subtraction (5.15) at each time step is detonated as z_t, where the noise covariance R_t is a scalar determined by the variance of the ground truth data.

Algorithm 1 Predictive beamforming

Require: $t = 1$, perform conventional beam training to obtain $\hat{\theta}^c$.

1: Set the initial state as: $\hat{\mathbf{x}}_t = \begin{bmatrix} \hat{\theta}^c \\ v \end{bmatrix}$
2: **for** $t \in 2, 3, ...$ **do**
3: State prediction: $\hat{\mathbf{x}}_{t|t-1} = \mathbf{F}\hat{\mathbf{x}}_{t-1}$
4: Predicted state covariance matrix: $\mathbf{P}_{t|t-1} = \mathbf{F}\mathbf{P}_{t-1}\mathbf{F}^\top + \mathbf{Q}_{t-1}$
5: Kalman gain matrix: $\mathbf{K}_t = \mathbf{P}_{t|t-1}\mathbf{h}_t(\mathbf{h}_t^\top \mathbf{P}_{t|t-1}\mathbf{h}_t + R_t)^{-1}$
6: **switch do**
7: **case** Proposed method
8: $\mathrm{z}_t = \hat{\theta}_t^{\mathrm{sub}}$
9: **end case**
10: **case** Data association method
11: $\mathrm{z}_t = \arg\min_j |z_{j,t} - \mathbf{h}_t^\top \hat{\mathbf{x}}_{t|t-1}|$
12: **end case**
13: **end switch**
14: Innovation (pre-fit residual): $\tilde{\mathrm{y}}_t = \mathrm{z}_t - \mathbf{h}_t^\top \hat{\mathbf{x}}_{t|t-1}$
15: Update/correct state: $\hat{\mathbf{x}}_t = \hat{\mathbf{x}}_{t|t-1} + \mathbf{K}_t\tilde{\mathrm{y}}_t$
16: Update covariance matrix: $\mathbf{P}_t = (\mathbf{I} - \mathbf{K}_t\mathbf{h}_t) + \mathbf{P}_{t|t-1}$
17: The transmit beamforming vector is constructed by:
18: $\mathbf{f}_t = \mathbf{a}_{\mathrm{T}}^*(\hat{\theta}_t^{\mathrm{pre}}) \in \mathbb{C}^{N_{\mathrm{T}} \times 1}$, as (5.6) expressed, where $\hat{\theta}_t^{\mathrm{pre}}$ is the predicted
19: angle obtained from $\hat{\mathbf{x}}_t$ (line 15).
20: **end for**

5.5.3 Data association beam training

Tracking a single UE may be complicated for scenarios where background subtraction is not considered. Given the high clutter density in proposed subscenarios, multiple measurements/uncertainties can arise within the area stemming from multiple echoes. In a downlink scenario without uplink feedback from the UE, the BS might need to associate those UE echoes with the predictive state.

To this end, some extensions of linear KF [103] arise in conventional sensing applications. The nearest neighbor method [104] represents one of the most straightforward approaches, involving the BS in calculating the Euclidean distance between measurements and the predictive state. This method is also outlined in [52] as a beam association technique for multiple targets. Due to its significant presence in the literature, this paper selects it as a baseline method within the SAC framework to comprehensively compare with the proposed approach.

The process begins by identifying the most suitable measurement to achieve a reliable predictive state. Therefore, it is assumed that the BS can receive multiple candidate measurements $z_{j,t}$ from $j = 1, ..., J$ at every t. These J candidate measurements are chosen from the backscattered signal with a constant false alarm rate (CFAR) threshold. In this way, only measurements with similar and highest amplitudes are considered to compute the Euclidean distance between the current a priori prediction and the current observation. In Algorithm 1, line 10 defines the process mentioned above as a *case*, in which the closest measurement state would yield the smallest Euclidean distance, as is described in line 11.

5.6 Analysis and results

The previously described beam training algorithms deliver valuable results for the presented use case. In this section, simulations are performed with several assumptions taken into account. The analysis presented here is based on findings from [101].

The InF sub-scenarios described in Chapter 2, Section 2.2.1 have served as a basis to model the scenario for the RT tool. Specifically, the InF-Sparse High (InF-SH) and InF-Dense High (InF-DH) sub-scenarios are considered since the UE detection might perform better with the antenna BS higher than the clutter as a first assumption. Figure 5.3 shows each sub-scenario modeling considered for the simulations.

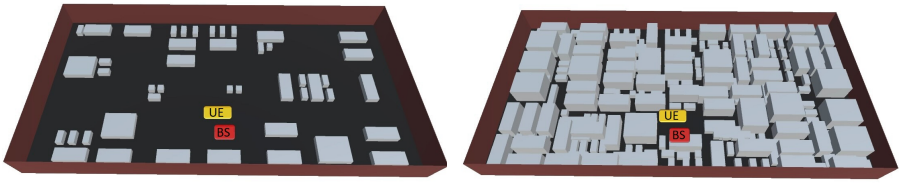

(a) Sparse High (b) Dense High

Figure 5.3: The 3GPP Indoor Factory sub-scenarios are replicated in the RT tool. The red square represents the BS, and the yellow square represents the UE

Walls, obstacles, and ground are constructed of concrete material. Meanwhile, the UE is made of metal since it is considered a mini Automatic Guided Vehicle (AGV). The AGV follows a straight-line trajectory of 10 meters in

front of the BS in Line of Sight (LoS). The acceleration is neglected in these cases since the simulations are snapshots at every time step. However, the ray generation has spatial consistency. The simulations are performed from this view, and the RT channel dataset is extracted. Table 5.1 summarizes the configuration parameters, and the following subsections further explain the benchmark and highlight the findings.

Parameters	**Value**
Frequency	28 GHz
Bandwidth	100 MHz
Transmit power	21 dBm
Noise variance (σ_N^2)	10^{-9}
N_T	64
Time frame (T)	1 ms
Algorithm 1	
σ_θ	1 [deg]
σ_v	0.01 [deg/s]
$\bar{\sigma}_\theta$	Based on 3dB beam width
$\bar{\sigma}_v$	0.01 [deg/s]
Scenario layout	
Room size (WxL)	L = 120 m, W = 60 m
Ceiling height	10 m
BS antenna height	8 m
UE (WxLxH)	0.2 x 0.2 x 0.2 m
Clutter density	Low clutter density: 20% High clutter density 60%
Clutter height	Low clutter density: 2 m High clutter density: 6 m
Distance between clutter	Low clutter density: 10 m High clutter density: 2 m
UE Trajectory	10 m
Time steps	100

Table 5.1: Simulation assumptions for Sensing-assisted Beam Training use case

5.6.1 Benchmark descriptions

Although the beam training algorithms have been explained in previous sections, detailed descriptions of the different performances to be compared are included here to help readers better understand the results. The following tag name is used:

- *Perfect knowledge (PK)*: This is the ideal case where the BS can obtain the UE location, neglecting the overhead of downlink and uplink pilots in SAC systems.
- *Conventional beam training (CBT)*: The beam training from a communication-only system is determined here, explained in Section 5.5.1.
- *SAC - no method (SAC-NM)*: This alternative is the optimal beams by finding the angle that maximizes the output of the spatial matched filter applied to the backscattered sensing signal in (5.1) at every time step without background subtraction, i.e.,

$$\hat{\theta}^{\text{sen}} = \arg\max_{\theta} \sum_{n=1}^{N} |\mathbf{a}_{\text{R}}^{*}(\theta)\mathbf{y}_{n}^{\text{sen}}|^{2}. \tag{5.16}$$

  This has opted to illustrate the case of misaligned beamforming without filtering since it estimates the AoD without any predictive method.
- *SAC - Data Association (SAC-DA)*: This benchmark is the predictive beamforming, which deals with multiple measurements, such as the Data Association in Section 5.5.3.
- *SAC - Background Subtraction (SAC-BS)*: This is the proposed solution for this use case described in Section 5.5.2. The background subtraction and predictive beamforming are considered.

5.6.2 Numerical results

The levels of SNR over the time steps for all the aforementioned alternatives are illustrated in Figure 5.4. In both sub-scenarios, the behavior of *PF* and *CBT* exhibits some similarities. In conventional communication, beam training aims to establish robust links using highly directional beams that precisely align the transmitter beam with the UE. However, this process might introduce high overhead that affects data transmission resources.

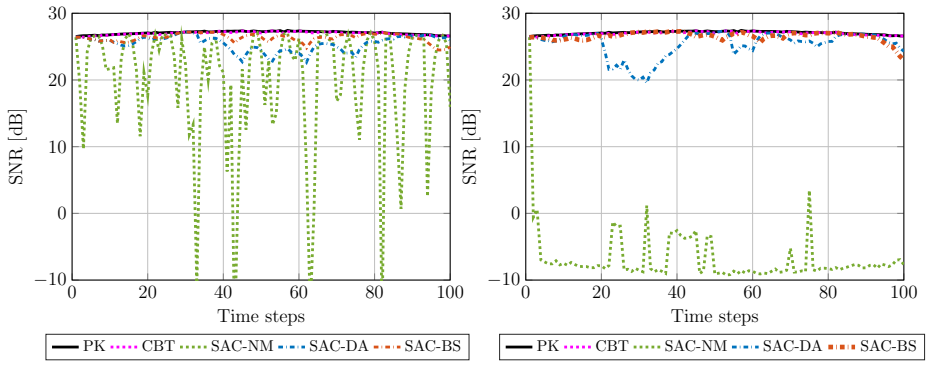

(a) Sparse High (b) Dense High

Figure 5.4: SNR performance for the proposed method and benchmark cases

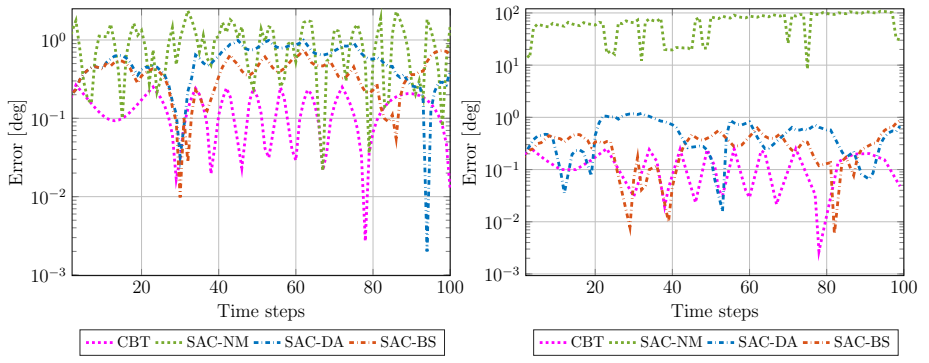

(a) Sparse High (b) Dense High

Figure 5.5: Error performance to give a visual correlation with the low levels of SNR

The performance of *SAC-NM* yields low SNR levels since the highest power selects the optimal beam. The highest power echo here might be a nearby obstacle, such as the ground. This underscores the importance of incorporating

specialized techniques, such as predictive beamforming and background subtraction, to leverage sensing information effectively.

In addition, although the *SAC-DA* obtains a significant level of SNR, the *SAC-BS* slightly overcomes it. This behavior demonstrates that background subtraction may leverage a strong link in SAC performance.

A noteworthy aspect is that the SNR levels are directly related to detection accuracy, i.e., the detection error. This implies that the accuracy of the information used to direct the transmitted beam must be exceptionally high. Thus, examining the error between the ground truth and the estimated or predicted information is essential. Figure 5.5 exhibits a correlation between high error levels and low SNR levels in both sub-scenarios. Even though the *Dense High* sub-scenario is the most affected, *SAC-BS* has lower error levels in more time steps than *SAC-DA*.

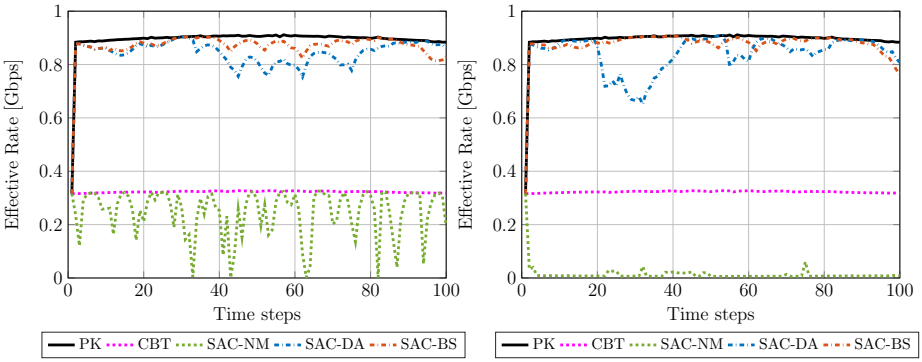

(a) Sparse High

(b) Dense High

Figure 5.6: Effective data rate performance for the proposed method and benchmark cases

Concerning data transmission resources, the overhead is another critical aspect that needs to be analyzed. Figure 5.6 shows the effective data rate over time steps. Assuming the overhead of conventional beam training should be considered at the first time step, both *SAC-DA* and the *SAC-BS* obtain high levels of effective data rate. Since both alternatives consider predictive beamforming, they disregard overhead for the remainder of the time. This behavior offers promising data rates under their respective conditions, demonstrating that SAC with predictive beamforming can effectively provide a communication link operating at almost 0.9 gigabit-per-second (Gbps).

5.7 Conclusions

This chapter has examined the potential of ISAC systems in an industrial use case. The findings are based on quasi-realistic measurements obtained using an RT tool, focusing on developing one SAC technique: sensing-assisted beam training. Given the complexity of factory environments with high clutter density, a strategic technique like background subtraction has been utilized. This approach has been developed to mitigate all possible non-target/UE sensing interference. When applied to the predictive beamforming algorithm, this has highlighted the efficacy of user detection and prediction.

The results showcased that while conventional beam training methods can introduce significant overhead, SAC, especially with background subtraction, can achieve superior SNR levels and effective data rates. In this manner, the IIoT application would benefit since high-reliability communication is paramount in such environments.

This approach has contributed to the pioneering use of background subtraction within the ISAC framework. Specifically, it could be employed in other algorithms, such as for detecting distance, velocity, and positioning.

Chapter 6

Conclusions and Future Work

6.1 Concluding remarks

With the integration of smart factories into wireless networks, particularly Fifth Generation (5G) and Next Generation Communication Systems (NGCS), Industrial Internet of Things (IIoT) applications have become one of the primary focus over the last few years. However, these applications often operate in cluttered environments where signal propagation is easily degraded. This problem affects the communications system and disrupts optimal factory production. This thesis identifies several challenges in channel modeling and system characterization within this framework.

A channel model is essential to construct any wireless system, as mandated by the International Telecommunications Union (ITU). However, it was not until 2019, just one year before the global deployment of 5G, that a channel model for industrial scenarios was published and considered. A study was conducted on the Third Generation Partnership Project (3GPP) channel model for Indoor Factory (InF) scenarios (Chapter 2) to analyze the situation of this framework.

This study has led to several notable conclusions. Firstly, the channel model was published early in Release 16, leaving industrial scenarios out of the 5G simulation scope and under-explored. Besides, conventional channel modeling has some limitations, such as less accurate characterization of essential parameters and failure to capture the complexity of industrial environments fully.

This trend, combined with the increasing interest in exploring innovative alternatives for the Sixth Generation (6G), indicates a growing inclination to develop and propose a new technology better aligned with the industry's demanding requirements. This technology could be Integrated Sensing and Communications (ISAC) systems. Despite the limited contributions related to industrial scenarios, this Thesis has argued that ISAC systems have the potential to enhance communication links in such environments significantly. Therefore, Chapter 3 introduced a channel model for ISAC systems as a first step in this novel exploration.

The 3GPP channel model has been considered the basis for constructing the sensing mono-static channel model for an ISAC system. Despite its limitations, this model remains the most recognized and standardized. During the modeling of ISAC channel, it has been discovered that the correlation between communication and sensing channels is a fundamental aspect to be considered in geometry-based stochastic model (GBSM).

Using the approach above, this Thesis has taken a step further by assessing the viability of ISAC systems in industrial environments, with the next step focused on developing a methodology to evaluate the effectiveness of these systems. The methodology presented in Chapter 4 is directly related to the key factors involved in ISAC channel modeling. It outlines the steps needed to develop a comprehensive system and guides the evaluation of its performance. The results suggested that key features such as the correlation between communication and sensing channels and spatial consistency in ISAC systems are critical aspects that must be considered.

Although the mentioned findings come from a simple use case, to study the viability of ISAC, it would be necessary to test scenarios in a quasi-realistic industrial environment. Chapter 5 presents a more complete ISAC industrial use case and introduces a new solution to improve detection and enhance communication systems. Background subtraction is the solution applied in sensing-assisted beam training applications.

The results have shown that background subtraction addresses the challenges of multiple obstructions, particularly in industrial scenarios. This technique demonstrates that sensing predictive beamforming enhances communication performance, specifically regarding effective data rate. This approach underscores the argument that ISAC is a suitable technology for InF, particularly under the conditions provided by this technique.

The following items comprehensively analyze how this Thesis has addressed the hypotheses formulated in Chapter 1.

- Hypothesis 1: The emergence of 6G technologies may have caused the 3GPP-InF channel model to not be fully exploited. This hypothesis may

require further research to be fully validated. Nevertheless, this Thesis has explored the 3GPP channel model for industrial scenarios, revealing certain limitations in fully addressing the inherent complexity of factory environments. Therefore, the following hypothesis suggests that the adoption of an alternative technology may be the most effective solution.

- Hypothesis 2: ISAC systems might open new paradigms for industrial environments. It is important to develop an ISAC channel model to evaluate it. This hypothesis has been driven by the initial step in the construction of any wireless system: channel modeling. Since ISAC is a key trend of 6G, developing a channel model for this system is crucial for future evaluations and testing, not only for industrial use cases but also for other scenarios. This Thesis has presented the novel ISAC channel model using the 3GPP channel model as a basis.

- Hypothesis 3: Developing an evaluation methodology gives criteria to assess an ISAC system in any scenario. This hypothesis is supported by the need for a methodology to evaluate the emerging ISAC system. As the literature lacks established evaluation methodologies, developing technical criteria like those used by the ITU in conventional standardization is crucial. Within this methodology, it was identified that characteristics such as the correlation between communication and sensing channels and spatial consistency are essential factors to consider when constructing an ISAC system.

- Hypothesis 4: ISAC may potentially meet the industry's needs by leveraging sensing to enhance communication systems. This Thesis explores this hypothesis through a use case set in a quasi-realistic industrial scenario. The findings suggest that sensing information, achieved through the background subtraction technique, can significantly enhance communication performances, particularly regarding effective data rate. Employing a predictive beamforming algorithm minimizes the need for pilot signal transmission, allowing communication resources to be dedicated entirely to data transmission.

6.2 Future research lines

Although this Thesis has primarily focused on the physical layer, specifically channel modeling, and has demonstrated promising ISAC results in industrial scenarios, there remains significant scope for further research. This work opens the door to the following research directions:

- Building on the extensive research in link-level simulation presented in this Thesis, the next logical step is to advance toward system-level simulation. This process might begin with investigating and implementing physical layer abstraction models, which have been recommended by the ITU to mitigate the high computational costs associated with conventional communication systems simulations. Since ISAC involves the coexistence of two systems, it is crucial to identify the key performance indicator (KPI) to abstract for each system, tailored to the specific requirements of the use case.

- ISAC's innovative vision for the industrial sector opens the door to exploring additional use cases, particularly those focused on analyzing communication latency, reliability, availability, and connection density, which are inherent requirements in IIoT applications.

- Regarding sensing configurations, this Thesis has focused on mono-static sensing as a first approach. However, bi-static or multi-static sensing may be further studied. Having multiple base station (BS) for sensing may improve the environment's prior knowledge, i.e., having the channel between the BS and other points in the scenario; therefore, as the communication system gains more information about the scenario, its ability to make informed decisions and enhance performance increases. For instance, this increased awareness might optimize beamforming alignments and inform whether to use pencil beamforming or adjust beamwidth, depending on the target size.

- Sensing-assisted resource allocation could be a convincing application of ISAC in industrial environments. Conventionally, resource allocation in communication-only systems primarily focuses on power control, spectral efficiency, energy efficiency, and spectrum allocation. However, by incorporating sensing and prior knowledge of the scenario, the spectrum can be more efficiently reused, leading to higher performance and increased data rates compared to communication-only systems. Mutual interference may arise with a high density of users or targets, as in such scenarios. Knowing the users' specific requirements and estimating their location or trajectory through sensing echo signals makes it possible to design tailored bandwidth allocation schemes for each user based on the available spectrum.

- For the sake of simplicity, this Thesis has not accounted for Doppler's effects in channel modeling. However, future research should improve sensing algorithms to incorporate spatial consistency models that accommodate high velocities and mobility, similar to those used in vehicular

scenarios. This addition would enhance the accuracy and effectiveness of such algorithms.

- The background subtraction technique has demonstrated its effectiveness and can be extended to other sensing algorithms, such as distance estimation, positioning, and velocity estimation in vehicular scenarios. Its applicability is not limited to cluttered environments, paving the way for further research in various scenarios.

Appendix A

3GPP Spatial Consistency Model

Procedure A of the Spatial Consistency (SC) model presented in the Third Generation Partnership Project (3GPP) Technical Report (TR) 38.901 [65] modifies the stepwise method to generate a radio communication channel by replacing the operations to generate small-scale parameters (SSPs). On the one hand, equations to generate cluster delays and angles in steps 5 and 7 in the 3GPP geometry-based stochastic model (GBSM) now consider the velocity vector of the receiver (Rx), $\mathbf{v}_{\mathrm{rx}}$, and the time elapsed between channel realizations, Δt, to update delays and angles from the previous ones, rather than generating new, uncorrelated sets of these parameters derived from probability distributions.

On the other hand, random variables used in generating other SSPs that are still calculated in the same way are conveniently treated to ensure that they are correlated to those used in a previous channel realization so that the corresponding SSPs will also be correlated. The changes introduced to the standard procedure are described below.

A.1 Generate updated cluster delays

The following method replaces Step 5 of the 3GPP GBSM. At the initial instant, t_0, cluster delays are calculated as

$$\tilde{\boldsymbol{\tau}}_n\left(t_k\right) = \boldsymbol{\tau}_n\left(t_0\right) + \tau_\Delta\left(t_0\right) + \frac{d_{3\mathrm{D}}\left(t_0\right)}{c}, \tag{A.1}$$

where $\boldsymbol{\tau}_n(t_0)$ are the cluster delays calculated as in Step 5 of the standard procedure, $\tau_\Delta(t_0)$ is either 0 in Line of Sight (LoS) condition or the minimum of non-normalized delays generated earlier, $\boldsymbol{\tau}'_n(t_0)$, in Non Line of Sight (NLoS), d_{3D} denotes the Three Dimensions (3D) distance between transmitter (Tx) and Rx, and c is the speed of light. Then, at the k_{th} time epoch, t_k, cluster delays are updated as

$$\tilde{\boldsymbol{\tau}}_n(t_k) = \tilde{\boldsymbol{\tau}}_n(t_{k-1}) - \frac{\hat{\mathbf{r}}_{\mathrm{rx},n}(t_{k-1})^T \mathbf{v}_{\mathrm{rx}}(t_{k-1})}{c}\Delta t, \tag{A.2}$$

where $\hat{\mathbf{r}}_{\mathrm{rx},n}(t_{k-1})^T$ is the transpose of the spherical unit vector, which is defined as

$$\hat{\mathbf{r}}_{\mathrm{rx},n}(t_{k-1}) = \begin{bmatrix} \sin(\theta_{n,\mathrm{ZOA}}(t_{k-1}))\cos(\phi_{n,\mathrm{AOA}}(t_{k-1})) \\ \sin(\theta_{n,\mathrm{ZOA}}(t_{k-1}))\sin(\phi_{n,\mathrm{AOA}}(t_{k-1})) \\ \cos(\theta_{n,\mathrm{ZOA}}(t_{k-1})) \end{bmatrix}. \tag{A.3}$$

In (A.3), $\theta_{n,\mathrm{ZOA}}$ and $\phi_{n,\mathrm{AOA}}$ are the angles of arrival in the elevation and azimuth dimensions are specific to each cluster, respectively. Finally, the delay normalization step is replaced by

$$\boldsymbol{\tau}_n(t_k) = \tilde{\boldsymbol{\tau}}_n(t_k) - \min\left(\{\tilde{\boldsymbol{\tau}}_n(t_k)\}_{n=1}^N\right). \tag{A.4}$$

The normalized delays are then used in the cluster powers generation (Step 6 of the 3GPP procedure).

A.2 Generate updated cluster departure and arrival angles

The following method replaces the method to generate cluster departure and arrival angles described in Step 7 of the 3GPP GBSM. At the beginning of the simulation, cluster delays are calculated as in the standard procedure. Then, at time t_k, cluster arrival angles in the azimuth and elevation dimensions are updated as

$$\begin{aligned} \boldsymbol{\phi}_{n,\mathrm{AOA}}(t_k) = \boldsymbol{\phi}_{n,\mathrm{AOA}}(t_{k-1}) \\ - \frac{\mathbf{v}_{\mathrm{rx}}(t_{k-1})^T \hat{\boldsymbol{\phi}}}{c \cdot \tilde{\boldsymbol{\tau}}_n(t_{k-1}) \sin(\boldsymbol{\theta}_{n,\mathrm{ZOA}}(t_{k-1}))}\Delta t, \end{aligned} \tag{A.5}$$

$$\boldsymbol{\theta}_{n,\mathrm{ZOA}}(t_k) = \boldsymbol{\theta}_{n,\mathrm{ZOA}}(t_{k-1}) - \frac{\mathbf{v}_{\mathrm{rx}}(t_{k-1})^T \hat{\boldsymbol{\theta}}}{c \cdot \tilde{\boldsymbol{\tau}}_n(t_{k-1})}\Delta t, \tag{A.6}$$

with $\tilde{\boldsymbol{\tau}}_n(t_{k-1})$ being the non-normalized spatially consistent cluster delays calculated in (A.2). $\hat{\boldsymbol{\phi}}$ and $\hat{\boldsymbol{\theta}}$ are the spherical unit vectors defined as

$$\hat{\boldsymbol{\phi}} = \begin{bmatrix} -\sin\left(\boldsymbol{\phi}_{n,\mathrm{AOA}}(t_{k-1})\right) \\ \cos\left(\boldsymbol{\phi}_{n,\mathrm{AOA}}(t_{k-1})\right) \\ 0 \end{bmatrix}, \tag{A.7}$$

$$\hat{\boldsymbol{\theta}} = \begin{bmatrix} \cos\left(\boldsymbol{\phi}_{n,\mathrm{AOA}}(t_{k-1})\right)\cos\left(\boldsymbol{\theta}_{n,\mathrm{ZOA}}(t_{k-1})\right) \\ \cos\left(\boldsymbol{\theta}_{n,\mathrm{ZOA}}(t_{k-1})\right)\sin\left(\boldsymbol{\phi}_{n,\mathrm{AOA}}(t_{k-1})\right) \\ -\sin\left(\boldsymbol{\theta}_{n,\mathrm{ZOA}}(t_{k-1})\right) \end{bmatrix}. \tag{A.8}$$

Similarly to (A.5) and (A.6), cluster departure angles are updated as

$$\begin{aligned} \boldsymbol{\phi}_{n,\mathrm{AOD}}(t_k) = \boldsymbol{\phi}_{n,\mathrm{AOD}}(t_{k-1}) \\ + \frac{\mathbf{v}'_{n,\mathrm{rx}}(t_{k-1})^T \hat{\boldsymbol{\phi}}}{c \cdot \tilde{\boldsymbol{\tau}}_n(t_{k-1}) \sin\left(\boldsymbol{\theta}_{n,\mathrm{ZOD}}(t_{k-1})\right)} \Delta t, \end{aligned} \tag{A.9}$$

$$\boldsymbol{\theta}_{n,\mathrm{ZOD}}(t_k) = \boldsymbol{\theta}_{n,\mathrm{ZOD}}(t_{k-1}) + \frac{\mathbf{v}'_{n,\mathrm{rx}}(t_{k-1})^T \hat{\boldsymbol{\theta}}}{c \cdot \tilde{\boldsymbol{\tau}}_n(t_{k-1})} \Delta t, \tag{A.10}$$

where $\hat{\boldsymbol{\phi}}$ and $\hat{\boldsymbol{\theta}}$ are the spherical unit vectors in (A.7) and (A.8), but replacing arrival angles with $\phi_{n,\mathrm{AOD}}(t_{k-1})$ and $\boldsymbol{\theta}_{n,\mathrm{ZOD}}(t_{k-1})$. $\mathbf{v}'_{n,\mathrm{rx}}$ is a per cluster transformation of the Rx velocity vector given by

$$\mathbf{v}'_{n,\mathrm{rx}}(t_{k-1}) = \begin{cases} \mathbf{v}_{\mathrm{rx}}(t_{k-1}) & \text{for LoS} \\ \mathbf{R}_{n,\mathrm{rx}} \cdot \mathbf{v}_{\mathrm{rx}}(t_{k-1}) & \text{for NLoS} \end{cases} \tag{A.11}$$

with $\mathbf{R}_{n,\mathrm{rx}}$ being a combination of rotation matrices defined in the SC model (Procedure A).

A.3 Generate correlated random variables

Whereas cluster delays and angles follow a different procedure to be calculated, the rest of SSPs, i.e., cluster powers, cross-polarization power ratios (XPR), and initial random phases, are generated following Steps 6, 9, and 10 of the 3GPP GBSM, respectively. However, to ensure that these SSPs are also spatially consistent, it is necessary to correlate the random variables used in their calculation. The generation of spatially consistent cluster and ray-specific random variables is based on the distance-dependent exponential auto-correlation function given by

$$R(\Delta x) = e^{-\frac{|\Delta x|}{d_{cor}}}, \tag{A.12}$$

where $|\Delta x|$ is the Two Dimensions (2D) distance from the last position in which the channel was updated, and d_{cor} is the correlation distance, a specific parameter to each of the scenarios defined in the 3GPP GBSM. Once the auto-correlation is calculated, a random variable, y_k, correlated to its previous realization, y_{k-1}, with correlation R can be generated as follows:

$$y_k = R(\Delta x)y_{k-1} + \sqrt{1 - R^2}z, \quad z \sim N(0, 1). \tag{A.13}$$

In (A.13), it is assumed that y is a random variable drawn from the standard Gaussian distribution. However, suppose random variables from other probability distributions are needed. For instance, random variables drawn from a uniform distribution are assigned as random phases of each ray. They can be obtained by applying known transformations to the above result.

Moreover, other considerations when implementing the SC model include sorting the delays as described in Step 5 of the 3GPP GBSM after applying the SC procedure and keeping the sign of the cluster angles generated at the beginning of the simulation throughout it. The random coupling of rays performed in Step 8 and sub-cluster delays do not change either.

References

[1] V. Pereira and T. Sousa, "Evolution of Mobile Communications: from 1G to 4G," *Department of Informatics Engineering of the University of Coimbra, Portugal*, vol. 4, pp. 20–0, 2004.

[2] A. Osseiran, J. F. Monserrat, and P. Marsch, *5G Mobile and Wireless Communications Technology*. Cambridge University Press, 2016.

[3] T. Jiang, J. Zhang, P. Tang, L. Tian, Y. Zheng, J. Dou, H. Asplund, L. Raschkowski, R. D'Errico, and T. Jämsä, "3GPP Standardized 5G Channel Model for IIoT Scenarios: A Survey," *IEEE Internet of Things Journal*, vol. 8, no. 11, pp. 8799–8815, 2021.

[4] M. A. Yülek and M. A. Yülek, "The industrialization process: A streamlined version," *How Nations Succeed: Manufacturing, Trade, Industrial Policy, and Economic Development*, pp. 171–182, 2018.

[5] K. Zhou, T. Liu, and L. Zhou, "Industry 4.0: Towards future industrial opportunities and challenges," in *2015 12th International conference on fuzzy systems and knowledge discovery (FSKD)*. IEEE, 2015, pp. 2147–2152.

[6] G. Aceto, V. Persico, and A. Pescapé, "A survey on information and communication technologies for Industry 4.0: State-of-the-art, taxonomies, perspectives, and challenges," *IEEE Communications Surveys & Tutorials*, vol. 21, no. 4, pp. 3467–3501, 2019.

[7] F. Zezulka, P. Marcon, I. Vesely, and O. Sajdl, "Industry 4.0–An Introduction in the phenomenon," *IFAC-PapersOnLine*, vol. 49, no. 25, pp. 8–12, 2016.

[8] ITU-R, "Guidelines for evaluation of radio interface technologies for IMT-2020," ITU, ITU-R M. 2412-0, 2017.

[9] U. Farooq and G. M. Rather, "Millimeter wave (MMW) communications for fifth generation (5G) mobile networks," in *Progress in Advanced Computing and Intelligent Engineering*. Springer, 2019, pp. 97–106.

[10] F. Lemic, J. Martin, C. Yarp, D. Chan, V. Handziski, R. Brodersen, G. Fettweis, A. Wolisz, and J. Wawrzynek, "Localization as a feature of mmWave communication," in *2016 International Wireless Communications and Mobile Computing Conference (IWCMC)*. IEEE, 2016, pp. 1033–1038.

[11] Federal Communications Commission, "Wireless E911 location accuracy requirements," *FCC-15-9, Ps Docket*, no. 07-114, 2015.

[12] F. Che, Q. Z. Ahmed, P. I. Lazaridis, P. Sureephong, and T. Alade, "Indoor Positioning System (IPS) Using Ultra-Wide Bandwidth (UWB)—For Industrial Internet of Things (IIoT)," *Sensors*, vol. 23, no. 12, p. 5710, 2023.

[13] 3GPP TSG RAN, "Study on NR positioning support (Release 16)," 3GPP, Tech. Rep. 38.855 V16.0.0, Mar 2019.

[14] S. Parkvall, Y. Blankenship, R. Blasco, E. Dahlman, G. Fodor, S. Grant, E. Stare, and M. Stattin, "5G NR Release 16: Start of the 5G evolution," *IEEE Communications Standards Magazine*, vol. 4, no. 4, pp. 56–63, 2020.

[15] E. S. Lohan, M. Koivisto, O. Galinina, S. Andreev, A. Tolli, G. Destino, M. Costa, K. Leppanen, Y. Koucheryavy, and M. Valkama, "Benefits of positioning-aided communication technology in high-frequency industrial IoT," *IEEE Communications Magazine*, vol. 56, no. 12, pp. 142–148, 2018.

[16] S. Gimenez, S. Roger, P. Baracca, D. Martín-Sacristán, J. F. Monserrat, V. Braun, and H. Halbauer, "Performance evaluation of analog beamforming with hardware impairments for mmw massive mimo communication in an urban scenario," *Sensors*, vol. 16, no. 10, 2016. [Online]. Available: https://www.mdpi.com/1424-8220/16/10/1555

[17] A. Shahmansoori, G. E. Garcia, G. Destino, G. Seco-Granados, and H. Wymeersch, "5G position and orientation estimation through millimeter wave MIMO," in *2015 IEEE Globecom Workshops (GC Wkshps)*. IEEE, 2015, pp. 1–6.

[18] I. Da Silva, S. El Ayoubi, M. Boldi, O. Bulakci, P. Spapis, M. Schellmann, J. F. Monserrat, T. Rosowski, G. Zimmermann, D. Telekom, and M. Tesanovic, "5G RAN architecture and functional design. METIS II white paper." *METIS-II*, 2016.

[19] ITU-R, "Minimum requirements related to technical performance for IMT-2020 radio interface(s)," ITU, ITU-R M. 2410-0, 2017.

[20] S. Jaeckel, L. Raschkowski, K. Börner, L. Thiele, F. Burkhardt, and E. Eberlein, "QuaDRiGa-quasi deterministic radio channel generator, user manual and documentation," Fraunhofer Heinrich Hertz Institute, Tech. Rep. v2. 0.0, 2017.

[21] V. Nurmela, A. Karttunen, A. Roivainen, L. Raschkowski, V. Hovinen, J. Y. EB, N. Omaki, K. Kusume, A. Hekkala, R. Weiler *et al.*, "Deliverable D1. 4 METIS channel models," *Proc. Mobile Wireless Commun. Enablers Inf. Soc.(METIS)*, p. 1, 2015.

[22] K. Haneda, S. Nguyen, A. Karttunen, J. Järveläinen, A. Bamba, R. D'Errico, J. Medbo, F. Undi, S. Jaeckel, N. Iqbal, J. Luo, M. Rybakowski, C. Diakhate, J.-M. Conrat, A. Naehring, S. Wu, A. Goulianos, E. Mellios, and M. Peter, "Measurement results and final mmmagic channel models," HHI, Berlin, Germany, Tech. Rep. H2020-ICT-671650-mmMAGIC/D2.2, May 2017.

[23] M. Zhu, G. Eriksson, and F. Tufvesson, "The COST 2100 Channel Model: Parameterization and Validation Based on Outdoor MIMO Measurements at 300 MHz," *IEEE Transactions on Wireless Communications*, vol. 12, no. 2, pp. 888–897, 2013.

[24] 3GPP TSG RAN, "Study on Channel Model for Frequencies from 0.5 to 100 GHz (Release 16)," 3GPP, Tech. Rep. 38.901 V16.0.0, Oct 2019.

[25] Z. Yu, Z. Liu, F. Meyer, A. Conti, and M. Z. Win, "Localization Based on Channel Impulse Response Estimates," in *2020 IEEE/ION Position, Location and Navigation Symposium (PLANS)*, 2020, pp. 1014–1021.

[26] X. Li, H. Xiao, Y. Wang, Q. Luo, X. Yang, X. Tu, C. Jiang, and B. Han, "New Radio Indoor Positioning Enhancement via Deep Learning Methods," in *2022 International Wireless Communications and Mobile Computing (IWCMC)*, 2022, pp. 205–210.

[27] G. Torsoli, M. Z. Win, and A. Conti, "Selection of Reference Base Station for TDOA-based Localization in 5G and Beyond IIoT," in *2022 IEEE Globecom Workshops (GC Wkshps)*, 2022, pp. 317–322.

[28] G. Torsoli, M. Z. Win, and A. Conti, "Blockage Intelligence in Complex Environments for Beyond 5G Localization," *IEEE Journal on Selected Areas in Communications*, vol. 41, no. 6, pp. 1688–1701, 2023.

[29] L. Terças, H. Alves, C. H. M. de Lima, and M. Juntti, "Bayesian-Based Indoor Factory Positioning Using AOA, TDOA and Hybrid Measurements," *IEEE Internet of Things Journal*, pp. 1–1, 2024.

[30] J. Nikonowicz, A. Mahmood, M. I. Ashraf, E. Björnson, and M. Gidlund, "Indoor positioning trends in 5G-Advanced: Challenges and solution towards centimeter-level accuracy," *arXiv preprint arXiv:2209.01183*, 2022.

[31] A. Fouda, R. Keating, and H.-S. Cha, "Toward cm-Level Accuracy: Carrier Phase Positioning for IIoT in 5G-Advanced NR Networks," in *2022 IEEE 33rd Annual International Symposium on Personal, Indoor and Mobile Radio Communications (PIMRC)*, 2022, pp. 782–787.

[32] A. A. Esswie and K. I. Pedersen, "Analysis of Outage Latency and Throughput Performance in Industrial Factory 5G TDD Deployments," in *2021 IEEE 93rd Vehicular Technology Conference (VTC2021-Spring)*, 2021, pp. 1–6.

[33] C.-T. Liu and J.-Y. Pan, "Worst-M CQI Reporting and MCS Selection for Indoor Factory Scenario," in *2021 IEEE Conference on Standards for Communications and Networking (CSCN)*, 2021, pp. 26–29.

[34] M. U. Sheikh, K. Ruttik, R. Jäntti, and J. Hämäläinen, "Distributed Antenna System in 3GPP Specified Industrial Environment," in *2021 IEEE 93rd Vehicular Technology Conference (VTC2021-Spring)*, 2021, pp. 1–6.

[35] C. S. M. García, R. L. Bruun, T. B. Sørensen, N. K. Pratas, T. K. Madsen, J. Lianghai, and P. Mogensen, "Cooperative Resource Allocation for Proximity Communication in Robotic Swarms in an Indoor Factory," in *2021 IEEE Wireless Communications and Networking Conference (WCNC)*, 2021, pp. 1–6.

[36] M. Schmieder, T. Eichler, S. Wittig, M. Peter, and W. Keusgen, "Measurement and Characterization of an Indoor Industrial Environment at 3.7 and 28 GHz," in *2020 14th European Conference on Antennas and Propagation (EuCAP)*, 2020, pp. 1–5.

[37] Y. Guan, J. Zhang, L. Tian, P. Tang, and T. Jiang, "A Comparative Study for Indoor Factory Environments at 4.9 and 28 GHz," in *2020 14th*

European Conference on Antennas and Propagation (EuCAP), 2020, pp. 1–5.

[38] Z. Ying, T. Jiang, P. Tang, J. Zhang, and L. Tian, "Analysis Of Delay Characteristics At 4.9 Ghz And 28 Ghz In An Indoor Industrial Scenario," in *2020 14th European Conference on Antennas and Propagation (EuCAP)*, 2020, pp. 1–5.

[39] Y. Wang, T. Jiang, P. Tang, Q. Song, X. Zhao, L. Tian, J. Zhang, and B. Liu, "Measurement-based Analysis and Modeling of Channel Characteristics in an Industrial Scenario at 28 GHz," in *2021 IEEE 94th Vehicular Technology Conference (VTC2021-Fall)*, 2021, pp. 1–5.

[40] B. B. Cebecioglu, Y. K. Mo, S. Dinh-Van, D. S. Fowler, A. Evans, A. Sivanathan, E. Kampert, B. Ahmad, and M. D. Higgins, "Sub-6 GHz Channel Modeling and Evaluation in Indoor Industrial Environments," *IEEE Access*, vol. 10, pp. 127 742–127 753, 2022.

[41] D. Chizhik, J. Du, R. A. Valenzuela, D. Samardzija, S. Kucera, D. Kozlov, R. Fuchs, J. Otterbach, J. Koppenborg, P. Baracca, M. Doll, I. Rodriguez, R. Feick, and M. Rodriguez, "Directional Measurements and Propagation Models at 28 GHz for Reliable Factory Coverage," *IEEE Transactions on Antennas and Propagation*, vol. 70, no. 10, pp. 9596–9606, 2022.

[42] ITU-R, "Future technology trends of terrestrial International Mobile Telecommunications systems towards 2030 and beyond," ITU, ITU-R M. 2516-0, Nov 2022.

[43] E. Y. Menta, N. Malm, R. Jäntti, K. Ruttik, M. Costa, and K. Leppänen, "On the performance of AoA-based localization in 5G ultra-dense networks," *IEEE Access*, vol. 7, pp. 33 870–33 880, 2019.

[44] ITU-R, "Framework and overall objectives of the future development of IMT for 2030 and beyond," ITU, ITU-R M. 2160-0, 2023.

[45] A. Ramos, A. Mrozowski, D. Prado-Alvarez, J. F. Monserrat, Y. Zhang, Z. Yu, and Y. Chen, "Evaluation Methodology for 6G Sensing-Assisted Communication System Performance," *IEEE Access*, vol. 12, pp. 7841–7852, 2024.

[46] Y. Cui, F. Liu, X. Jing, and J. Mu, "Integrating Sensing and Communications for Ubiquitous IoT: Applications, Trends, and Challenges," *IEEE Network*, vol. 35, no. 5, pp. 158–167, 2021.

[47] F. Liu, Y. Cui, C. Masouros, J. Xu, T. X. Han, Y. C. Eldar, and S. Buzzi, "Integrated Sensing and Communications: Towards Dual-functional Wireless Networks for 6G and Beyond," *IEEE Journal on Selected Areas in Communications*, vol. 40, no. 6, pp. 1728–1767, 2022.

[48] Z. He, W. Xu, H. Shen, D. W. K. Ng, Y. C. Eldar, and X. You, "Full-Duplex Communication for ISAC: Joint Beamforming and Power Optimization," *IEEE Journal on Selected Areas in Communications*, vol. 41, no. 9, pp. 2920–2936, 2023.

[49] Z. Du, F. Liu, W. Yuan, C. Masouros, Z. Zhang, S. Xia, and G. Caire, "Integrated Sensing and Communications for V2I Networks: Dynamic Predictive Beamforming for Extended Vehicle Targets," *IEEE Transactions on Wireless Communications*, vol. 22, no. 6, pp. 3612–3627, 2023.

[50] Y. Li, F. Liu, Z. Du, W. Yuan, and C. Masouros, "ISAC-enabled V2I networks based on 5G NR: How many overheads can be reduced?" *arXiv preprint arXiv:2301.12787*, 2023.

[51] Y. Cui, Q. Zhang, Z. Feng, Q. Wen, Z. Wei, F. Liu, and P. Zhang, "Seeing Is Not Always Believing: ISAC-Assisted Predictive Beam Tracking in Multipath Channels," *IEEE Wireless Communications Letters*, 2023.

[52] F. Liu, C. Masouros, A. P. Petropulu, H. Griffiths, and L. Hanzo, "Joint radar and communication design: Applications, state-of-the-art, and the road ahead," *IEEE Transactions on Communications*, vol. 68, no. 6, pp. 3834–3862, 2020.

[53] F. Liu, W. Yuan, C. Masouros, and J. Yuan, "Radar-Assisted Predictive Beamforming for Vehicular Links: Communication Served by Sensing," *IEEE Transactions on Wireless Communications*, vol. 19, no. 11, pp. 7704–7719, 2020.

[54] F. Liu and C. Masouros, "A Tutorial on Joint Radar and Communication Transmission for Vehicular Networks—Part III: Predictive Beamforming Without State Models," *IEEE Communications Letters*, vol. 25, no. 2, pp. 332–336, 2020.

[55] C. Baquero Barneto, E. Rastorgueva-Foi, M. F. Keskin, T. Riihonen, M. Turunen, J. Talvitie, H. Wymeersch, and M. Valkama, "Millimeter-Wave Mobile Sensing and Environment Mapping: Models, Algorithms and Validation," *IEEE Transactions on Vehicular Technology*, vol. 71, no. 4, pp. 3900–3916, 2022.

[56] R. Du, H. Xie, M. Hu, Narengerile, Y. Xin, S. McCann, M. Montemurro, T. Xiao Han, and J. Xu, "An Overview on IEEE 802.11bf: WLAN Sensing," *arXiv preprint arXiv:2207.04859*, 2022.

[57] A. Ali, N. Gonzalez-Prelcic, R. W. Heath, and A. Ghosh, "Leveraging Sensing at the Infrastructure for mmWave Communication," *IEEE Communications Magazine*, vol. 58, no. 7, pp. 84–89, 2020.

[58] M. L. Rahman, J. A. Zhang, X. Huang, Y. J. Guo, and Z. Lu, "Joint communication and radar sensing in 5G mobile network by compressive sensing," *IET Communications*, vol. 14, no. 22, pp. 3977–3988, 2020.

[59] Z. Zhang, R. He, B. Ai, M. Yang, C. Li, H. Mi, and Z. Zhang, "A General Channel Model for Integrated Sensing and Communication Scenarios," *IEEE Communications Magazine*, vol. 61, no. 5, pp. 68–74, 2023.

[60] 3GPP TSG RAN, "Study on Channel Model for Frequencies from 0.5 to 100 GHz (Release 14)," 3GPP, Tech. Rep. 38.901 V14.3.0, Dec 2017.

[61] 3GPP TSG RAN, "Study on Channel Model for Frequencies from 0.5 to 100 GHz (Release 15)," 3GPP, Tech. Rep. 38.901 V15.1.0, Sept 2019.

[62] Ericsson, "New SI Proposal: Study on Channel Modeling for Indoor Industrial Scenarios," 3GPP, Tech. Rep. RP-182138, Sept 2018. [Online]. Available: https://www.3gpp.org/DynaReport/TDocExMtg-RP-81-18666.htm

[63] Ericsson, "List of Measurements," 3GPP, R1- 1909706, Aug 2019. [Online]. Available: https://www.3gpp.org/ftp/tsg_ran/WG1_RL1/TSGR1_98/Docs/

[64] M. Cantero, S. Inca, A. Ramos, M. Fuentes, D. Martín-Sacristán, and J. F. Monserrat, "System-Level Performance Evaluation of 5G Use Cases for Industrial Scenarios," *IEEE Access*, vol. 11, pp. 37 778–37 789, 2023.

[65] 3GPP TSG RAN, "Study on Channel Model for Frequencies from 0.5 to 100 GHz (Release 17)," 3GPP, Tech. Rep. 38.901 V17.0.0, Mar 2022.

[66] CMCC and BUPT, "New Measurements and Modelling on Fast Fading in IIoT Scenarios," 3GPP, R1- 1904743, Nov. 2018. [Online]. Available: https://www.3gpp.org/ftp/tsg_ran/WG1_RL1/TSGR1_96b/Docs/

[67] Nokia and Nokia Shanghai Bell, "Delay Spread Measurement Results and Observations From Two Operational Factory Halls at 3.5 GHz for Various Antenna Configurations," 3GPP, R1- 1902624,

Feb 2019. [Online]. Available: https://www.3gpp.org/ftp/tsg_ran/WG1_RL1/TSGR1_96/Docs/

[68] ZTE, BJTU, and Sanechips, "RMS Delay Spread Model in IIoT Scenario," 3GPP, R1- 1906492, May 2019. [Online]. Available: https://www.3gpp.org/ftp/tsg_ran/WG1_RL1/TSGR1_97/Docs/

[69] ns-3 Network Simulator. [Online]. Available: https://www.nsnam.org/

[70] A. Ramos, Y. Estrada, M. Cantero, J. Romero, D. Martín-Sacristán, S. Inca, M. Fuentes, and J. Monserrat, "Implementation and Calibration of the 3GPP Industrial Channel Model for Ns-3," in *Proceedings of the 2022 Workshop on Ns-3*, ser. WNS3 '22. New York, NY, USA: Association for Computing Machinery, 2022, p. 10–16. [Online]. Available: https://doi.org/10.1145/3532577.3532596

[71] 3GPP TSG RAN, "Indoor industrial channel model calibration results, WG1 Meeting #97," 3GPP, R1- 1909704, May 2019.

[72] 3GPP TSG RAN, "Summary of email discussion on indoor industrial channel model and calibration, WG1 Meeting #97," 3GPP, R1- 1907968, May 2019.

[73] M. K. Samimi and T. S. Rappaport, "3-D Millimeter-Wave Statistical Channel Model for 5G Wireless System Design," *IEEE Transactions on Microwave Theory and Techniques*, vol. 64, no. 7, pp. 2207–2225, 2016.

[74] T. S. Rappaport, S. Sun, and M. Shafi, "Investigation and Comparison of 3GPP and NYUSIM Channel Models for 5G Wireless Communications," in *2017 IEEE 86th Vehicular Technology Conference (VTC-Fall)*, 2017, pp. 1–5.

[75] F. Ademaj, S. Schwarz, K. Guan, and M. Rupp, "Ray-Tracing Based Validation of Spatial Consistency for Geometry-Based Stochastic Channels," in *2018 IEEE 88th Vehicular Technology Conference (VTC-Fall)*, 2018, pp. 1–5.

[76] D. Dupleich, N. Han, A. Ebert, R. Müller, S. Ludwig, A. Artemenko, J. Eichinger, T. Geiss, G. Del Galdo, and R. Thomä, "From Sub-6 GHz to mm-Wave: Simultaneous Multi-band Characterization of Propagation from Measurements in Industry Scenarios," in *2022 16th European Conference on Antennas and Propagation (EuCAP)*, 2022, pp. 1–5.

[77] S. Jaeckel, N. Turay, L. Raschkowski, L. Thiele, R. Vuohtoniemi, M. Sonkki, V. Hovinen, F. Burkhardt, P. Karunakaran, and T. Heyn, "Industrial Indoor Measurements from 2-6 GHz for the 3GPP-NR and QuaDRiGa Channel Model," in *2019 IEEE 90th Vehicular Technology Conference (VTC2019-Fall)*, 2019, pp. 1–7.

[78] D. K. Pin Tan, J. He, Y. Li, A. Bayesteh, Y. Chen, P. Zhu, and W. Tong, "Integrated Sensing and Communication in 6G: Motivations, Use Cases, Requirements, Challenges and Future Directions," in *2021 1st IEEE International Online Symposium on Joint Communications & Sensing (JC&S)*, 2021, pp. 1–6.

[79] M. A. Richards, *Fundamentals of Radar Signal Processing*, 2nd ed. McGraw-Hill Professional, 2014.

[80] A. López-Reche, D. Prado-Alvarez, A. Ramos, S. Inca, J. F. Monserrat, Y. Zhang, Z. Yu, and Y. Chen, "Considering correlation between sensed and communication channels in GBSM for 6G ISAC applications," in *2022 IEEE Globecom Workshops (GC Wkshps)*, 2022, pp. 1317–1322.

[81] S. Inca, A. Mrozowski, D. Prado-Alvarez, J. F. Monserrat, Y. Zhang, W. Yang, and Y. Chen, "Angular Correlation Study of Sensing and Communication Channels in V2X Scenarios for 6G ISAC Usage," in *2023 IEEE Globecom Workshops (GC Wkshps)*, 2023, pp. 1189–1194.

[82] S. Lu, F. Liu, Y. Li, K. Zhang, H. Huang, J. Zou, X. Li, Y. Dong, F. Dong, J. Zhu *et al.*, "Integrated Sensing and Communications: Recent Advances and Ten Open Challenges," *arXiv preprint arXiv:2305.00179*, 2023.

[83] S. Mandelli, M. Henninger, M. Bauhofer, and T. Wild, "Survey on Integrated Sensing and Communication Performance Modeling and Use Cases Feasibility," *arXiv preprint arXiv:2305.07144*, 2023.

[84] R. Yang, C.-X. Wang, J. Huang, E.-H. M. Aggoune, and Y. Hao, "A Novel 6G ISAC Channel Model Combining Forward and Backward Scattering," *IEEE Transactions on Wireless Communications*, vol. 22, no. 11, pp. 8050–8065, 2023.

[85] Y. Zhuo and Z. Wang, "Performance Analysis of ISAC System Under Correlated Communication-Sensing Channel," *IEEE Transactions on Vehicular Technology*, pp. 1–6, 2023.

[86] WINNER II, "WINNER II channel models," IST-WINNER II WP1, Deliverable D1.1.2, 2007.

[87] C. Ouyang, Y. Liu, H. Yang, and N. Al-Dhahir, "Integrated Sensing and Communications: A Mutual Information-Based Framework," *IEEE Communications Magazine*, vol. 61, no. 5, pp. 26–32, 2023.

[88] M. Fuentes, J. L. Carcel, C. Dietrich, L. Yu, E. Garro, V. Pauli, F. I. Lazarakis, O. Grøndalen, O. Bulakci, J. Yu *et al.*, "5G New Radio Evaluation Against IMT-2020 Key Performance Indicators," *IEEE Access*, vol. 8, pp. 110 880–110 896, 2020.

[89] J. Grythe and A. Norsonic, "Beamforming Algorithms-Beamformers," *Technical Note, Norsonic AS, Norway*, 2015.

[90] Y. Cui, Q. Zhang, Z. Feng, Q. Wen, Z. Wei, F. Liu, and P. Zhang, "Seeing Is Not Always Believing: ISAC-Assisted Predictive Beam Tracking in Multipath Channels," *IEEE Wireless Communications Letters*, pp. 1–1, 2023.

[91] 3GPP TSG RAN, "NR; User Equipment (UE) radio access capabilities (Release 16)," 3GPP, Tech. Spec. 38.306, Nov 2020.

[92] F. Wen, H. Wymeersch, B. Peng, W. P. Tay, H. C. So, and D. Yang, "A survey on 5G massive MIMO localization," *Digital Signal Processing*, vol. 94, pp. 21–28, 2019, special Issue on Source Localization in Massive MIMO. [Online]. Available: https://www.sciencedirect.com/science/article/pii/S1051200419300569

[93] H. Wymeersch, D. Shrestha, C. M. de Lima, V. Yajnanarayana, B. Richerzhagen, M. F. Keskin, K. Schindhelm, A. Ramirez, A. Wolfgang, M. F. de Guzman, K. Haneda, T. Svensson, R. Baldemair, and S. Parkvall, "Integration of Communication and Sensing in 6G: a Joint Industrial and Academic Perspective," in *2021 IEEE 32nd Annual International Symposium on Personal, Indoor and Mobile Radio Communications (PIMRC)*, 2021, pp. 1–7.

[94] Y. Wang, Z. Wei, and Z. Feng, "Beam Training and Tracking in MmWave Communication: A Survey," *arXiv preprint arXiv:2205.10169*, 2022.

[95] Y. Xu, Y. Guo, C. Li, B. Xia, and Z. Chen, "Predictive Beam Tracking with Cooperative Sensing for Vehicle-to-Infrastructure Communications," in *2021 IEEE/CIC International Conference on Communications in China (ICCC)*. IEEE, 2021, pp. 835–840.

[96] Z. Du, F. Liu, and Z. Zhang, "Sensing-assisted beam tracking in V2I networks: Extended target case," in *ICASSP 2022-2022 IEEE International Conference on Acoustics, Speech and Signal Processing (ICASSP)*. IEEE, 2022, pp. 8727–8731.

[97] W. Yuan, F. Liu, C. Masouros, J. Yuan, D. W. K. Ng, and N. González-Prelcic, "Bayesian Predictive Beamforming for Vehicular Networks: A Low-Overhead Joint Radar-Communication Approach," *IEEE Transactions on Wireless Communications*, vol. 20, no. 3, pp. 1442–1456, 2021.

[98] D. H. Parks and S. S. Fels, "Evaluation of Background Subtraction Algorithms with Post-Processing," in *2008 IEEE Fifth International Conference on Advanced Video and Signal Based Surveillance*, 2008, pp. 192–199.

[99] G. R. Maccartney, T. S. Rappaport, S. Sun, and S. Deng, "Indoor office wideband millimeter-wave propagation measurements and channel models at 28 and 73 GHz for ultra-dense 5G wireless networks," *IEEE access*, vol. 3, pp. 2388–2424, 2015.

[100] A. Shahmansoori, G. E. Garcia, G. Destino, G. Seco-Granados, and H. Wymeersch, "Position and Orientation Estimation Through Millimeter-Wave MIMO in 5G Systems," *IEEE Transactions on Wireless Communications*, vol. 17, no. 3, pp. 1822–1835, 2018.

[101] A. Ramos, M. F. Keskin, H. Wymeersch, S. Inca, and J. F. Monserrat, "Enhancing Sensing-Assisted Communications in Cluttered Indoor Environments Through Background Subtraction," in *2024 IEEE Wireless Communications and Networking Conference (WCNC)*, 2024, pp. 1–6.

[102] M. B. Rhudy, R. A. Salguero, and K. Holappa, "A Kalman filtering tutorial for undergraduate students," *International Journal of Computer Science & Engineering Survey*, vol. 8, no. 1, pp. 1–9, 2017.

[103] B.-n. Vo, M. Mallick, Y. Bar-Shalom, S. Coraluppi, R. Osborne, R. Mahler, and B.-t. Vo, "Multitarget Tracking," *Wiley encyclopedia of electrical and electronics engineering*, no. 2015, 2015.

[104] K. Taunk, S. De, S. Verma, and A. Swetapadma, "A brief review of nearest neighbor algorithm for learning and classification," in *2019 international conference on intelligent computing and control systems (ICCS)*. IEEE, 2019, pp. 1255–1260.